Stefan Grünenwald

HIGH POWER FIBER LASER WELDING OF THICK SECTION MATERIALS – PROCESS PERFORMANCE AND WELD PROPERTIES

ACTA UNIVERSITATIS LAPPEENRANTAENSIS 877

Stefan Grünenwald

HIGH POWER FIBER LASER WELDING OF THICK SECTION MATERIALS – PROCESS PERFORMANCE AND WELD PROPERTIES

Dissertation for the degree of Doctor of Science (Technology) to be presented with due permission for public examination and criticism in the Auditorium 2310 at Lappeenranta-Lahti University of Technology LUT, Lappeenranta, Finland on the 27th of November, 2019, at noon.

Acta Universitatis
Lappeenrantaensis 877

Supervisor Professor Antti Salminen
LUT School of Energy Systems
Lappeenranta-Lahti University of Technology LUT
Finland

Reviewers Associate Professor John C. Ion
Department of Physics
University of Western Australia
Australia

Professor Knut Partes
Department of Mechanical Engineering
Jade Hochschule Wilhelmshaven
Germany

Opponent Associate Professor John C. Ion
Department of Physics
University of Western Australia
Australia

ISBN 978-952-335-438-8
ISBN 978-952-335-439-5 (PDF)
ISSN-L 1456-4491
ISSN 1456-4491

Lappeenranta-Lahti University of Technology LUT
LUT University Press 2019

Abstract

Stefan Grünenwald
High Power Fiber Laser Welding of Thick Section Materials – Process Performance and Weld Properties
Lappeenranta 2019
85 pages
Acta Universitatis Lappeenrantaensis 877
Diss. Lappeenranta-Lahti University of Technology LUT
ISBN 978-952-335-438-8, ISBN 978-952-335-439-5 (PDF),
ISSN-L 1456-4491, ISSN 1456-4491

High power fiber laser systems have reached output powers far beyond 30 kW and a fiber laser source of 100 kW output power has recently become available for fundamental research. With the high laser power that is now attainable and the ability to deliver a high-quality beam in a flexible fiber with high wall plug efficiency and low maintenance requirements, high power fiber laser systems are becoming of increasing interest for joining thick section materials in industrial applications.

In this work, fiber laser systems with output power of up to 30 kW are used to investigate the feasibility of autogenous laser welding and laser arc hybrid welding for joining thick section materials. The focus is placed on joining pipe steels and shipbuilding steels of up to 28 mm thickness with the aim of developing welding strategies and parameter sets that can meet the requirements of industrial standards and guidelines. The reliability of the parameter sets developed for the joining processes is tested against process boundaries or limits such as maximum penetration depth, ability to compensate for linear misalignment, air gaps and change in welding position. To verify the quality of the welded joints, characterisation of the material properties is carried out using destructive and non-destructive test methods.

The results of the experimental test series and materials characterisation support the use of high power fiber laser sources as suitable tools for laser arc hybrid welding and autogenous laser welding of thick section materials. Considering especially the autogenous laser welding process, it is shown that varying the power density or oscillating the laser beam can benefit the weld result to the same extent than laser arc hybrid welding.

The research presented in this work provides an improved understanding of the behaviour of deep penetration welds in thick section material, referring to the properties of the welded joint and performance of the process. The achieved results are a solid foundation for meeting the requirements of industrial applications in the pipeline and shipbuilding industry.

Keywords: high power fiber lasers, laser arc hybrid welding, autogenous laser welding, thick section material, X65, X70, imperfections, air gap, linear misalignment, power density, oscillated laser beam welding

Acknowledgements

The studies for this thesis were carried out at the Bremer Institut für angewandte Strahltechnik (BIAS) and at Lappeenranta-Lahti University of Technology (LUT). The work on this thesis developed into a long-term project over several years and I wish to express my gratitude to all those persons who have accompanied me through this time.

First, I would like to express my sincere thanks to Professor Antti Salminen who agreed to supervise my thesis. I very much appreciated the valuable opportunity to carry out research at LUT and his support over this long period of time.

I am very grateful to Professor John Ion who gave valuable comments on my work and acted as an opponent in the public examination.

I very much appreciated feedback and comments from Professor Knut Partes during the process of writing this thesis.

My success in completing this thesis would not have been possible without the help of many people at BIAS and LUT. I had great pleasure working with, Antti Heikkinen, Pertti Kokko, Ilkka Poutiainen and Anna Unt. Thank you for the practical suggestions for my experiments and the constructive criticism on publications and my thesis. I would like to pay special thankfulness to Peter Jones for the thorough proofreading of the manuscript – you have done so much more than advising on grammar and spelling. Special thanks go to Minna Loikkanen who provided moral support and helpful advice from the day I started studying at LUT.

Finally, I would like to deeply thank my family for their patience and moral support during all of these years and especially during the last months of finalising this thesis.

Stefan Grünenwald
October 2019
Bremen, Germany

To Josephine Johanna

Contents

List of publications

This dissertation is based on the following publications, which are referred to in the text by Roman numbers I-V. The rights have been granted by the publishers to include the publications in the dissertation.

I. Vollertsen, F., Grünenwald, S., Rethmeier, M., Gumenyuk, A., Olschock, S. (2010). Welding Thick Steel Plates with Fibre Lasers and GMAW. Welding in the World, 54(3/4), pp. R62 – R70.

II. Grünenwald, S., Seefeld, T., Vollertsen, F., Gook, S., Gumenyuk, A., Rethmeier, M. (2010), Laser-MSG-Hybridschweißen dicker Bleche aus Rohrleitungsstahl mit Faserlasern hoher Leistung. Schweißen und Schneiden, 62, pp. 338 – 347.

III. Grünenwald, S., Seefeld, T., Vollertsen, F., Kocak, M. (2010). Solutions for joining pipe steels using laser-GMA-hybrid welding processes. Physics Procedia, 5, pp. 77-87.

IV. Unt, A., Poutiainen, I., Grünenwald, S., Sokolov, M., Salminen, A. (2017). High Power Fiber Laser Welding of Single Sided T-joint on Shipbuilding Steel with Different Processing Setups, Appl. Sci. 7(12), pp. 1276.

V. Grünenwald, S., Unt, A., Salminen, A. (2018). Investigation of the influence of welding parameters on the weld geometry when welding structural steel with oscillated high-power laser beam. Procedia CIRP, 74, pp. 461 – 465.

Author's contribution

Stefan Grünenwald is the main author and investigator in publications I – III and V. In publication IV, Anna Unt was the corresponding author and Stefan Grünenwald post-processed the experimental data, discussed the basic structure of the manuscript, and read and approved the final version prior to submission for publication.

Abbreviations

a	core radius of optical fiber	[mm]
B	brightness	
BM	base metal	
BOP	bead on plate	
BPP	beam parameter product	[mm mrad]
CMT	cold metal transfer	
cw	continuous wave	
CO_2	carbon dioxide	
DIN	Deutsches Institut für Normung (German Institute for Standardisation)	
DNVGL	Det Norske Veritas Germanischer Lloyd	
E	power density	[W/cm^2]
EN	Europäische Norm (European Standard)	
f_{pp}	focal point position	[mm]
FWM	four wave mixing	
GHz	gigahertz	
GMAW	gas metal arc welding	
GTAW	gas tungsten arc welding	
h	hours	
HV	hardness Vickers	
HAZ	heat affected zone	
ISO	International Organization for Standardization	
LP	linearly polarized	
M^2	beam quality factor	
MCVD	modified chemical vapour deposition	
n	refractive index	
NA	numerical aperture	
OVD	outside vapour deposition	
P	laser power	[kW]
PAW	plasma arc welding	
PCF	photonic crystal fiber	
PCVD	plasma chemical vapour deposition	
R_a	average surface roughness	[µm]
r_{cl}	cladding radius	[mm]
r_b	laser beam radius	[mm]
SAW	submerged arc welding	
SBS	stimulated Brillouin scattering	
SEM	scanning electron microscope	
SMAW	shielded metal arc welding	
SPM	self-phase modulation	
SRS	stimulated Raman scattering	
TEM	transverse electromagnetic mode	

THz	tetrahertz	
TIR	total internal reflection	
t	thickness	[mm]
VAD	vapour axial deposition	
v_w	welding speed	[m/min]
WM	weld metal	
YAG	Yttrium Aluminium Garnet	
α	angle of inclination	[°]
λ	wavelength	[nm]
θ_a	acceptance angle	[°]
θ_c	critical angle	[°]
θ_B	angle of divergence of the laser beam	[°]
ω_B	mode field radius of the laser beam	[mm]

Chemical elements

Er	Erbium
Ho	Holmium
Nd	Neodymium
Tm	Tulium
Yb	Ytterbium
Al	Aluminium
C	Carbon
Cr	Chromium
Cu	Copper
Mn	Manganese
Mo	Molybdenum
N	Nitrogen
Nb	Niobium
Ni	Nickel
P	Phosphorous
S	Sulphur
Si	Silicon
Ti	Titanium
V	Vanadium

1 Introduction

In this work, fiber laser sources with a maximum output power of 30 kW are used to study process performance and weld properties when joining thick section steel material. The aim is to experimentally examine the use of autogenous laser welding and laser arc hybrid welding processes to join thick section material and establish parameter sets, which provide welds of such a quality that meet requirements for industrial applications.

Employing a laser arc hybrid welding process, the first objective was to investigate boundaries or limits that influence the maximum weldable thickness and quality of the weld with the purpose of establishing a welding strategy with parameter sets that produce acceptable welds that meet industrial standards and guidelines. The most important process boundary investigated was the relationship between the material thickness and the available laser power. In the work, welding strategies were developed to adapt the welding process and joint preparation to different material thickness and laser power to maintain full penetration. Further process boundaries investigated were variation of the air gap size, linear misalignment and the welding position. Suitable parameter sets were developed to control the stability of the melt pool and avoid droplets on the root side of the weld.

The second objective was to explore the feasibility of an autogenous laser welding process for deep penetration welding as an alternative to laser arc hybrid welding. The focus of the research was on controlling the heat input, i.e. the energy absorbed by the material, by varying the power density and oscillating the laser beam.

To verify the quality of the welded joints, characterisation of the material properties was carried out by using destructive and non-destructive test methods. The approach employed to achieve the desired outcome is described in detail by presenting individual results of each test series and explaining the influence of the main parameters of the welding process on the weld result.

The scientific contribution of this work is an improved understanding of the behaviour of deep penetration welds in thick section material, referring to the properties of the welded joint and the performance of the process. The main findings are, first, experimental validation that up to 30 kW of laser power can be used for a controlled deep penetration welding process. Second, identification of the interaction of laser power and welding speed with other critical parameters to achieve high quality welds when the initial conditions are limited by given imperfections in the joint preparation and welding position. Third, research of the impact on the weld result when varying the power density and oscillating the laser beam. Fourth, contribution of a welding strategy with a knowledge base to be used for further developing deep penetration welding processes, simulation models and industrial applications.

The structure of this dissertation is organized in two parts. The first part reviews the state of the art, giving a detailed overview of the basic principles of fiber lasers and the development of high power fiber laser systems. In addition, it describes the principles of laser-based welding processes and gives a summary of welding of thick section materials with high power fiber lasers. The second part provides a detailed summary of the main findings of the publications. This includes the materials and equipment used for the experiments and the discussion of the achieved results from laser arc hybrid welding and autogenous welding. The publications are included at the end of the dissertation.

2 State of the art

Based on the theoretical description of Einstein, the principle of light amplification by stimulated emission of radiation was used by Maiman to develop the first ruby laser in 1960 (Einstein, 1916), (Maiman, 1960). Since then the development of different laser types and systems has led to a variety of applications for laser technology. For welding of thick section material, high power laser systems are particularly interesting. This chapter reviews the basic principle of fiber lasers and describes the development and current state of high power fiber lasers. The second part of the chapter focuses on welding with laser-based processes, the interaction between laser radiation and material, and definition of autogenous laser welding and hybrid laser welding processes. The third part gives an overview of welding of thick section materials, the influence of different parameters on the process and development of laser-based welding processes for industrial applications in the pipeline and shipbuilding industry.

2.1 High power fiber lasers

Snitzer laid the conceptual foundation for the fiber laser in the 1960s by initially considering a light pipe in which electromagnetic energy propagates by internal reflection off the pipe walls (Snitzer, 1961). The light pipe is there more accurately described as a cylindrical metallic or dielectric waveguide consisting of a core and cladding. A few years later, Koester et al. experimentally investigated parameters affecting the gain in a fiber laser. This work amplified a neodymium glass laser beam by pumping a 1 m long glass fiber with a Nd doped core coiled around a flashtube (Koester, 1964).

Further research in the development of rare earth doped optical fibers was carried out in the beginning of the 1980s (Hegarty, 1983), (Poole, 1986), (Mears, 1987). The availability of laser diodes as pump sources in the subwatt level (Hayashi, 1970), (Snitzer, 1988a), (Nakazawa, 1989) led to successful development of optical fiber amplifiers in the telecommunication industry in the 1980s and 1990s (Goodno, 2011), (Okhotnikov, 2012).

The step to high power fiber lasers became possible in 1988 when Snitzer (1988b) proposed the concept of cladding pumping, where the pump light is coupled into a cladding instead of the core. This approach allows the use of a high power pump source with a low beam quality to generate a much brighter and more intense laser output (Zervas, 2014).

In further review of high power fiber lasers, the focus in this dissertation is placed on laser configurations with continuous wave-operation (cw) for materials processing purposes.

2.1.1 Fiber design

The fundamental part of a high power fiber laser is the double clad fiber as proposed by Snitzer in 1988. A double clad fiber consists of a doped core which is surrounded by an inner cladding and an outer cladding that acts as a second waveguide (Eichler, 2006), Figure 2.1. Low brightness pump light is coupled into the inner cladding and because of the decreasing refractive index profile from the core towards the outer cladding the pump light is confined between the inner and outer cladding. As the light propagates along the fiber it is gradually absorbed by the doped core and the stimulated emission is generated as high brightness signal laser radiation.

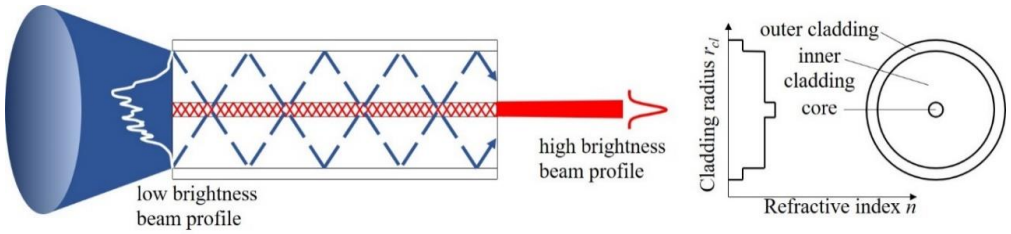

Figure 2.1: Structure of a double clad fiber showing the pumping scheme (left) and refractive index profile (right), based on Nilsson (2011) and Zervas (2014).

Power scaling of fiber lasers to levels in the range of several kilowatts of continuous wave single mode laser power and up to more than 100 kW multimode can be achieved by utilizing double clad fibers with suitable pump sources, the appropriate fiber design and material but also consideration of optical and thermal effects (Goodno 2011), (Okhotnikov 2012), (Richardson, 2012), (Zervas, 2014), (Dragic, 2018).

Optical fibers for high power laser applications are silica-based and drawn from glass, using a chemical vapour deposition process. Industrially applied processes are modified chemical vapour deposition (MCVD), outside vapour deposition (OVD), vapour axial deposition (VAD) and plasma chemical vapour deposition (PCVD). The manufacturing process of a cylindrical optical fiber involves fabrication of the preform of the raw material, drawing of the fiber and application of the required coating materials (MacChesney, 1990). In order to achieve the desired waveguiding and thermal and thermomechanical properties of the fiber, co-dopants are added. Relative to the base material, germanium dioxide (GeO_2) and silicon dioxide (SiO_2), for example, increase the refractive index and enhance the increase in reflectivity of the permanent refractive index, the so-called photosensitivity. Aluminium oxide (Al_2O_3) enhances the maximum concentration of lanthanide dopants. Phosphorous pentoxide (P_2O_5) raises the refractive index and reduces the viscosity (Li, 2018), (Peng, 2019).

To dope the active core itself, rare-earth elements such as erbium (Er), holmium (Ho), neodymium (Nd), thulium (Tm) or ytterbium (Yb) from the group of lanthanides can be used. Common rare-earth elements for the production of fibers for laser systems are erbium, thulium and ytterbium, which are incorporated in the silica-based fiber core as trivalent ions Er^{3+}, Tm^{3+} and Yb^{3+} (Träger, 2012). The most interesting fiber type for high power fiber lasers are Yb-doped fibers, which will be discussed in the following sections.

Yb-doped fibers have a simple electronic two-level system with only one excited state level ($^2F_{5/2}$) and a ground state level ($^2F_{7/2}$). In principle, this structure is a configuration in which population inversion leads to an equilibrium on both levels, and optical gain is thus not achieved and lasing is not be possible (Dragic, 2018). By placing the dopant ions into a glass or crystal structure, splitting of the energy level into different manifolds can be achieved, so-called Stark splitting (Stark, 1914). This splitting effect can enable operation of three- or four-level Yb^{3+} systems, with up to twelve levels being physically possible, and enables lasing activity (White, 2009), Figure 2.2.

The emission and absorption spectra vary depending on the composition of the co-dopants of the silica-base of the Yb-doped fiber. In general, the absorption band ranges from 850 nm to 1080 nm, which is particularly suitable for the wavelength spectrum at which high power pump laser diodes work best. The gain bandwidth extends from 975 nm to 1180 nm. High power fiber laser systems are mostly operated between 1060 nm and 1100 nm, (Lu, 2002), (Barua, 2008), (Träger, 2012), (Li, 2018), Figure 2.3.

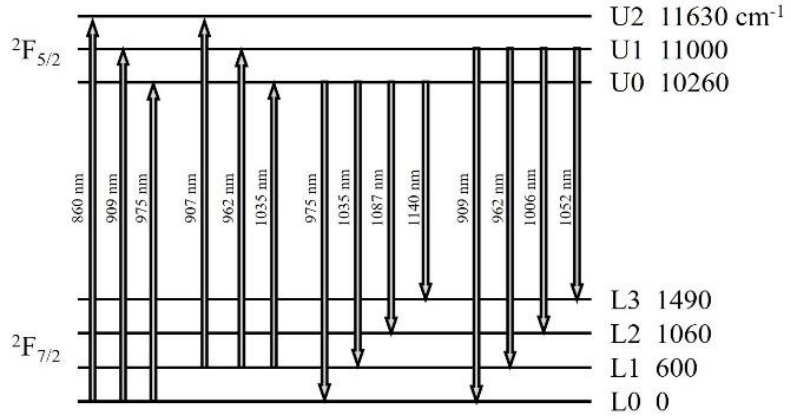

Figure 2.2: Energy level diagram for Yb^{3+} ions in a silica-base with approximate values for wavelength and splitting, based on Dieke (1963) and Pask (1995).

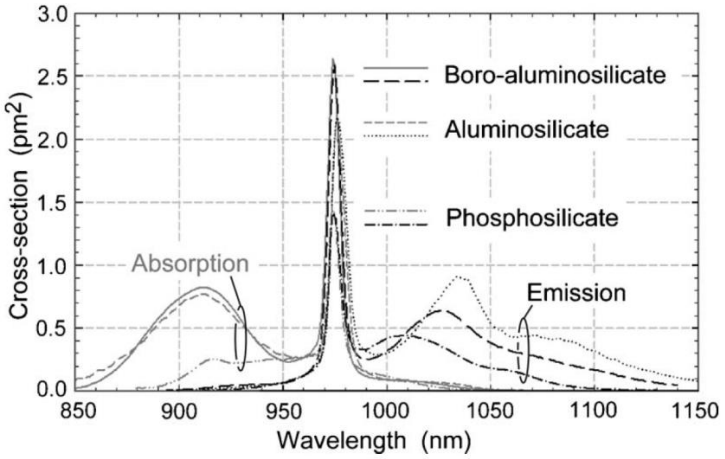

Figure 2.3: Emission and absorption spectrum of ytterbium ions in different silica-based fibers, (Richardson, 2012).

Using knowledge of the basic material properties and their effect on the stimulated emission of radiation, it is possible to design an optical fiber that fits the requirements of different laser applications and systems. The simplest and most common configuration of optical fibers is the step-index fiber, in which the core is surrounded by one or more cladding of a lower refractive index to ensure the required total internal reflection (TIR). Rays of light propagating in an optical fiber must meet the smallest angle of incidence that yields TIR, known as critical angle θ_c, according to Snell's law, to avoid losses between the interfaces of the cladding and the core. To fulfil this criterion, the ray of light must enter the fiber under the acceptance angle θ_a also expressed in terms of the numerical aperture (NA), Figure 2.4 (Pedrotti, 2002):

$$NA = n_0 \sin\theta_a = n_1 \sin\theta_c = \sqrt{n_1^2 - n_2^2} \tag{2.1}$$

where n_1 and n_2 represent the refractive indices of the core and the cladding, and $n_0 = 1$ is the refractive index of air.

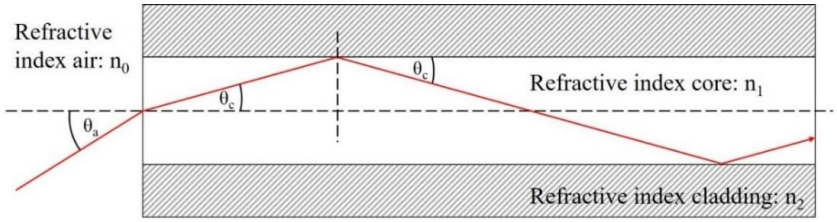

Figure 2.4: Propagation of light through a step-index fiber with total internal reflection.

The normalized frequency *V* is used to describe the spatial distribution of the energy that propagates through the fiber. The value of *V* is dependent on the optical wavelength λ, the core radius *a*, and the refractive indices contained in the numerical aperture *NA* (Gloge, 1971):

$$V = \frac{2\pi}{\lambda} a\ NA \tag{2.2}$$

For a value of *V* below 2.405, an optical fiber supports a single guided optical mode for a given wavelength, which can be approximated by a Gaussian distribution. For values > 2.405 the fiber is considered to be multimode. Based on a Gaussian or LP_{01}/TEM_{00} intensity profile of a single guided mode, the beam quality factor M^2 or the beam parameter product (BPP) can be derived (Eichler, 2006), (Ross, 2006):

$$M^2 = \frac{\pi}{\lambda} \omega_B \theta_B \tag{2.3}$$

$$BPP = \omega_B \theta_B \tag{2.4}$$

where ω_B is the mode field radius and θ_B is the angle of divergence of the laser beam. For an ideal Gaussian beam $M^2 = 1$ and for real laser beams $M^2 > 1$.

The maximum pump power (P_P) coupled into the inner cladding of a fiber is proportional to the brightness *(B)* of the pump source, and the radius (r_{cl}) and numerical aperture (NA_{cl}) of the outer cladding. According to the definition of brightness by Ross (2006):

$$B = \frac{P_P}{\pi^2 BPP^2} = \frac{P_P}{(M^2\lambda)^2} \tag{2.5}$$

with the given beam quality *BPP* or M^2, in combination with the wavelength λ, the maximum pump power coupled into a circular fiber can be described as:

$$P_P = B(\pi r_{cl}^2)(\pi NA_{cl}^2) \tag{2.6}$$

When considering the delivery of the pump light to the laser active core in a double clad fiber, one drawback is the rotational symmetric cladding-core design, which reduces the absorption of pump light. Different designs exist where the symmetry of the inner cladding is altered to increase the overlap of the pump light and direct skew rays towards the active core. Figure 2.5 shows different cross sections of non-symmetric inner claddings (Snitzer, 1988b), (Grubb, 2000). Investigations with numerical models of the local absorption rate of the pump light into the core show that already small deformations in the cladding can lead to improvement in pump light absorption (Kouznetzov, 2002a and 2002b), (Javadimanesh, 2016).

To avoid non-linear effects, limited thermal capabilities and a simultaneous increase in the numerical aperture, and to allow a higher pump power to be coupled into the fiber while still providing high brightness of the output laser beam, the fiber design can be adjusted further. For example, microstructuring the fiber can add properties to the fiber that enable the challenges inherent in the fiber design to be overcome. Photonic crystal fibers (PCF), Figure 2.6, with an array of cylindrically arranged air holes around the core throughout the whole length of the fibre allow a larger multimode core than is usually required when utilizing regular fibers whilst still enabling a single mode operation by adjusting the refractive index between the core and cladding. In combination with another adjustment, so-called air-cladding, on the boundary of the outer and inner cladding, the numerical aperture can be increased to values higher than 0.8 and the diameter of the inner cladding can be decreased. Both design features allow a considerable increase in the pump power, an increased absorption rate and shorter absorption lengths of the pump light in the fiber. If the diameter of the inner cladding is not reduced, the need for complex coupling structures of the pump light into the fiber can be avoided (Wadsworth, 2003), (Limpert, 2004), (Limpert, 2007), (Hansen, 2011).

Further microstructuring of optical fibers is also possible, such as leakage channel fibers, higher order mode fibers, chirally-coupled core fibers and photonic bandgap fibers. However, these designs and their applications concentrate on scaling of the effective mode area with the goal of, for example, improving single mode guidance with lower non-linear effects and a higher damage threshold. Further development is needed to be able to use these fiber designs in current high power fiber lasers systems; however, such fiber designs will be critical for further power scaling of fiber lasers (Dong, 2015).

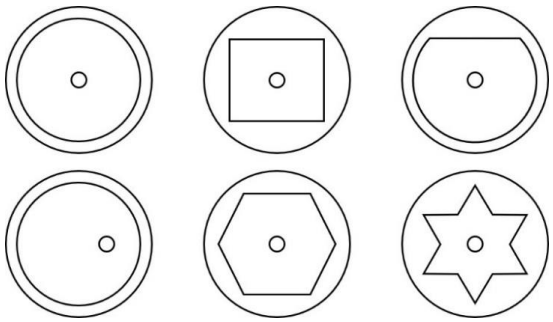

Figure 2.5: Cross sections of non-symmetric cladding structures to improve overlapping of pump light with the core, based on Snitzer (1988), Grubb (2000), Kouznetzov (2002b).

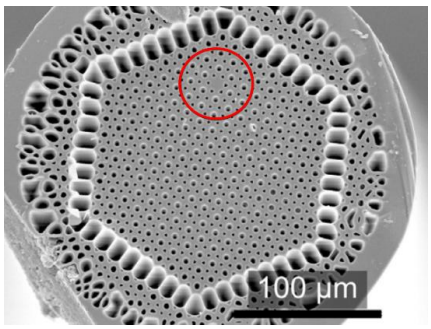

Figure 2.6: Scanning electron microscope (SEM) cross section of a PCF with air holes around the core (circled in red) and air cladding on the boundary between the inner and outer cladding (Wadsworth, 2003).

2.1.2 Cavity design

The cavity design of a fiber laser system for high power applications is typically based on either fiber-Bragg-gratings (FBG) or bulk optics such as lenses to form the beam or mirrors that act as reflectors. FBG are a periodic perturbation of the refractive index and are inscribed into the fiber core. They act as a wavelength specific optical filter and reflect or pass selected wavelengths. The pump light can be coupled into the cavity at the end of the fiber through the FBG or between the ends of the fiber, Figure 2.7 left (Archambault, 1997), (Giles, 1997), (Hill, 1997). A bulk mirror cavity comprises, for example, high reflectivity mirrors and low reflectivity output couplers in combination with lenses and dichroitic mirrors to couple the pump light into the cavity, Figure 2.7 right (Jeong 2004), (Boullet, 2008), (Wirth, 2011). Bulk mirror elements need to be properly aligned and the fiber end facets prepared with anti-reflective coatings or angle polishing to reduce the effective feedback Fresnel reflection and to prevent damage to optical components and the fiber itself (Wang, 2007).

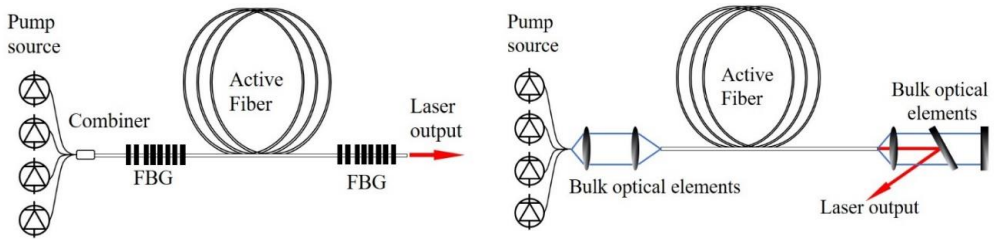

Figure 2.7: Fiber laser cavity with end-pumped design using fiber Bragg gratings (FBG), left and bulk optical elements, right, based on Giles (1997) and Boullet (2008).

Different aggregation or pumping schemes exist to deliver the pump light to the cavity and couple it into the cladding pumped optical fiber. Bulk optics can also be used as well as so-called combiners or a combination of both approaches (Fan, 1990), (Liu, 2004), (Calles-Arriaga, 2008). Combiners are designed to combine the output from one or several fiber-coupled pump diodes into the inner cladding of the double clad fiber. In general, two methods of coupling the pump light into the optical fiber can be distinguished, side pumping and end pumping, see Figure 2.8, (DiGiovanni, 1999), (Noordegraaf, 2012), (Stachowiak, 2018). To keep the benefit of the high initial efficiency and brightness of the diode pump source, a combination of both pumping schemes can be employed, in two steps, for high power fiber laser systems. The pump light from several diode stacks or single emitter diodes is collected in the first step and in a second step is fed into a tapered multi-fiber bundle, Figure 2.9, (Krummrich, 2014), (Zervas, 2014).

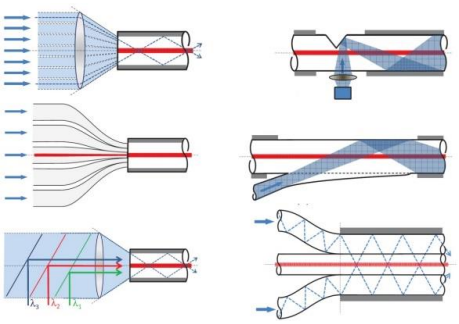

Figure 2.8: Schemes for cladding pumping, end pumping (left side) and side pumping (right side), (Zervas, 2014).

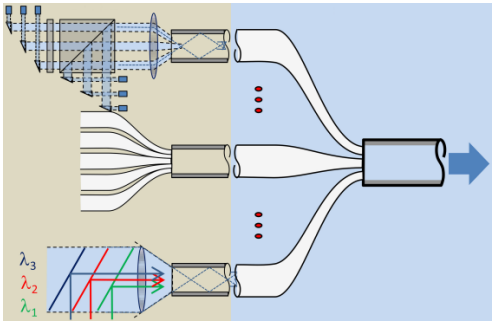

Figure 2.9: Combination of cladding pumping schemes for high power fiber laser systems, step 1 (left side) and step 2 (right side), (Zervas 2014).

2.1.3 Pump sources

The most common pump sources are diode lasers as they possess the highest wall plug efficiency, are available in different configurations, and provide output in a wide optical spectrum from UV radiation to the mid-infrared range (Fan 1988), (Röhner, 2013), (Midilli, 2017). To pump high power fiber lasers, either diode bars or stacks and a broad-area single emitter can be employed. The advantage of bars and stacks is the high power-to-package volume provided; however, they have a low brightness and thus require a complicated optical arrangement for the pump light to be coupled into the optical fiber. Furthermore, because of the high thermal load produced within a small volume of bars and stacks, the technical demands for cooling are very high. Broad-area single emitters, in comparison, have a high brightness but lower power and thus thermal management is much simpler (Leers, 2008), (Richardson 2010), (Träger, 2012), (Abed, 2015).

Other pump sources can be thin disk lasers or other fiber lasers. If the fiber laser is pumped with a high brightness beam source, an even higher beam quality in the diffraction limited regime can be achieved. In this case, the fiber laser is merely a converter to enhance the brightness of the pump beam (Popp, 2010).

2.1.4 Power scaling

Power scaling of fiber lasers has several limiting effects that need to be considered when increasing the output power of fiber laser systems. While the development of improved fibers, optical components and pump sources to increase the output power is a limiting

factor, non-linear optical effects, transverse mode instability (Jauregui, 2016) and thermal limitations (Codemard, 2009) also need to be considered (Dawson, 2008), (Zervas 2014), (Dragic, 2018).

Non-linear effects are linked to energy transfer in unwanted spectral regions. Specifically, long fiber lengths with the light confined and propagating in the core lead to non-linear effects even at modest laser powers. The effects with greatest impact are stimulated Raman scattering (SRS) and stimulated Brillouin scattering (SBS). Furthermore, because of the optical Kerr effect, self-focusing, four wave mixing (FWM) and self-phase modulation (SPM) occur as unwanted non-linear effects.

SRS and SBS arise from inelastic scattering processes involving acousto-optic interaction. SRS is the interaction of light with vibrations of the glass lattice, where above a certain threshold of ~13 THz part of the radiation energy is transferred as excited vibrational modes into the silica base of the fiber. SRS acts on broadband signals and the scattered light can propagate in the core in both directions and destabilize the laser cavity which limits the maximum output power. These two interactions constrain cw-fiber lasers in particular (Smith, 1972), (Jauregui, 2013). Strategies to minimize SRS are, for example, to inscribe long-period FBG to attenuate the scattered beam (Nodop, 2010), the use of special fibers with wavelength-selective transmission to prevent the propagation of radiation with the scattered light in the core (Kim, 2006), (Alkeskjold, 2009) or the use of shorter fiber lengths, which is a technique applied for high peak pulsed lasers (Morasse, 2013).

SBS is the interaction of light with acoustic waves propagating in the fiber. The power threshold at which the lasing energy is transferred to a down-shifted laser beam is around 11 GHz. This down-shifted beam propagates in the opposite direction to the lasing energy and can thus cause catastrophic effects. The scattered beam propagating backwards can break up the original pulse and produce high peak power sub-pulses that can cause optical damage and catastrophic fiber failure (Stiller, 2012), (Jauregi, 2013), (Zervas 2014). Techniques to minimize SBS include, for example, increasing the mode area by using fiber with an appropriate NA (Taverner, 1997) and the use of fibers that reduce the overlap between the light and the acoustic modes (Li, 2007) or are highly doped to absorb the pump light in a short length (Dajani, 2010).

Research is being undertaken to further improve the power scalability and also to enhance the reliability and robustness of laser systems. For example, by optimizing the fiber design and use of dopants, improving the methods of pumping the laser or minimizing non-linear effects as described above.

In development of new fibers, nanoparticle-doping is one area of current research interest. Rare-earth ions, which are currently incorporated directly into the glass matrix, may also be incorporated into nanoparticles, which are then doped into the glass matrix. Thus, improved performance can be achieved by adjustment of the distribution of the rare-earth ions and the chemical environment (Baker, 2017). By developing a direct nanoparticle

deposition method that maximizes the physical separation of the Yb atoms it was possible to reduce deleterious optical effects such as photodarkening and increase the efficiency of the laser operation (Tammeta, 2006). Other research, for example, investigated the introduction of heavy metal ions into the glass matrix with the aim of reducing the phonon energy while still enabling a relatively low NA in the fiber core (Lezal, 2001), (Vermillac, 2017).

Improvement in pumping of the fiber laser can be achieved by employing the tandem pumping method. Yb-doped fiber lasers are usually pumped at around 900 nm, where high power laser diodes are available and the absorption maximum of the pump energy is achieved. However, the output power is limited by non-linear effects or detrimental thermal and optical effects in the fiber. To increase further the power output of a fiber laser, the brightness of the pump source needs to be increased. Consequently, disk or fiber lasers emitting at around 1000 nm, are used as the initial pump source. Even though at this wavelength the absorption rate of the pump light in the core is up to 10 times lower, the brightness of the output beam can be up to 100 times higher. (Codemards, 2009), (Xiao, 2015), (Zhou, 2017). Using this approach, losses arising from the quantum defect can be reduced and a shorter fiber length can be used, thus minimizing thermal and non-linear effects. High power fiber lasers with near diffraction-limited output in the range of several kW of laser power are possible (Hecht, 2018).

2.1.5 High power fiber laser systems for industrial applications

From the above description of the physical principles of fiber lasers, it can be seen that several physical attributes distinguish high power fiber lasers from other types of lasers. The design of the fiber laser allows a controlled spatial distribution of the laser beam in the active fiber, enabling high beam qualities with low transmission losses, which results in high efficiency. The fiber itself has a large heat-dissipating surface which allows effective thermal management. The power scalability of fiber lasers has surpassed 100 kW of output power for cw-multimode fiber laser systems and the 10 kW limit for cw-single mode fiber lasers, Figure 2.10, (Hecht, 2018). Comparing the basic properties of different laser sources for materials processing purposes, fiber lasers outperform gas lasers and other solid state lasers in wall plug efficiency, expected lifetime and maintenance requirements, Table 2.1, (Olsen, 2009), (Shiner, 2010) (Beyer, 2012), (Shi, 2014), (Zervas, 2014).

Since becoming commercially available in the beginning of the 1990s, the output power and brightness of fiber lasers have increased continuously and high power fiber laser systems have become the first choice for material processing applications (Shiner, 2006), (Shiner, 2016). Fiber lasers have increased their market share and they are slowly replacing the more established CO_2 (carbon dioxide laser) laser (Overton, 2013), (Overton, 2019). Figure 2.11 gives an overview of the global market share of lasers for materials processing in 2018, (Mayer, 2019).

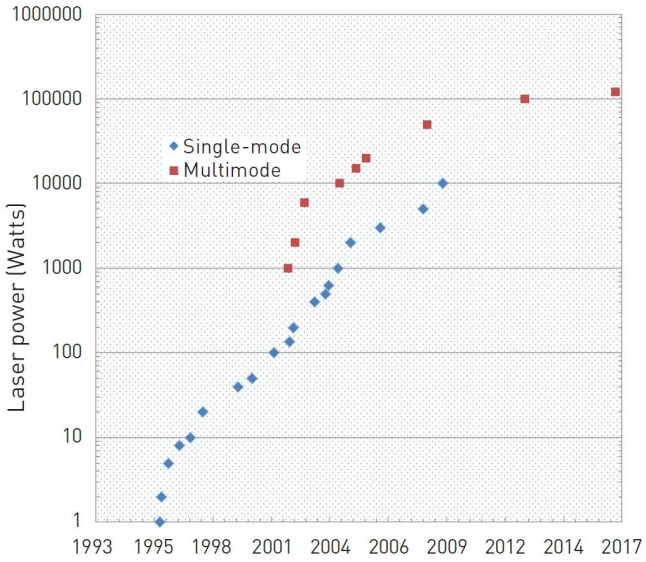

Figure 2.10: Growth in laser power of commercial fiber lasers from IPG Laser (Hecht, 2018).

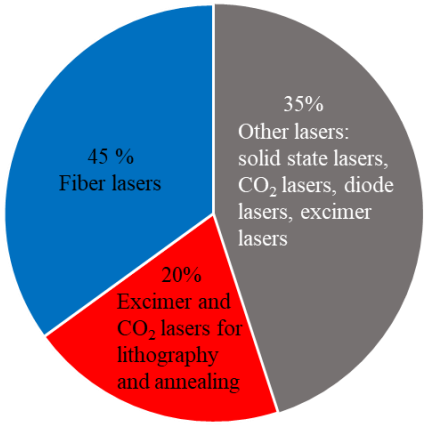

Figure 2.11: Global market share for lasers for materials processing in 2018 (Mayer, 2019).

Table 2.1: Comparison of basic properties for laser sources used for material processing (Olsen, 2009), (Zervas, 2014), (Rominger, 2015) (IPG-Photonics, 2018), (Laserline, 2019), (Trumpf, 2019).

		Fiber laser	CO_2 laser	Disc laser	Nd:YAG laser (diode pumped)	Diode laser
Lasing medium		Doped fiber	Gas mixture	Crystalline disc	Crystalline rod	Semi-conductor
Emitted wavelength	[µm]	1.07	10.6	1.03	1.06	0.808-0.98
Power efficiency	[%]	> 40	10-15	20-30	10-30	> 40
Max. output power	[kW]	> 100	20	> 20	6	45
BPP at 4 kW	[mm mrad]	0.35	4	1	12	30
M^2		1.1	1.2	1.4	35	100
Mobility		High	Low	Medium	Low	High
Maintenance interval	[h]	> 30,000	1,000	> 25,000	10,00	> 25,000
Lifetime	[h]	100,000	20,000	20,000	20,000	> 25,000

2.2 Laser beam welding processes

Laser beam welding is a fusion welding technique that utilizes the electromagnetic radiation of a laser beam to transfer energy onto the surface of a given metallic material or substrate. In general, two processes can be distinguished: heat conduction welding and keyhole welding. Keyhole welding without the use of any filler materials is a so-called autogenous laser welding process. Keyhole welding in combination with a gas metal arc welding (GMAW) process is called laser arc hybrid welding. Both processes will be reviewed further in the following chapters.

2.2.1 Interaction of laser beam radiation and material

In laser materials processing, the required energy in the form of heat for the welding process is supplied by the radiation energy of the laser beam. Using optical elements, the laser beam is focused as a small spot on the material surface, the energy is absorbed by the material and converted into heat. The temperature on the surface can be determined based on the balance of released energy and absorbed energy, which defines the resulting thermal mechanisms. Thus, the effect of the laser beam radiation is determined by the absorbed energy, the interaction time with the workpiece, and the geometrical and material properties of the workpiece. The power density E on the workpiece surface is calculated with the beam power P and the laser beam radius r_b as:

$$E = \frac{P}{\pi r_b^2}. \tag{2.7}$$

Power density can be used to determine the principal physical mechanism of the interaction with the material, see Figure 2.12. At power densities lower than 10^3 W/cm^2 to 10^4 W/cm^2, radial heat conduction will dominate. In this range, significant heating of the workpiece takes place while the temperature remains below the melting point of the material. When increasing the power density to the order of 10^5 W/cm^2, by raising the laser power or reducing the radius of the laser beam, the melting point in the zone of interaction is reached, which leads to the generation of a melt pool. This state satisfies the conditions for heat conduction welding. When the power density is between 10^5 W/cm^2 and 10^6 W/cm^2, the vaporisation temperature is reached and a cavity, called a keyhole is generated in the workpiece. Heat conduction ensures that there is sufficient melting of the walls of the keyhole to enable a weld to be made. Intensifying the power density further to around 10^7 W/cm^2 to 10^8 W/cm^2 increases the vaporisation rate in the keyhole. This can lead to high pressure in the interaction zone which, consequently, rapidly expels liquid melt and increases the generation of plasma and metal vapour. Both the plasma and metal vapour can be ionised, which absorbs the laser beam energy to a great extent and impairs energy transfer into the workpiece. Figure 2.13 gives an overview of the power densities and interaction times applicable for the most important laser processes (Kroos, 1993), (Steen, 2003), (Ion, 2005), (Olsen, 2009).

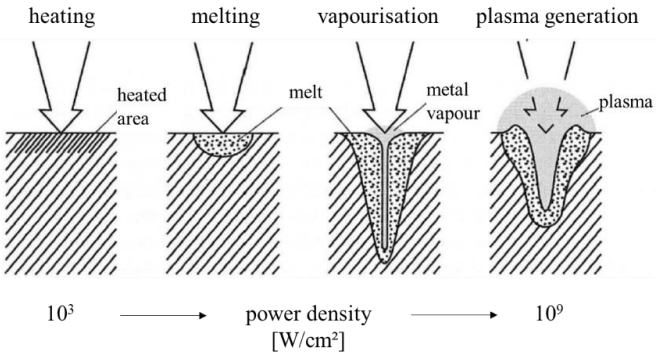

Figure 2.12: Laser material interaction at increasing power density and principal physical principles of material interaction, based on Kroos (1993).

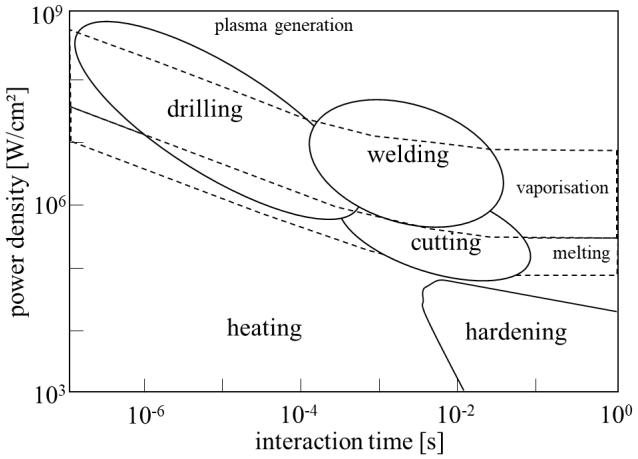

Figure 2.13: Range of laser processes mapped against power density and interaction time for metallic materials, based on Steen (2003), Ion (2005) and Hügel (2009).

When the laser beam radiation delivers sufficient energy onto the surface of the workpiece to first start melting and then vaporising the material, the recoil force of vaporisation from the liquid surface expels the melt and forms a cavity. Once this cavity is deep enough the laser beam radiation is reflected from the cavity wall. This causes a sudden increase of the vaporisation process which leads to further deepening of the cavity until a stationary keyhole is formed. The actual welding process is performed by moving the keyhole relative to the workpiece. Liquid material is generated at the front side of the keyhole, flows around it, solidifies behind the keyhole and produces a deep and narrow weld with

a high aspect or depth to width ratio, Figure 2.14, (Beyer, 1995), (Ion, 2005), (Poprawe, 2005), (Hügel, 2009).

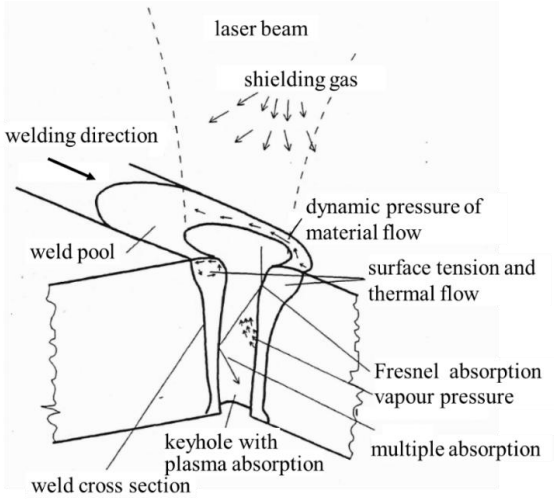

Figure 2.14: Principal physical mechanisms in the keyhole, based on Kaplan (1994).

The most important physical processes for the absorption of energy in the keyhole and for maintaining the equilibrium between opening and closing forces are (Kroos,1993), (Kaplan, 1994) (Beck, 1996):

- Fresnel absorption, which describes the angular dependent absorption of laser beam radiation on the wall of the keyhole. It is guided through the keyhole to the base of the keyhole or, in the case of full penetration reflected out at the bottom side of the keyhole.
- Absorption by multiple reflections on the keyhole wall, which increases the absorption rate, especially in the formation phase of the keyhole.
- Plasma absorption by inverse Bremsstrahlung, which is the transfer of energy from photons to electrons. The incident radiation into the keyhole is partly absorbed by the plasma in and above the keyhole. The absorbed energy is conducted into the melt pool.
- Recoil pressure created by the vaporisation process, which accelerates vapour particles desorbed from the condensed phase to the keyhole wall and thus keeps the keyhole open.
- Surface tension pressure, which is dependent on the material properties and tries to close the keyhole.

- Hydrodynamic pressure, which is proportional to the density of the melt, the depth of the keyhole and gravity. It acts to close the keyhole.
- Dynamic pressure of material flow around the keyhole, which creates a higher pressure at the front of the keyhole and a lower pressure at the back.

By determining the single forces of the pressure balance, it can be calculated that recoil pressure and pressure from surface tension are of equal value. The hydrostatic pressure is negligible and the dynamic pressure of the material flow around the keyhole gains significance only at very high welding speeds.

2.2.2 Autogenous laser welding and laser hybrid welding

Autogenous or keyhole welding is the dominant welding process in laser welding applications as it can produce a deep and narrow weld at higher welding speeds than conventional arc welding processes such as GMAW or even submerged arc welding (SAW). With the high power density of a focused laser beam, the required energy can be directed precisely onto the fusion zone. The heat conduction losses are smaller and the thermal load of the workpiece is decreased (Katayama, 2013). High power solid state lasers, especially fiber lasers, continuously increased their share in material processing since the beginning of the 1990s, benefiting from a higher beam quality and a shorter wavelength compared with CO_2 lasers (Hügel, 2000). The shorter wavelength allows a higher absorptivity in metals (Dausinger, 1995) and a lower sensitivity to laser induced plasmas (Shcheglov, 2012). These two effects result in a wider processing window (Vollertsen, 2009), increased process stability (Quintino, 2007) and better weld quality (Kawahito, 2007).

The combination of an autogenous laser welding process with a GMAW process is called laser arc hybrid welding and will be referred to as laser hybrid welding in this work. The development of laser hybrid welding started in the late 1970s with the idea of Steen and Eboo to utilize a laser beam and an electric arc in the same processing zone (Eboo, 1978), (Steen, 1979), (Steen, 1980). In this common zone of interaction both processes share and contribute to a variety of parameters. These parameters can be grouped into parameters for the combined laser hybrid process with sub-processes for the laser beam and the arc, material parameters and design parameters, as shown in Figure 2.15 (Olsen, 2009). The characteristic properties of the laser hybrid welding process arise from the benefits and limitations of both individual processes (Victor, 2011), (Unt, 2018). Table 2.2 compares the advantages and disadvantages of autogenous laser and laser hybrid welding as regards the welding process, and also considers economic aspects.

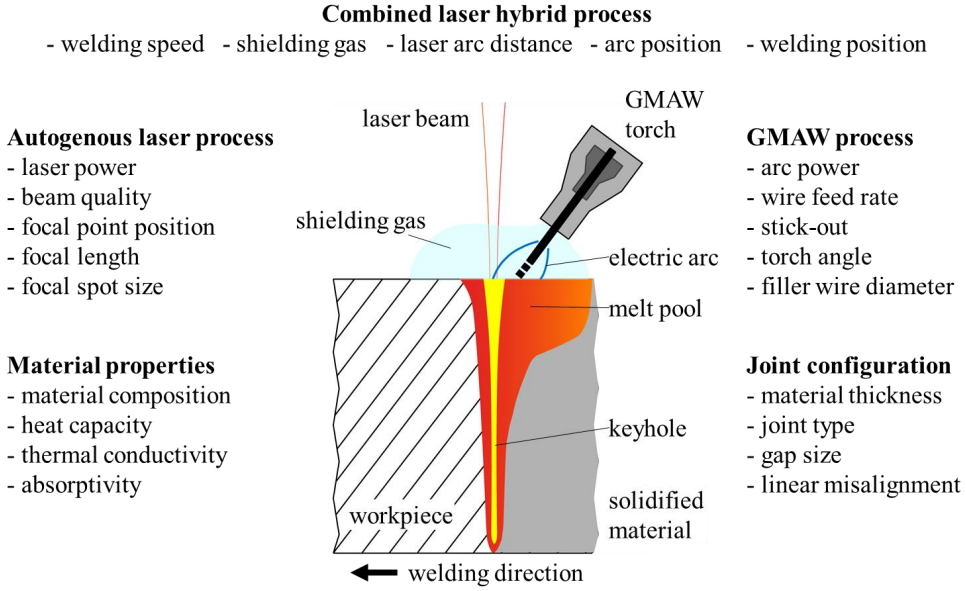

Figure 2.15: Schematic drawing of a hybrid welding process with full penetration and an overview of principle parameters, based on Olsen (2009).

Table 2.2: Comparison of advantages and disadvantages of autogenous laser welding and laser hybrid welding as regards the welding process and economic aspects.

Advantages	Disadvantages
Autogenous laser welding	
– High power density provides deep penetration and narrow welds at high welding speeds – Lower heat input with less distortion – All welding positions possible	– Precise preparation of workpieces and alignment required – Fast cooling cycles may result in brittle microstructure and formation of hot cracks
Laser Hybrid welding	
– Greater tolerance to joint gaps and joint preparation – Provision of filler metal allows control of mechanical and metallurgical properties – Increased energy utilization from laser radiation into the material	– Complex process with larger number of process parameters – Higher cost for filler material, shielding gas, equipment and maintenance

Laser hybrid welding has been intensively studied for scientific purposes and, as a result of international research and development activities, the technique is now utilized in many different industrial applications. Numerous publications on the topic can be found in scientific journals as research articles, review papers, books and book contributions. These publications present, in comprehensive detail, descriptions of laser hybrid welding processes, process parameters and their effects on the welding process and the resulting welds, available welding systems, and applications for welding, see Table 2.3.

Table 2.3: Overview of publications reviewing laser hybrid welding processes, parameters and applications.

Seyffarth et. al	2002	Book about processes and applications in welding and material treatment such as development of combined laser arc processes for joining of different materials, laser beam arc plasma interaction and combined discharge, integrated plasma torches for laser arc processes and practical applications.
Shelyagin et. al	2002	Review article on scientific publications on hybrid and combined laser arc processes.
Bagger et. al	2005	Review article of fundamental phenomena in laser arc interaction, on governing process parameters, and examples of industrial applications.
F. O. Olsen	2009	Book summarising research on laser hybrid welding processes and its applications such as fundamental characteristics on plasma interaction, dynamics and stability of the weld pool, effect of shielding gases and joint properties, quality control and weld quality assessment, heat sources for hybrid welding processes and applications for shipbuilding, magnesium and aluminium alloys and steels.
Hübner et. al	2010	Review article of laser hybrid welding with different arc sources for practical applications.
Casalino et. al	2010	Book chapter reviewing laser hybrid welding processes for different materials such as stainless steels, mild steels, and aluminium and magnesium alloys with a focus on the process parameters of welding speed, shielding gas and laser arc distance.
Victor et. al	2011	Review article of laser hybrid welding processes summarising the modes of operation and giving a detailed overview of the influence of process parameters such as welding speed, laser

		power, laser arc distance, arc orientation, shielding gas, wire feed rate and arc current and voltage, as well as joint design with gap size and joint mismatch.
P. Kah	2012	Review article comparing autogenous laser welding processes and conventional arc welding processes with laser hybrid welding processes describing the combination of different types of lasers with arc welding sources.
S. Katayama	2013	Book chapters on topics related to laser hybrid welding and combined laser beam technologies, with a focus on thick section materials, including modelling and simulation of autogenous laser and hybrid laser welding.
B. Acherjee	2018	Review article on laser hybrid arc welding systems with GMAW, gas tungsten arc welding (GTAW) and plasma arc welding (PAW) sources and their arrangements relative to the laser source. Discussion of the influence of parameters such as laser power, welding speed, relative position of the laser beam and arc electrode, focal point position, electrode angle, shielding gas composition, modulation of the arc welding system, wire feed rate, joint gap and joint configuration on the hybrid welding process. Description of the performance characteristics and weld quality and industrial applications.

2.3 Overview of welding of thick section material

This chapter reviews scientific applications of thick section welding of steel materials with high power lasers. The focus is on solid state lasers and fiber lasers, and the chapter includes comparison with CO_2 lasers where appropriate. An overview is given of process parameters and their influence on autogenous and laser hybrid welding, single-pass and multi-pass welding techniques, joint configurations and, different variations of arc and laser sources.

2.3.1 Influence of process parameters on weld quality

High power CO_2 lasers have shown their application potential for joining thick plates (Petring, 2007), (Nielsen, 2001). The effects of the laser power on the process and process parameters during deep penetration welding have been reported, for example by Goussian (1997) and Kawaguchi (2006). Following the commercial introduction of high power fiber laser systems, welding of thick section material with autogenous and laser hybrid welding processes has become a topic of research interest. The available laser power for research activities has increased steadily since the beginning of the year 2000, starting from 8 kW to 17 kW (Vollertsen, 2005) to over 30 kW (Kessler, 2010) and up to 100 kW (Katayama, 2015). The main issues considered in this research are the effect of increasing laser power on the penetration depth and the mutual dependence of welding speed and laser power independent of the welding system set up or the material welded. As well as laser power and welding speed as the main influencing parameters on the penetration depth, the focal point position also has an influence in welding of thick section material. Using 10 kW of laser power and an autogenous laser welding process it has been shown that the deepest penetration is achieved with a focal point position on or beneath the surface of the workpiece (Thomy, 2006), (Katayama, 2010), (Vänskä, 2014). Experimental data from El Rayes (2004) and Kawaguchi (2006) support these findings for CO_2 lasers.

Reducing the ambient pressure for the welding process from 1 bar to vacuum conditions significantly increased the penetration depth at low welding speeds between 0.3 m/min and 1 m/min (Katayama, 2011). Another effect of reduced ambient pressure is a change of the appearance of the weld to a very parallel and thin shaped form (Jiang, 2019).

The influence of surface roughness on the penetration depth and weld quality was studied for welding of thick section materials with autogenous laser welding (Sokolov, 2012) and laser hybrid welding (Farrokhi, 2016) using between 10 kW and 15 kW laser power. The results indicated that an increased surface roughness level on the joining edge up to R_a 6.3 µm positively influenced the penetration depth for autogenous laser welding. In laser hybrid welding experiments, it was demonstrated that a higher surface roughness benefits full penetration and improves the weld quality. Both studies also reported a positive

influence of a small gap between 0.05 mm and 0.5 mm on the penetration depth and the quality of the weld.

A general investigation of the quality of 20 mm and 25 mm thick samples welded as I-butt joints with up to 30 kW of laser power following the requirements of standard EN ISO 13919-1 is presented by Sokolov (2011). To fully penetrate the given material thickness of 20 mm, the focal point position was set to -7.5 mm at 15 kW and further decreased to -15 mm at higher laser powers and 25 mm thickness. Acceptable weld qualities were achieved at welding speeds between 1.8 m/min and 2.4 m/min.

To establish a suitable parameter window for thick section welding of stainless steel with an autogenous laser welding process using a 10 kW laser source, parameters such as welding position, beam incident angle, welding speed and the use of a gas jet were examined and tested for a maximum plate thickness of 15 mm by Zhang (2018). As regards the weld quality, the most influential parameters were the welding position and beam incident angle. Welding in PC (horizontal) position supported the melt pool against gravitational effects and reduced root sagging. Changing the incident angle of the laser beam by 10° reduced spatter and produced a smoother weld seam. It was also found that variation of the gas jet influenced penetration depth and weld appearance. Similar findings were made in work, investigating a variety of gas nozzles to suppress the vapour plume in a laser hybrid process with a Nd:YAG laser source when welding 12 mm and 15 mm thick plates (Fuhrmann, 2007). The process stability and consequently the weld result improved significantly when the vapour plume was successfully suppressed.

Further investigations on the stability of a laser hybrid welding process used in thick section welding of I-butt and V-butt joints were carried out with a 15 kW fiber laser source by Bunaziv (2018). A pulsed arc and cold metal transfer (CMT) arc were applied to weld the two different joint types. The position of the arc relative to the laser beam and the welding speed chosen had the greatest influence on the stability of the process and the weld quality, especially the generation of pores in the weld. The effect of the joint preparation on the process stability was negligible.

Another aspect impacting the weld quality is the distortion of the welded sample or overall structure. In a test series with a laser hybrid welding process, the influence of a leading and trailing arc on the angular distortion was measured (Cao, 2011). A 5 kW fiber laser, using its maximum power, was employed at a welding speed of 1.5 m/min to fully penetrate 9.5 mm thick material in a single pass. The angular distortion measured was least for the process with a trailing arc at 0.22° and highest for a leading arc with 0.44°. A sample welded with a GMAW process in three passes was produced for comparison purposes and showed an angular distortion of more than 2.44°.

2.3.2 Single-pass welding

Welding thick section material in a single pass is the most economic joining method. It is suitable for I-butt joints and does not require additional welding passes, which increase production time and material cost (Nielsen, 2015). Producing a fully penetrated weld with a sound root and acceptable quality is the goal for every welding task. Thicker materials require good control of the welding process because the volume of liquid in the melt pool is greater, which can lead to sagging of the melt or droplet formation on the root side (Frostevarg, 2015). Increasing the welding speed is one feasible option for achieving the required penetration, should sufficient laser power be available (Bachmann, 2016), (Kawahito, 2018). Other methods to control the welding process and stabilize the root formation are the use of root support or a backing made from ceramic (Farrokhi, 2017) or a bed of flux powder (Seffer, 2012), (Wahba, 2016).

A technique to directly influence the root formation is the use of an electromagnetic field to counteract the hydrostatic pressure of the molten material on the root side (Fritzsche, 2016), (Üstündag, 2018). In experimental investigations, it was shown that using a laser hybrid process with 19 kW of laser power, up to 28 mm thick material could be welded at low welding speeds down to 0.5 m/min. With the right choice of parameters and good process control, acceptable welds for single pass welding can be achieved without supporting techniques. This was shown, for example, for welding 13.5 mm thick duplex stainless steel plates with a laser hybrid welding process using 2.2 m/min welding speed and 14 kW of laser power (Westin, 2011).

2.3.3 Multi-pass welding

In contrast to single-pass welding, multi-pass welding requires several passes to join the workpiece. The face or height of the so-called root pass, the first pass to be welded can be prepared according to the selected welding process and the parameter set most suitable for producing an acceptable weld. However, the preparation of the joint configuration involves an additional step in the production process. Common to all approaches applying multi-pass welding is to choose the root face as high as possible to reduce the number of fill passes. The preparation of the groove differs depending on the plate thickness, welding process and access strategy of the joint. Research with autogenous laser welding and laser hybrid welding processes has examined, for example, the effect of the groove geometry (Coste, 2001b), (Li, 2014), (Guo, 2016), the angle of filler metal feed into the groove (Jokinen, 2003) and the focal length (Coste, 2001a) on the weld result and the number of fill passes needed. Double-sided access with different joint geometries has been investigated with the aim of reducing the number of fill passes and improving the mechanical properties of the weld (Gook, 2014), and increasing the maximum weldable thickness from 30 mm to 50 mm (Tarasawa, 2010).

2.3.4 Variation of joint configuration and welding position

The joint configuration and welding position are determined by the welding task and the manufacturing process. In investigation of welding of T-joint configurations with autogenous laser welding and laser hybrid welding, test series has been carried out to study the effects of different parameters on the welding results. Butthoff (2002) investigated the general feasibility of welding T-joints with a laser hybrid welding process. It was shown that 10 mm thick fillet joints could be successfully welded from both sides using a 4.4 kW Nd:YAG laser. Unt (2015) examined the geometry of 8 mm thick T-joints when the inclination angle, welding position and heat input was varied. The results showed that the inclination angle had the greatest impact on the penetration depth for laser hybrid welding and autogenous laser welding with a 10 kW fiber laser source.

For I-butt joints, edge misalignment on the top side of the workpiece was successfully bridged with a laser hybrid welding process in PA (flat) position. Experiments in PB (horizontal vertical) position showed that the deviation of the solidified material on the top side was more pronounced at higher welding speeds (Petronis, 2017). Similar experiments were carried out by welding 16 mm thick stainless steel in PB position with a laser hybrid welding process and a 10 kW fiber laser (Sun, 2017). Joint preparation helped to achieve full penetration at sufficiently high welding speeds of around 2 m/min and maintain control of the melt pool. Without joint preparation, the welding speed of samples welded as a regular I-butt joint was reduced to 0.8 m/min. Full penetration could be achieved and sagging of the melt was avoided.

All position welding with a 10 kW fiber laser as an autogenous laser welding process was demonstrated for 11 mm thick material (Thomy, 2006). A welding speed of 2.2 m/min was required in all positions to control the melt pool and achieve a weld with acceptable quality that did not indicate sagging on the top or root side. An experimental test series with a practical background investigated the weldability of three different joint types for application in offshore steel foundations (Kristiansen, 2017). Laser hybrid welding and autogenous laser welding with a 16 kW disk laser was applied to weld 16 mm I-butt-joints and lap joints in PA, PF (vertical up) and PG (vertical down) positions. The results showed that adequate penetration depth of up to 23 mm was achieved in PA position for both joint types. Controlling the melt pool in vertical positions required higher welding speeds and a lower heat input. Welding vertical down with a trailing arc turned out to be more stable than vertical up.

2.3.5 Pipe welding

Large diameter pipes with high wall thicknesses are welded, for example, in the oil and gas industry, where pipes need to withstand pressures of more than a hundred bar (Spinelli, 2012). Autogenous laser welding and laser hybrid welding processes have the potential to reduce the number of passes required to join thick sections and increase the

welding speed (Reutzel, 2006), (Komizo, 2008). Table 2.4 gives a comparison of three welding processes, shielded metal arc welding (SMAW) as a manual process, tandem GMAW and laser hybrid welding. Laser hybrid welding has better performance than the other two processes in all three studies categories: filler metal consumption, weld time and energy consumption in welding of a 40" diameter pipe with 20 mm wall thickness.

Table 2.4: Comparison of welding processes when joining a 40" diameter pipe with 20 mm wall thickness (Gumenyuk, 2010).

Welding process	Filler metal consumption [kg]	Welding time [min]	Wall plug energy consumption [kWh]
Manual SMAW	780	190	30
Tandem GMAW	200	12	2.7
Laser hybrid	50	1.5	2.2

As part of efforts to realize the potential of laser hybrid welding and autogenous laser welding for joining thick section pipe material, much scientific research has been undertaken in the areas of process development and characterisation of mechanical properties. A number of general parameter studies investigating the joining of pipeline steels and testing the applicability of fiber lasers and Nd:YAG lasers for autogenous laser welding and laser hybrid welding have been carried out for single passes and multiple passes. The overall conclusion of these studies was that laser welding processes using an Nd:YAG laser are suitable for joining pipeline steel grades. However, the mechanical properties of the welded samples did not meet the acceptance criteria (Moore, 2004a), although they can be significantly improved by using suitable process parameters and selecting appropriate filter metals (Moore, 2004b). A comparison with CO_2 laser welding results showed that deeper penetration and higher welding speeds could be achieved in pipeline steels with similar laser powers (Howse, 2005), (Vollertsen, 2005).

A multi-pass welding approach where the root pass is joined with a laser-based process and the remaining groove is filled with conventional GMAW processes has been reported to increase productivity of the pipeline construction (Yapp, 2004), (Coste, 2005). Based on the multi-pass approach a girth welding process using a laser hybrid welding process to join the root face and a high deposition GMAW process for the fill passes has been developed in cooperation with an industrial partner (Yapp, 2010). Further investigations in orbital welding were carried out focusing on the use of fiber lasers for the welding task. Technical equipment was designed and tested especially for laser hybrid welding processes (Gook, 2009), (Vänskä, 2011), (Turichin, 2014). The common challenge independent of the laser power used or material thickness welded, is controlling the effect of gravity in the different welding positions, especially for the GMAW dominated part in the melt pool.

2.3.6 Welding for shipbuilding applications

Laser based welding processes are already established in several shipyards around the world (Olsen, 2009), (Turichin, 2017). The main benefits for industrial implementations are the high welding speed and lower heat input, which reduces distortion compared with conventional GMAW processes (Lezzi, 2013). Laser hybrid welding is the preferred process to join, for example, flat panels, sandwich panels or stiffeners in T-joint and I-butt joint configurations (Lembeck, 2002), (Miebach, 2003), (Roland, 2004), (Jasnau, 2008).

Despite the widespread industrial application of laser-based welding processes, research and development activities are still ongoing. The reduction of distortion has been investigated for laser hybrid welding and SAW with the aim to further reduce the cost and increase the productivity which is of high interest for industrial applications (Kelly, 2009). Increasing the productivity by combining high deposition GMAW processes with laser beams has been studied for flat panels with a V-butt and I-butt joint (Wieschemann, 2001). Several studies have been carried out to examine the effect of process parameters of laser hybrid welding and autogenous welding on the weld quality and penetration depth of T-joint configurations, for example (Unt, 2014), (Unt, 2015), and (Turichin, 2017).

3 Experimental work

This chapter gives an overview of the experimental test series carried out in investigation of joining of thick section material with high power fiber lasers. The materials welded and the experimental setup employed are detailed at the beginning of the chapter. The process parameters used for the welding tasks are then described, followed by an overview of the key parameters. Mechanical tests to characterise the welded samples and assess the weld quality are listed at the end of the chapter.

3.1 Material

Five different steel grades as flat plates with thicknesses ranging from 8 mm to 30 mm were used for the welding experiments. The chemical compositions are given in Table 3.1. Two pipe steel grades X65 and X70 with a high yield strength of at least 460 MPa and a high impact toughness of at least 450 J at -40°C were used for single-pass and multi-pass welding and the shipbuilding steel AH36 with a minimum yield strength of 355 MPa was examined for T-joint welding. One fine-grained steel S355MC with a minimum yield strength of 355 MPa and one structural steel S235J2C with a minimum yield strength of 235 MPa were welded with an oscillated laser beam.

Table 3.1: Chemical composition of the materials in (wt %) and plate thicknesses welded.

C	Si	Mn	P	S	Al	Cr	Cu	Mo	N	Nb	Ni	Ti	V
X65, t = 9.5 mm, t = 16 mm, t = 20 mm													
0.05	0.18	1.07	0.012	0.002	0.03	0.03	0.01	-	0.006	0.057	0.02	0.002	0.035
X70, t = 14 mm													
0.083	0.228	1.73	0.013	0.003	0.049	0.031	0.047	0.002	0.005	0.051	0.055	0.005	0.082
AH36, t = 8 mm													
0.111	0.149	0.77	0.035	0.15	0.03	0.051	0.031	0.01	-	-	0.041	-	0.008
S355MC, t = 12 mm, t = 15 mm													
0.09	0.50	1.00	0.02	0.01	0.015	-	-	-	-	0.07	-	0.05	0.05
S235J2C, t = 8 mm													
0.09	0.03	1.2	0.02	0.02	-	-	-	-	-	-	-	-	-

For the laser hybrid welding process, the shielding gases were chosen in accordance with EN 439, M21 as gas mixtures with 82 % – 90 % argon and 10 % – 18% CO_2. The filler

metal for the GMAW process was a wire electrode of the type G3Si1 and G4Si1 according to EN 440. Pure argon was used as the shielding gas for the autogenous laser welding processes.

3.2 Equipment

The basic experimental set-up consisted of a welding head with collimating and focusing optics, process gas supply and fixtures for clamping down the workpiece. In addition, depending on the experiments carried out, a GMAW torch for a laser hybrid welding process or an oscillating unit were used, Figure 3.1. The welding torch was used for the laser hybrid welding experiments only. The oscillating unit was used in combination with an autogenous laser welding process. Different high power fiber laser sources were used for the experiments with output powers ranging from 8 kW to a maximum of 30 kW, see Table 3.2.

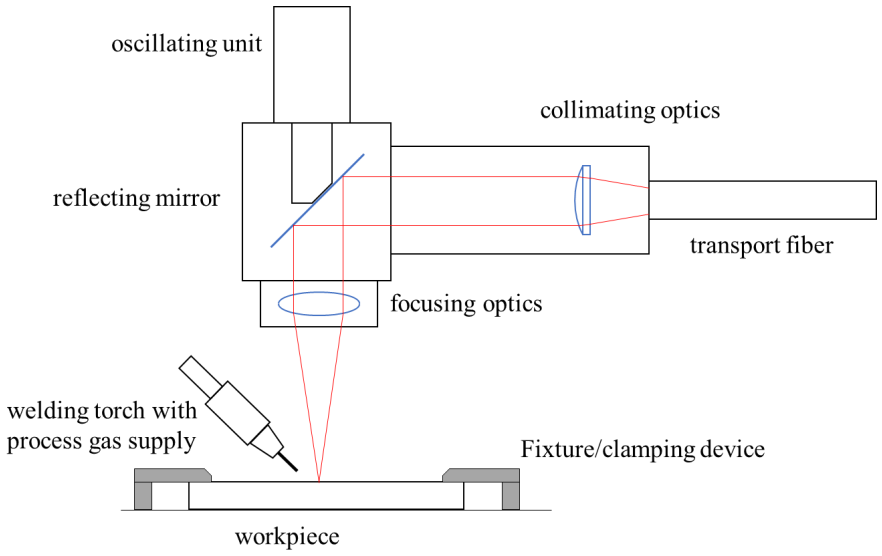

Figure 3.1: Schematic drawing of set-up used for welding experiments.

3.3 Welding processes and parameter study

To study the general applicability of laser hybrid and autogenous laser welding processes for different welding tasks, a set of experiments was carried out to investigate the process capabilities. First, the maximum weldable thickness for a given laser power with a single pass was determined by adapting the heat input and varying individual laser and arc related parameters like focal point position or wire feed speed. If the laser power was insufficient to weld a single pass, multi-pass welding was investigated as an alternative approach with the aim to reduce the number of required passes. For single-pass and multi-pass welding, different parameter sets, including I-butt and V-butt joints, were tested. The process parameter sets developed from the experiments were adapted to further determine the process boundaries when welding joints with linear misalignment and air gaps. Figure 3.2 gives an overview of the configurations with joint type and imperfections, including the welding positions tested. To complete the research on different joint types, T-joint configurations were examined for their potential to be welded with autogenous laser processes when varying the power density on the workpiece surface. The final experimental test series was carried out with an oscillated laser beam to be used for thick section welding, focusing on the effect of the oscillation frequency on the geometry of the weld. An overview of the key parameters applied in publications I – IV is given in Table 3.2.

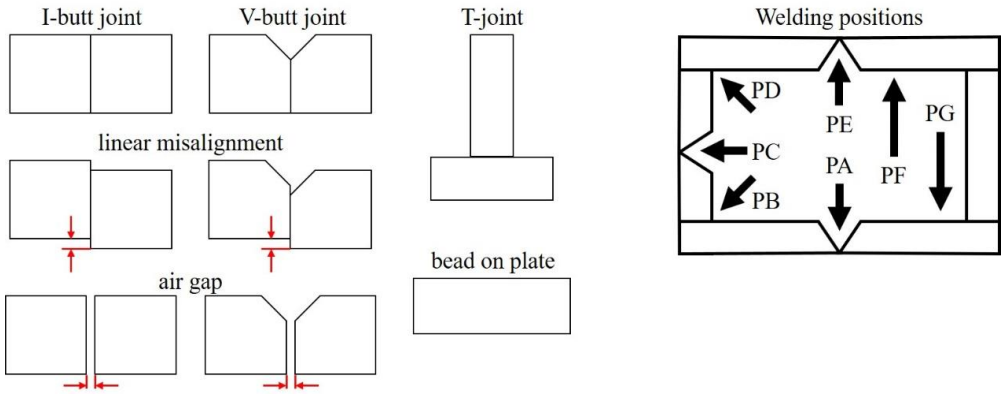

Figure 3.2: Configurations of joint types studied in combination with linear misalignment and air gaps (left) and welding positions according to EN ISO 6947 (right).

3.4 Weld assessment and characterisation

To investigate the weld quality of the produced samples, non-destructive testing by visual inspection and destructive test procedures were applied. The characterisation and assessment of the welded samples was carried according to the following testing methods:

- Visual inspection of the root and bead surface of the weld, according to EN ISO 13919.
- Preparation of the specimen according to EN ISO 17639.
- Hardness testing of the weld metal, heat affected zone (HAZ) and base metal of the prepared specimen, according to DIN EN ISO 6507-1.
- Charpy V-notch testing of cut specimens with notches in the weld metal, weld metal-HAZ 50-50 and base metal, according to EN 10045-1.
- Tensile testing according to EN 10002-1 and micro tensile testing based on a technique developed by Kocak et al. (Kocak, 1998).

Table 3.2: Overview of key parameters applied for welding experiments in publications I – V.

	Publication I	Publication II	Publication III	Publication VI	Publication V
Parameters for experimental set-up					
Laser source	YLR-8000S YLR-20000	YLR-8000S YLR-20000 YLR-30000	YLR-8000S	YLR-10000	YLR-10000
Laser power [kW]	8 – 19	8 – 30	8	6 – 10	5; 6; 8; 10
Focal length [mm]	280; 350	280; 350; 300	280	300	300
Fiber diameter [µm]	100	100; 200	100	200; 300; 600	200
Beam quality [mm mrad]	4.2; 11.5	4.2; 11.5	4.2	9.1; 12; 22.3	6.9
Oscillation frequency [Hz]	-	-	-	-	100 – 1000
Material					
Grade	X65	X65	X65; X70	AH36	S355MC S235J2C
Thickness [mm]	16	16; 20; 28	9.5; 14	8	8; 12; 15
Main process parameters					
Welding speed [m/min]	0.4** – 2.5*	0.4** – 2.2*	1 – 2	0.75 – 1.75	1; 2; 3
Wire feed speed [m/min]	6 – 18	6 – 15	6.5 – 9	-	-
GMAW heat input [kJ/cm]	1.8 – 6.4	1.8* – 12.7**	2.3* – 12.5**	-	-
Focal position [mm]	-6 – 0	-2	-2	-6 – -2	-10 – 10
Welding position	PA	PA; PF; PG	PA	PB	PA
* laser hybrid welded root pass, ** GMAW fill pass					
Joint configuration					
Bead on plate	I-butt joint V-butt joint	I-butt joint V-butt joint	I-butt joint	T-joint	Bead on plate
Air gap [mm]	0.35 – 1.2	0.6 – 1.2	0 – 0.5	0	-
Linear mis-alignment [mm]	0.5 – 3	0.5 – 3	-	-	-
Weld assessment and characterisation test methods					
	EN ISO 13919 EN ISO 17639	EN ISO 13919 EN ISO 17639	EN ISO 13919 EN ISO 17639 EN ISO 6507 EN 10045 EN 10002	EN ISO 13919 EN ISO 17639 EN ISO 6507	EN ISO 13919 EN ISO 17639

4 Results and discussion

The results are divided into three different parts. The focus of the first part is utilization of autogenous laser welding and laser hybrid welding processes to weld thick section material with the aim of achieving weld results that are acceptable for industrial applications. The main research concentrates on investigating process boundaries corresponding to the maximum weldable plate thickness. The process limitations to compensate for imperfections and different welding positions are experimentally tested to determine suitable process parameters. The second part presents material characterisation of the welds according their mechanical properties using the test methods described in chapter 3. The last part examines autogenous welding of thick section materials with the objective to identify those parameters that influence the welding process, and can be used to overcome the constraints of a laser hybrid welding process to expand the process parameter windows.

4.1 Investigation of process boundaries and limitations on the weld result

Using the different laser sources and experimental set-ups, a significant number of process parameters was tested for welding the given materials. In the following sections, the exemplary results of the experimental investigation of the process parameters are illustrated and integrated in a graphical overview at the end of each subchapter. The correlation of the results on the process performance and weld quality is analysed and discussed in detail. Evaluation of the weld quality is based on the standard EN ISO 13919 - 1. The quality levels used in this work are “acceptable”, “medium” and “moderate”. Consideration of the quality levels of the welded joints focuses on incomplete penetration and linear misalignment, including air gaps. Other designated imperfections are considered where applicable.

4.1.1 Variation of material thickness

Laser sources with 8 kW, 10 kW, 20 kW and 30 kW laser power were available for joining plate thicknesses up to 28 mm in a single pass or multiple passes. In the welding experiments, full penetration of the material was achieved, by either varying the laser power, or adjusting the height of the root face for the respective joint preparation. Figure 4.1 presents weld results achieved with single-pass welding for different material thicknesses. The maximum penetration achieved with 8 kW laser power and a laser hybrid welding process was 9.5 mm thickness with an I-butt joint preparation. Using up

to 20 kW of laser power allowed full penetration of 16 mm and 20 mm thick plates with autogenous and laser hybrid welding processes. The welding parameters and joint preparation were altered when changing the welding process and thickness of the material. 30 kW of laser power was sufficient to join 28 mm thick plates with a laser hybrid process.

All samples shown in Figure 4.1 were welded with an I-butt joint, except for Figure 4.1 d) which had a V-butt joint configuration with a 16 mm root face and a 30° included angle. This joint preparation was necessary to be able to weld 20 mm thick plates a single-pass with a higher welding speed and a lower laser power. If the same material was preheated up to 160°C, an I-butt joint instead of a V-butt joint could be welded with the same parameter set.

Based on the quality levels introduced, the results achieved with the parameter set for 9.5 mm thick material attained the level “acceptable”. The welds produced with 16 mm and 20 mm material achieved “medium” and “moderate” levels depending on the process used. The results from experiments with 28 mm material failed to meet the criteria because of incomplete penetration. Even though the quality of the 28 mm thick plates is of “moderate” quality, the results show the potential of the hybrid welding process for even thicker materials. Welding experiments carried out by Katayama (2015) with a 100 kW fiber laser source, using an autogenous laser welding process indicated that, for example, increasing the penetration depth is possible, while maintaining the welding speed, aspect ratio and weld geometry on the surface.

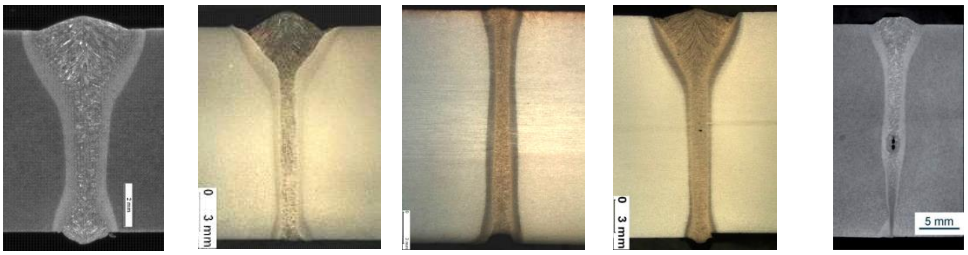

a)	b)	c)	d)	e)
t = 9.5 mm	t = 16 mm	t = 20 mm	t = 20 mm	t = 28 mm
P = 8 kW	P = 17 kW	P = 19 kW	P = 17 kW	P = 30 kW
v_w = 1.6 m/min	v_w = 2.3 m/min	v_w = 1.3 m/min	v_w = 1.8 m/min	v_w = 2.5 m/min
acceptable	medium	medium	acceptable	moderate

Figure 4.1: Results for single-pass laser hybrid welding of different material thicknesses with laser powers up to 30 kW.

If the laser power available was insufficient to join a given material thickness in a single-pass, multi-pass welding was investigated as an optional joining strategy. In this case, a V-butt joint with a root face between 6 mm and 8 mm and an included angle of 45° or 60° was used as joint preparation, Figure 4.2. To join the root face a laser hybrid welding process with a maximum laser power of 8 kW was employed. Applying a GMAW process only for one or several passes produced the best results. Welding fill and cap passes with a laser hybrid welding process did not achieve acceptable results because of the high number of pores and clustered porosity, occurring in the weld, see Figure 4.4 d) and Figure 4.6 b) and c).

Limitations for multi-pass welding arise from choosing the right joint preparation. If the root face was not chosen according to the available laser power, full penetration could not be obtained. Applying the quality levels based on standard EN ISO 13919-1 for multi-pass welds with suitable parameter sets resulted in "acceptable" quality level. Quality level "medium" was achieved in several cases because of porosity located along the whole length of the weld. Quality level "moderate" was achieved due to a lack of penetration when the root face as was too high. The approach of multi-pass welding has been proposed for pipe welding applications to increase the productivity for the construction of pipe lines (Yapp, 2004). In this case, the root pass would be welded with a laser hybrid process at a high welding speed and the fill passes produced with a high deposition GMAW process. The root pass welding then governs the overall speed of the pipeline construction and the fill passes define the number of welding stations following the root pass.

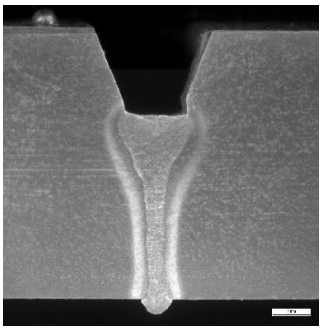

a) root pass
t = 14 mm
P = 8 kW
v_w = 1.6 m/min
root face 6 mm
acceptable

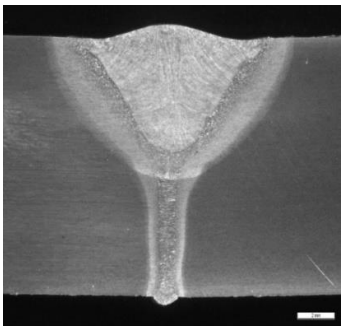

b) cap pass for a)
GMAW only
v_w = 0.4 m/min

acceptable

c) root pass
t = 16 mm
P = 7.6 kW
v_w = 1.4 m/min
root face 10 mm
moderate

Figure 4.2: Results for multi-pass welding of 14 mm and 16 mm thick material with 8 kW of laser power.

An overview of the produced weld quality from the different experimental series carried out is given in Figure 4.3. The basic parameters used to compare the results of the different welding experiments were heat input per unit length and penetration depth which equals the plate thickness for single-pass welding or the prepared root face for multi-pass welding. Several other parameter variations such as air gap, linear misalignment or change of welding position are included in this overview, they are indicated within the description of the weld quality. Further presentation and more detailed discussion are given in the following subchapters.

The dashed lines in Figure 4.3 depict ranges in which an acceptable and a medium weld quality could be achieved. Whether the extrapolation beyond the actual results is correct needs to be validated with further experiments. Comparing these results with those from available literature reporting experimental results of joining thick section material with autogenous laser processes or laser hybrid welding processes shows that the parameter sets chosen are in a comparable range and similar or equal weld results are achieved (Nilsen, 2015), (Sokolov, 2015), (Turichin, 2015), (Farrokhi, 2017).

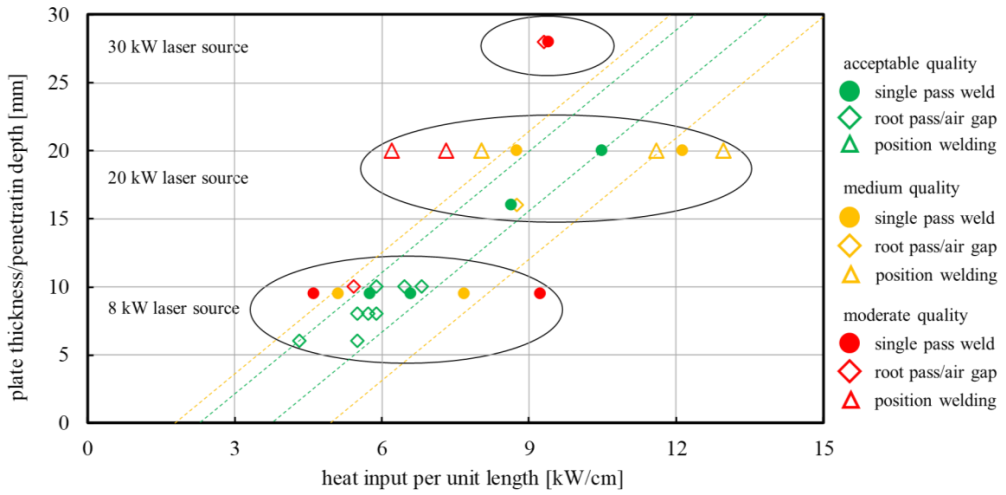

Figure 4.3: Overview of achieved weld quality from experiments performed with different material thicknesses, joint preparations and laser sources.

4.1.2 Variation of air gap size

Experiments investigating the gap bridging capability of different parameters sets were carried out with the same laser sources described in the previous subchapter. Gap sizes from 0.35 mm to 1.2 mm were welded with different joint configurations, Figure 4.4.

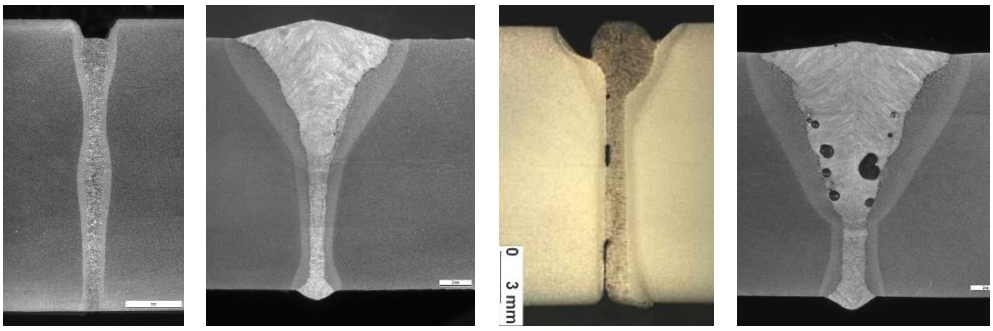

a) 0.35 mm gap single-pass weld	b) 0.5 mm gap multi-pass weld	c) 0.5 mm gap single-pass weld	d) 1.2 mm gap multi-pass weld
t = 28 mm	t = 16 mm	t = 16 mm	t = 16 mm
P = 30 kW	P = 7.6 kW	P = 17 kW	P = 7.6 kW
v_w = 2.5 m/min	vw = 1.6 m/min	vw = 2.1 m/min	vw = 1.6 m/min
moderate	root face 10 mm acceptable	moderate	root face 10 mm acceptable

Figure 4.4: Results for welding joints with air gaps up to 1.2 mm in different material thicknesses and with laser powers up to 30 kW.

Especially with 8 kW of laser power and the respective parameter sets, see Figure 4.4 b) and d), gaps up to 1.2 mm could be bridged and acceptable were achieved. To fill the gap volume the necessary wire feed speed was calculated and adapted to welding speed and gap size. Figure 4.4 a) shows an example with an incompletely filled groove, where the wire feed speed of the GMAW source, limited to 24 m/min, was insufficient to completely fill the gap, even though, theoretically, a value of around 21.6 m/min wire feed speed should have been required to fill the existing gap. Larger gap sizes also helped to increase the penetration depth, thus the maximum weldable root face can be increased when the joint configuration was kept constant. For V-butt joints the root face could be increased from 6 mm with zero gap up to 10 mm with 0.5 mm air gap or larger, see Figure 4.4 b) and d) with Figure 4.2 c). For an I-butt joint configuration as shown in Figure 4.1 e) and Figure 4.4 a), a gap of 0.35 mm benefited full penetration. This effect has also been investigated by Farrokhi (2016) for laser hybrid welding of double-sided welds. Keeping the parameter set constant during welding but changing the air gap size did not give successful welding results.

Figure 4.5 gives an overview of the welding experiments carried out, to investigate the gap bridging capability of the different process parameters used. To enable comparison of the different plate thicknesses and root faces welded, the ratio of plate thickness and air gap was determined and plot against the calculated heat input per unit length. Circled in black in this overview are two sets of experiments, where the gap was varied from 0.35 mm to 0.5 mm but all other parameters were kept constant. The achieved quality level for 0.35 mm was rated acceptable, whereas with a 0.5 mm gap the quality was inadequate, see also Figure 4.4 c).

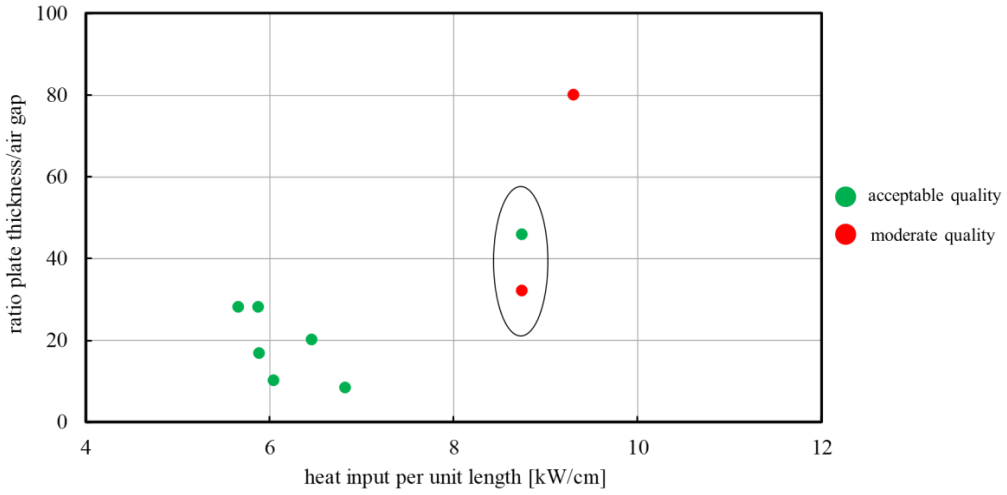

Figure 4.5: Overview of achieved gap bridging ability with different material thicknesses, joint preparations and laser source.

4.1.3 Variation of linear misalignment

Linear misalignment in the joint configuration to be welded, is classified as an imperfection in the standard EN ISO 13919. The lowest quality level allows a maximum value of linear misalignment of 3 mm. Hence, the experimental test series was carried out with a maximum linear misalignment of 3 mm for the given joint configurations, Figure 4.6.

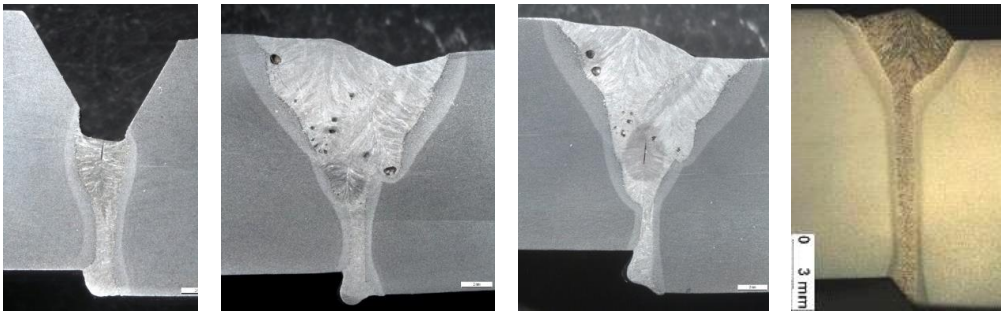

a) 0.5 mm linear misalignment	b) 1.5 mm linear misalignment	c) 3.0 mm linear misalignment	d) 2.0 mm linear misalignment
t = 16 mm	t = 16 mm	t = 16 mm	t = 16 mm
P = 7.6 kW	P = 7.6 kW	P = 7.6 kW	P = 17 kW
v_w = 1.8 m/min	v_w = 1.8 m/min	v_w = 1.8 m/min	v_w = 2.5 m/min
root face 8 mm	root face 8 mm	root face 8 mm	
acceptable	moderate	moderate	acceptable

Figure 4.6: Results for welding joints with linear misalignment of up to 3.0 mm in different material thicknesses and with laser powers up to 20 kW.

Linear misalignment reduces the effective penetration depth and allows full penetration with larger root faces, higher welding speeds or less laser power. When welding V-butt joint configurations, for example, the root face could be increased from 6 mm to 8 mm with zero gap; even at 0.5 mm linear misalignment full penetration was achieved, see Figure 4.6 and Figure 4.2. Acceptable weld results with the 8 kW laser source were achieved for a maximum linear misalignment of 0.5 mm. With the 20 kW laser source linear misalignment of up to 2 mm could be welded. The essential limit for compensating linear misalignment, is given by the formation of droplets on the root side. From the overview of the experimental welding results, for varying linear misalignment, Figure 4.7, it can be seen that keeping process parameters such as laser power or welding speed with wire feed speed constant while changing linear misalignment will achieve only a moderate quality, as shown by the values circled in black. The resulting weld quality could be improved, by changing the focal point position, a parameter that was kept constant throughout the experimental test series, from -4 mm to 0 mm on top of the surface, Figure 4.6 d).

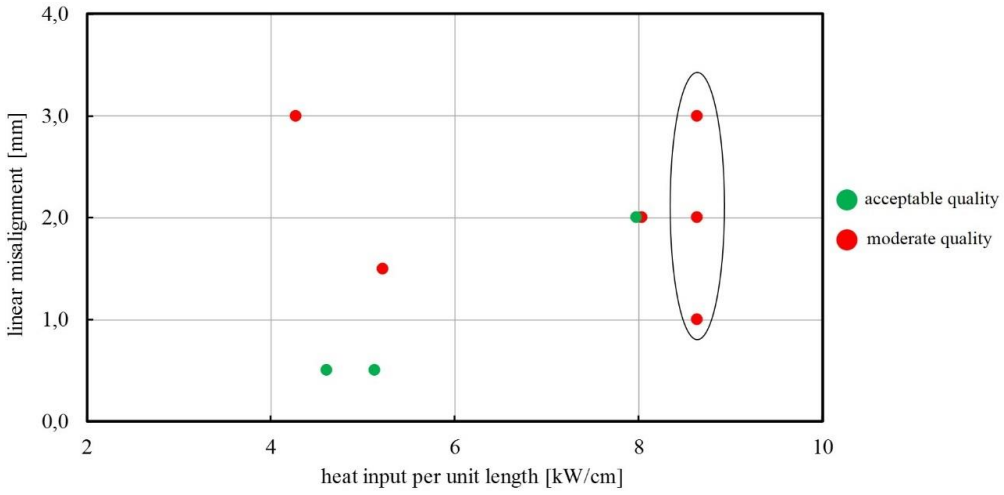

Figure 4.7: Overview of results for linear misalignment with different material thicknesses, joint preparations and laser sources.

4.1.4 Variation of welding position

Investigation of the effect of welding position was carried out for 16 mm thick plates in an I-butt joint configuration and with 8 mm thick plates as a T-joint. The test series included PF and PG position at 30°, 60° and 90° for I-butt joints, Figure 4.8, as well as PB position, where the angle of inclination of the laser beam was varied from 6° to 15°, Figure 4.9.

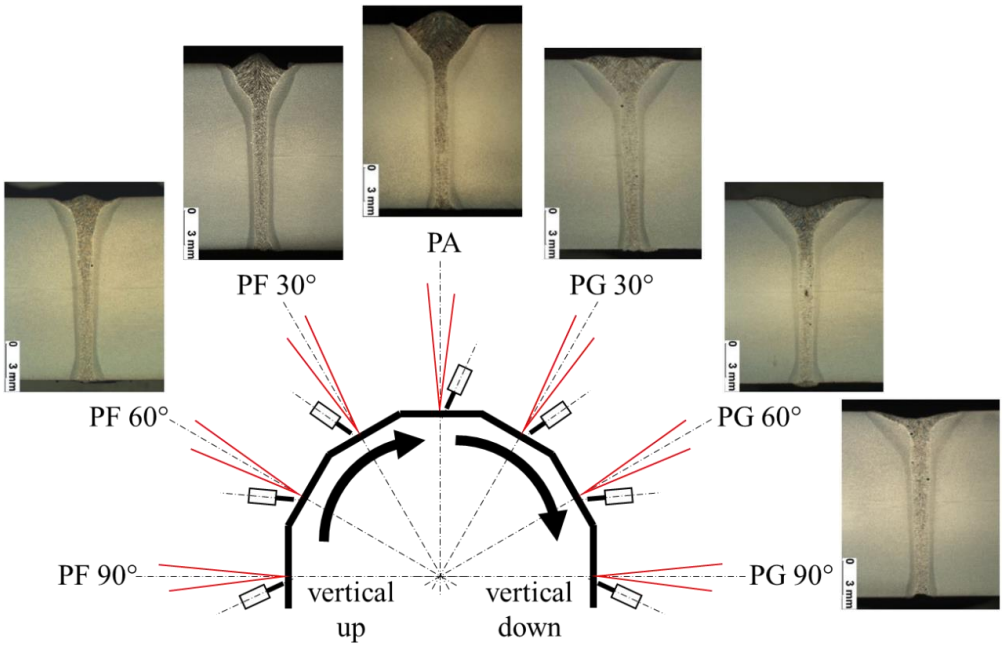

Figure 4.8: Overview of results achieved in PF and PG welding positions when joining 20 mm thick plate material in an I-butt joint configuration with a 20 kW laser source. Parameter set: P = 17 kW, v_w = 2 m/min, heat input per unit length = 6.3 – 9 kW/cm.

Changing the welding position requires good control of the process. The liquid melt experiences gravitational effects in the different welding positions, which needs to be countered in the GMAW process in particular. With vertical down welding, the process parameter set used for flat position welding could also be utilized for the PG 30° position. For better control of the melt pool in PG 60° and PG 90° position, the wire feed speed was reduced. Welding vertical up showed that only the PF 30° position could be controlled and welded with acceptable parameters. In PF 60° droplets were formed on the top side of the seam due to the instable melt pool in which the molten material could not be contained. Similar observations were made for welding I-butt joints for offshore structures with a laser hybrid process using a 16 kW disk laser by Kristiansen (2017). As

regards the laser-dominated part of the weld, it was seen that there is only little effect on the shape and quality when varying the weld position. This has also been observed when employing an autogenous laser welding process for orbital welding (Thomy, 2006) or supported by slow beam oscillation with up to 60 Hz and cold wire feeding (Vänskä, 2011). Control of the process in vertical welding and overhead positions is crucial for welding applications such as orbital welding or girth welding to maintain weld quality and meet the requirements of classifications and guidelines.

In addition to laser hybrid welding test series, autogenous laser welding experiments were carried out in PB position as a T-joint configuration to investigate the effect of changing the angle of inclination of the laser beam, Figure 4.9. Full penetration with minimal deviation from the joint axis was achieved with an inclined angle of 6°. Higher angles of inclination led to incomplete penetration as the deviation from the specified joint axis was too high.

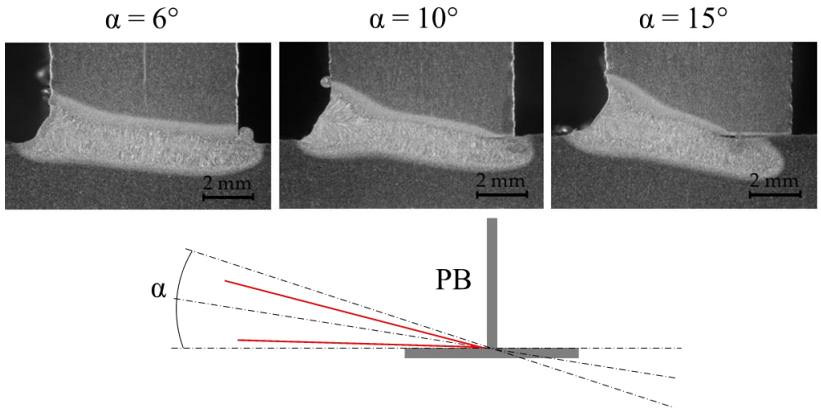

Figure 4.9: Overview of autogenous laser welding experiments, varying the angle of inclination of the laser beam, carried out in PB position as a T-joint configuration using a 10 kW laser source.
Parameter set: P = 6 kW, v_w = 1.25 m/min, heat input per unit length = 2.8 kW/cm.

The results of the experiments show that autogenous laser welding can be an alternative process to laser hybrid welding if the parameters are adjusted to the welding task and to the requirements of the joint configuration. Comparable results from other publications are not yet available, hence more research work is needed to validate these results prior to adoption in industrial applications.

4.2 Characterisation of material properties

Characterisation of the material properties was carried out in detail for the experimental test series examining 8 mm thick AH36 welded with an autogenous laser process as well as 9.5 mm thick X65 and 14 mm thick X70 plate material welded with a laser hybrid process. As described in chapter 4.1, the 8 mm material was welded in a T-joint configuration, the 9.5 mm material in a single-pass as an I-butt joint, and the 14 mm material in a V-butt joint which required a root pass and an additional cap pass welded with a GMAW process, see Figure 4.1, Figure 4.2 and Figure 4.9. To determine the characteristics of the welded samples, non-destructive testing and destructive testing methods were carried out. Non-destructive testing in the form of visual inspection was carried out to check the visual appearance of the root and fill passes as described in detail in chapter 4.1. Destructive testing comprised metallographic preparation of specimens to evaluate the hardness, mechanical testing of the tensile and micro tensile strength as well as Charpy V-notch impact toughness. Table 4.1 gives an overview of the test results of the experimental test series carried out with the above-specified materials. In order to compare the mechanical properties of the single results, the acceptance criteria from the classification society DNVGL for ships and submarine pipeline systems were chosen as a reference.

With the AH36 material grade, the hardness tests were carried out with HV5 instead of HV10 as required by the standard. Nevertheless, the results indicate that the hardness level required can be achieved with the chosen process parameters. In the case of an acceptance test, however, this criterion needs to be repeated with the correct load for HV10.

The tensile testing results for the material grades X65 and X70 show that the welds comply with the acceptance criteria of the standards. The impact toughness for X65 welded in a single-pass produced two results with 25 J which would have failed the acceptance test. For the multi-pass weld with the X70 material, the relatively highest hardness values can be found in the weld metal (WM) and HAZ of the root pass. These hardness values are above the requirements of the standard for this material grade. Even though a GMAW fill pass reduces the speed and efficiency of the overall welding process, the tested specimen revealed that the upper part of the root pass is softened by the deposition of the GMAW cap pass. A further outcome of all multi-pass welded samples was that the tested filler wires and different bevel types had a minor effect on the mechanical properties. To increase the reliability of the produced welds and meet the acceptance criteria of the respective standards, the process parameters need to be refined. Additionally, a different choice of filler metal and preheating could be taken into consideration.

Table 4.1: Overview of results from mechanical testing of material grades AH36, X65 and X70.

		Hardness [HV10]	Acceptance criteria	Tensile strength [MPa]	Acceptance criteria	Charpy V-notch [J]	Acceptance criteria
AH36 (T-joint, 8 mm)							
HAZ	max.	386 (HV5)	380[1]				
WM	max.	373 (HV5)					
X65 (I-butt joint, 9.5 mm)							
base metal (BM)	range avg.	187-220 198	270[2]	range 610-623 avg. 617	535[2]		mean 45[2] single 38[2]
HAZ	range avg.	207-245 215				174-323 (0°C) 210 (0°C)	
WM	range avg.	215-256 234				25-342 (0°C) 25-307 (-20°C) 171 (0°C) 175 (-20°C)	
X70 (V-joint, 14 mm) root pass and cap pass							
BM root pass	range avg.	201-257 215	300[2]	range 620-623 avg. 621	570[2]	250-297	mean 50[2] single 40[2]
BM cap pass	range avg.	201-208 206					
HAZ root pass	range avg.	268-345 315				189-246	
HAZ cap pass	range avg.	260-329 310					
WM root pass	range avg.	321-333 327				130-152	
WM cap pass	range avg.	241-252 245					

[1]DNVGL-RU-SHIP Part 2 Chapter 4 Section 5
[2]DNV OS F101 Section 6

4.3 Potential welding processes for joining thick section material

Autogenous laser welding processes are investigated in this chapter as a feasible option to the use of laser hybrid welding processes. The experimental test series comprised different parameter sets for welding T-joint configurations with an autogenous laser beam and basic study of an oscillated laser beam for welding purposes.

4.3.1 Variation of power density

To study the potential of the autogenous laser welding process, 8 mm thick T-joints from AH36 material were joined from one side with a 10 kW laser source. The diameter of the delivery fiber was varied between 200 µm, 300 µm and 600 µm to manipulate the power intensity on the joint surface of the weld. The effects on the welding result of the parameters of angle of inclination α of the laser beam, focal point position f_{pp} and beam offset from the flange were investigated. An overview of the welding results and parameter sets used is given in Figure 4.10 for the 300 µm delivery fiber and Figure 4.11 for the 600 µm delivery fiber. For comparison, welded joints with the 200 µm fiber and variation of the angle of inclination are shown in Figure 4.9.

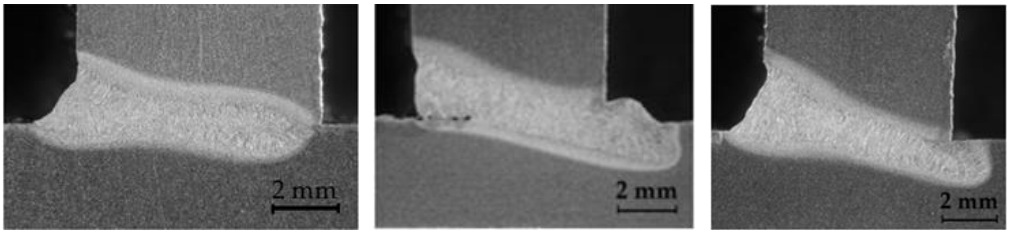

a) P = 6 kW	b) P = 8 kW	c) P = 8 kW
v_w = 1.25 m/min	v_w = 1.25 m/min	v_w = 1.25 m/min
f_{pp} = -2 mm	f_{pp} = -2 mm	f_{pp} = -4 mm
α = 6°	α = 15°	α = 15°
beam offset = 0.5 mm	beam offset = 1.5 mm	beam offset = 1.0 mm

Figure 4.10: Results for autogenous welding of T-joints with a 300 µm delivery fiber.

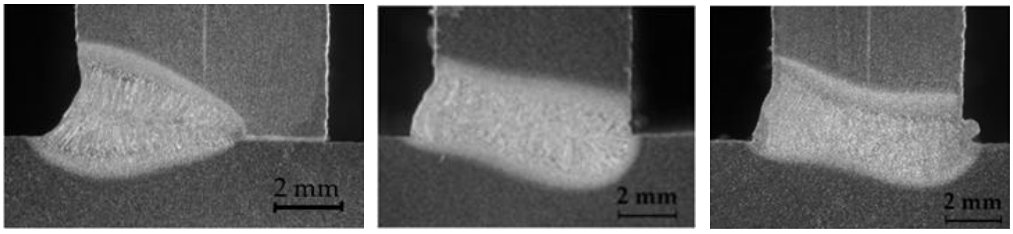

a) P = 6 kW	b) P = 10 kW	c) P = 10 kW
v_w = 1.25 m/min	v_w = 1.25 m/min	v_w = 1.25 m/min
f_{pp} = -2 mm	f_{pp} = -2 mm	f_{pp} = -4 mm
α = 6°	α = 15°	α = 15°
beam offset = 0.5 mm	beam offset = 1.5 mm	beam offset = 1.5 mm

Figure 4.11: Results for autogenous welding of T-joints with a 600 µm delivery fiber.

Optimum parameter sets were found for angles of inclination at 6°, focal point positions at -4 mm and a beam offset of 1 mm from the flange. These parameters in combination with the 600 µm delivery fiber achieved weld results with the highest quality level. Moreover, the welds had a wider fusion zone, which increases the tolerance of the process to possible displacement of the beam relative to the workpiece and imperfections within the joint configuration. The surface of the welded joints is very smooth and without visible defects on the root and face side. This result supports the hypothesis put forward by Vänska (2014) that a change in power density on the joint surface because of a lager fiber diameter affects the energy distribution and melt flow in the keyhole.

A GMAW process or laser hybrid welding process is usually employed to weld T-joint configurations. Laser hybrid welding processes have the advantage of giving full penetration welds, whereas GMAW with a fillet weld, for example, only partly penetrates the base metal and generates the joint by deposition of molten filler metal between the web and flange (Lezzi, 2013). For industrial applications, the mechanical properties of these welds are especially interesting, and need to be thoroughly examined before implementing such a process into production (Levshakov, 2015), (Turichin, 2017). To increase the reliability of process quality, a possible alternative to single-sided welding would be to weld the joint from both sides. The benefit of autogenous laser welding compared to laser hybrid welding is that there are fewer parameters to control, which reduces the complexity of the overall process, and the process provides cost savings as regards filler wire, shielding gas and energy.

4.3.2 Variation of laser beam oscillation frequency

Another way to influence the geometry of the welded joint is to oscillate the laser beam. The experimental test series in this work carried out as bead-on-plate (BOP) welds with 8 mm, 12 mm and 15 mm material. The parameter sets were chosen to investigate the effect of the oscillation frequency on the geometry of the weld and the penetration depth. The main parameters that were varied were oscillation frequency, laser power, welding speed and focal point position.

Depicted in Figure 4.12 is the effect on the penetration depth of changes in the oscillation frequency with different laser powers and welding speeds. It was found that the heat input per unit length determined by laser power and welding speed dependant on the oscillation frequency led to the expected change in penetration depth. Further experimental test series investigating the influence of the focal point position showed only a minor effect on the penetration depth.

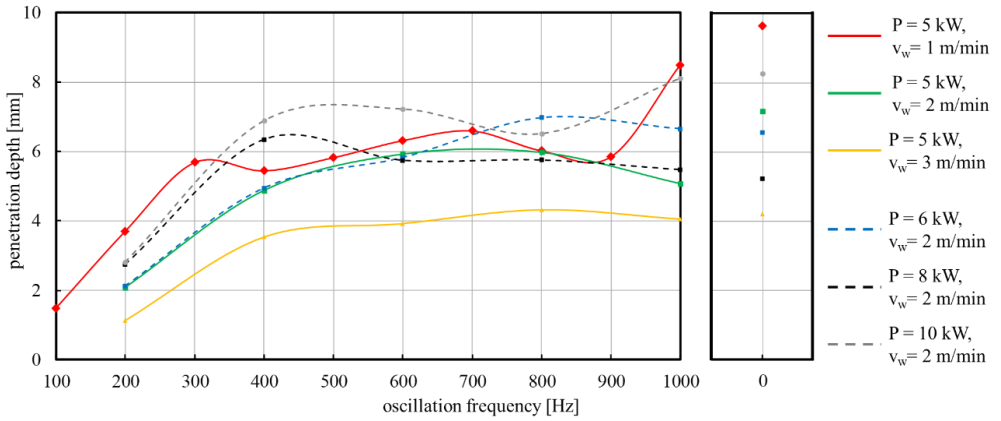

Figure 4.12: Effect of oscillation frequency from 100 Hz to 1000 Hz (left side) and 0 Hz (right side) on the penetration depth with different of laser power and welding speed.

Another effect of the oscillation frequency that was studied was its effect on the geometry of the weld fusion zone. Measurements of the width of the fusion zone were taken at five different locations equally distributed along the depth of penetration from the middle of the weld fusion zone to the outline of the weld fusion zone. The measurements were statistically processed to make them comparable to each other. Figure 4.13 shows the average distance from the middle of the weld. The graph is plotted for positive values on the x-axis only, the indicated grey outline of the weld cross-section in the background gives an orientation of the geometrical shape. The graph clearly shows that the welds produced with 200 Hz are the widest – independent of the parameter set applied – and

have the highest statistical variance, as can be seen from the upper and lower band of confidence. Welds produced with oscillation frequencies of 400 Hz and higher, including 0 Hz, have a rather narrow band of confidence and are closer together, resembling the geometry of a high power laser weld the most.

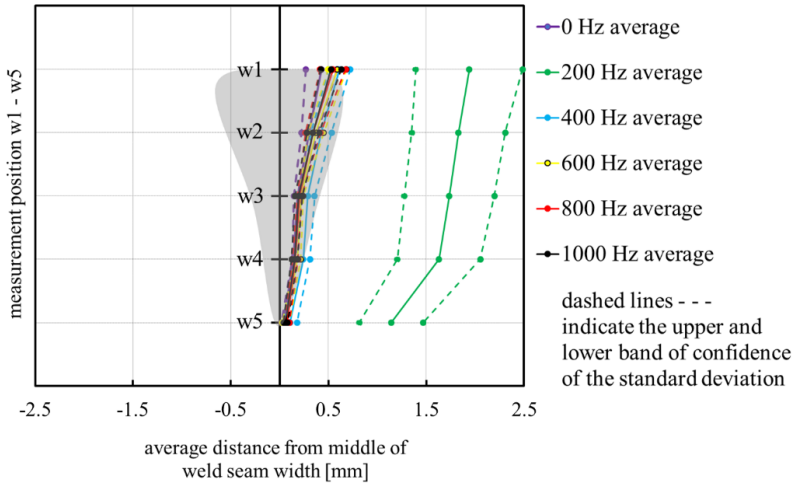

Figure 4.13: Overview of standardized weld geometry at different positions in the fusion zone.

Oscillating the laser beam decreases the penetration depth but helps to widen the weld fusion zone, thus opening the possibility to increase tolerance to workpiece displacement, small gaps or linear misalignment. However, as shown from examples in the chapters above, when welding thick section material with a given laser source and defined parameter set, the maximum achievable penetration depth plays the most important role in weld process outcome. Further experiments are needed, especially with higher laser power, to identify the full capability of oscillated laser beam welding for material thicknesses well above 10 mm.

5 Conclusion

In this work the use of high power fiber lasers was studied to weld thick section material with laser hybrid and autogenous laser welding processes with a focus on the process performance and weld properties. The research activities concentrated on three different topics. First, investigation of the process boundaries correspondent to the maximum weldable plate thickness and determination of the limits for compensating imperfections and welding positions. Second, characterisation of the weld samples according to their mechanical properties and comparison of the results to applicable classification standards. Third, investigation of autogenous laser welding processes as an approach for thick section welding. The main findings were as follows:

- 16 mm, 20 mm and 28 mm thick material could be welded as an I-butt joint with autogenous laser and laser hybrid welding processes in a single pass using 20 kW and 30 kW laser sources.
- T-joints of 8 mm thick material could be welded with an autogenous laser welding process. Changing the power density on the workpiece surface by employing a 600 µm fiber improved the weld result.
- 8 kW laser power was sufficient to join 9.5 mm thick material with a laser hybrid process in a single pass. Thicker materials required joint preparation such as a V-butt joint and multiple weld passes.
- Welding fill and cap passes with a laser hybrid welding process produced excessive porosity. The most effective approach was to weld the highest possible root face with a laser hybrid welding process and fill the remaining groove with a GMAW process.
- Gap bridging was successful up to 1.2 mm with a laser hybrid welding process. Linear misalignment could be compensated up 0.5 mm, the limit is determined by the formation of droplets on the root side.
- Welding in different positions showed that vertical down welding was possible with good control of the laser hybrid process and acceptable to moderate results were achieved for positions PG 30°, PG 60° and PG 90°. Controlling the process for vertical up welding was possible for PF 30°.
- Process parameter sets applied to achieve acceptable weld qualities for autogenous laser welding and laser hybrid welding processes needed to be adapted for each welding task separately. The heat input and power density had the most significant effect on the welded result, especially the penetration depth.

- Characterisation of the material properties showed that welded samples can meet requirements from classification standards, although there were certain limitations to the hardness and toughness values of laser hybrid welded samples.

It was shown in the study that high power fiber lasers employed for autogenous welding processes and in combination with an arc welding process are able to produce deep penetration welds of high quality. The reliability of the parameter sets used during the experimental test series to achieve these results were suitable for welding similar joint configurations with slight deviations such as air gap and linear misalignment. A change in material thickness, joint type or welding position required a different parameter set which needed to be adapted to each new task.

In light of the findings of this work it can be concluded that established processes can be readily transferred to industrial applications to replace older laser systems and to improve the efficiency and sustainability of the welding process.

6 Future work

Future research should take the opportunity to investigate two fields to further develop effective joining of thick section material. The first area of interest is the feasibility of using even higher laser powers for laser hybrid and autogenous laser welding processes than those used in the experimental studies carried out in this work. An indication of the prospects for such high power laser welding has already been given by this work with lasers up to 30 kW. Published research reported experiments with laser powers up to 100 kW. Especially interesting for industrial applications could be investigation of the sustainability of a fiber laser-based process in comparison with other laser types. When considering the physical and technical limitations of high power lasers, it should be noted that laser systems with powers up to 500 kW are offered by manufacturers. The focus of such future research should be placed on understanding of the physical and thermodynamic phenomena in the melt pool and keyhole, and control the different parameters of the welding process to fully utilize the capability of high power lasers for joining thick section material.

The second area of interest is investigation of approaches and techniques to improve the robustness of the welding process itself by developing methods to control the reliability of the welded results when faced with imperfections and other flaws that cause weld defects. Of particular interest for industrial applications would be assessment of autogenous laser welding and hybrid laser welding processes for higher grade material such as X80 or X120 and orbital welding for the approval of pipeline construction.

References

Abed, R. N. (2015). The Thermal Management System of Laser Diode: A Review. *ARPN Journal of Engineering and Applied Sciences, 10*(12), 5250 - 5260.

Acherjee, B. (2018). Hybrid laser arc welding: State-of-art review. *Optics and Laser Technology, 99*, 60 - 71.

Alkeskjold, T. (2009). Large-mode-area ytterbium-doped fiber amplifier with distributed narrow spectral filtering and reduced bend sensitivity. *Optics Express, 17*(19), pp. 16394 - 16405.

Archambault, J.-L., & Grubb, S. G. (1997). Fiber Gratings in Lasers and Amplifiers. *Journal of Lightwave Technology, 15*(9), 1378 - 1390.

Bachmann, M., Gumenyuk, A., & Rethmeier, M. (2016). Welding with high-power lasers: trends and developments. *Physics Procedia, 83*, 15 - 25.

Bagger, C., & Olsen, F. (2005). Review of laser hybrid welding. *Journal of Laser Applications, 17*(1), 2 - 14.

Baker, C., Friebele, E., Burdett, A., Rhonehouse, D., Fontana, J., Kim, W., . . . Haub, J. (2017). Nanoparticle doping for high power fiber lasers at eye-safer wavelengths. *25*, 13903 - 13915.

Barua, P., Sekiya, H., Saito, K., & Ikushima, A. (2008). Influences of Yb3+ ion concentration on the spectroscopic properties of silica glass. *Journal of Non-Crystalline Solids, 354*, 4760 – 4764.

Basu, P. (2006). *Combustion and gasification in fluidized beds.* Boca Raton, FL, USA: CRC Press. Retrieved June 15, 2009, from Combustion and gasification in fluidized beds: http://www.engnetbase.com/books/4502/3396_C000.pdf

Beck, M. (1996). *Modellierung des Lasertiefschweißens.* Stuttgart: Teubner Verlag.

Beyer, E. (1995). *Schweißen mit Laser.* Berlin Heidelberg: Springer Verlag.

Beyer, E., Herwig, P., Hunze, S., Lasagni, A. F., Lütke, M., Mahrle, A., . . . Thieme, S. (2012). High-Power Laser Materials Processing. *International Congress on Applications of Lasers & Electro-Optics. 2012*, pp. 1 - 10. LIA.

Boullet, J., Zaouter, Y., Desmarchelier, R., Cazaux, M., Salin, F., Saby, J., . . . Cormier, E. (2008). High power ytterbium-doped rod-type threelevel. *Optics Express, 16*(22), 17891 - 17902.

Bunaziv, I., Frostevarg, J., Akselsen, O., & Kaplan, A. (2018). Process stability during fiber laser-arc hybrid welding of thick steel plates. *Optics and Lasers in Engineering, 102*, 34-44.

Butthoff, H., Keitel, S., & Neubert, J. (2002). MSG-Laserstrahl-Hybridschweißen an unterschiedlichen Stoßarten. *DVS - Berichte, 220*, 148 - 152.

Calles-Arriaga, C., Duran-Ramirez, V., Barbosa-Garcia, O., Selvas-Aguilar, R. J., Martínez-Rios, A., Torres-Gomez, I., & Mata-Chavez, R. I. (2008). Beam pump combination for fiber lasers. Optical Engineering. *Optical Engineering, 47*(2), 020502-1 - 020502-3.

Cao, X., Wanjara, P., Huang, J., Munro, C., & Nolting, A. (2011). Hybrid fiber laser – Arc welding of thick section high strength low alloy steel. *Materials and Design, 32*, 3399-3413.

Casalino, G., Dal Maso, U., & Campanelli, A. (2010). *Hybrid Laser Welding: A Review*. DAAAM International Scientific Book.

Codemard, C. A., Shirakawa, A., Sahu, J. K., Yoo, S., Jeong, Y., & Nilsson, J. (2009). Thermal Resilience of Polymer-Coated Double-Clad Fiber. *The European Conference on Lasers and Electro-Optics* (pp. CJ-P5). Munich, Germany: Optical Society of America.

Coste, F., Fabbro, R., Allais, C., & Mas, J. (2005). Laser and hybrid welding of high strength steel application to pressure vessel manufacturing. *Proceedings of the Laser Materials Processing Conference ICALEO 2005.* Laser Institute of America, Paper 546.

Coste, F., Sabatier, L., Dubet, O., Aubert, P., & Jones, L. (2001). 20 mm thickness Nd:Yag Laser Welding of 316L stainless steel with long focal length. *Proceedings of the Laser Materials Processing Conference ICALEO 2001*. Laser Institute of America, 2001, Section C 1706.

Coste, F., Sabatier, L., Dubet, O., Aubert, P., & Jones, L. (2001). Nd:YAG laser welding of 60 mm thickness 316L parts using multiple passes. *Proceedings of the Laser Materials Processing Conference ICALEO 2001*. Laser Institute of America, 2001, Section C 1706.

Dajani, I., Zeringue, C., Lu, C., Vergien, C., Henry, L., & Robin, C. (2010). Stimulated Brillouin scattering suppression through laser gain competition: Scalability to high power. *Optics Letters, 35*, 3114 – 3116.

Dausinger, F. (1995). *Strahlwerkzeug Laser: Energieeinkoppling and Prozeßeffektivität.* Stuttgart: Teubner Verlag.

Dawson, J., Messerly, M., Beach, R., Shverdin, M., Stappaerts, E., Sridharan, A., . . . Barty, C. (2008). Analysis of the scalability of diffraction-limited fiber lasers and amplifiers to high average power. *Optics Express, 16*(17), pp. 13240 - 13266.

Dieke, G., & Crosswhite, H. (1963). The Spectra of the Doubly and Triply Ionized Rare Earths. *Applied Optics, 7*(2), 675 - 686.

DiGiovanni. (1999). *USA Patent No. 5,864,644.*

Dong, L. (2015). Advanced Optical Fibers for High Power Fiber Lasers. In M. Yasin, *Advances in Optical Fiber Technology: Fundamental Optical Phenomena and Applications.* London, UK: InTech.

Dragic, P., Cavillon, M., & Ballato, J. (2018). Materials for optical fiber lasers: A review. *Applied Physics Reviews, 5*, 041301.

Eboo, M., & Steen, W. (1978). Arc - augmented laser welding. *Fourth International Conference on Advances in Welding Processes*, (pp. 257 - 265, Paper 17). Harrogate, U.K.

Eichler, J. (2006). *Laser - Bauformen, Strahlführung, Anwendungen.* Berlin Heidelberg: Springer-Verlag.

Einstein, A. (1916). Strahlungsemission und Absorption nach der Quantentheorie. *Verhandlungen der Deutschen Physikalischen Gesellschaft, 18*, 318 - 323.

El Rayes, M., Walz, C., & Sepold, G. (2004). The Influence of Various Hybrid Welding Parameter on Bead Geometry. *Welding Journal, 83*(5), 147S - 153S.

EN 10002-1: Metallic materials - Tensile testing - Part 1 Method of testing at ambient temperature. (2001). Berlin, Germany: Beuth Verlag.

EN 10045-1: Metallic materials - Charpy impact test - Part 1 Test method. (1990). Berlin, Germany: Beuth Verlag.

EN 439: Welding consumables - Shielding gases for arc welding and cutting. (1995). Berlin, Germany: Beuth Verlag.

EN 440: Welding consumables - wire electrodes and deposits for gas-shielded metal arc welding of non-alloy and fine grain steels. (1994). Berlin, Germany: Beuth Verlag.

EN ISO 13919-1: Welding - Electron and laser-beam welded joints - Guidance on quality levels for imperfections - Part 1 Steel. (1996). Geneva, Switzerland: International Organization for Standardization.

EN ISO 17639: Destructive Tests on Welds in Metallic Materials - Macroscopic and Microscopic Examination of Welds. (2003). Geneva, Switzerland: International Organisation for Standardization.

EN ISO 6507: Metallic materials - Vickers hardness test - Part 1 Test. (2005). Geneva, Switzerland: International Organization for Standardization.

EN ISO 6947: Welding and allied processes - Welding positions. (2011). Geneva, Switzerland: International Organization for Standardization.

Fan, T. (1990). Diode-Pumped Solid State Lasers. *The Lincoln Laboratory Journal, 3*(3), 413 - 426.

Fan, T., & Byer, R. (1988). Diode Laser-Pumped Solid-state Lasers. *IEEE Journal of Quantum Electronics, 24*(6), 895 - 912.

Farrokhi, F., & Kristiansen, M. (2016). A practical approach for increasing penetration in hybrid laser-arc welding of steel. *Physics Procedia, 83*, 577 - 586.

Farrokhi, F., Larsen, R., & Kristiansen, M. (2017). Single-pass hybrid laser welding of 25 mm thick steel. *Physics Procedia, 89*, 49 - 57.

Fritzsche, A., Avilov, V., Gumenyuk, A., Hilgenberg, K., & Rethmeier, M. (2016). High power laser beam welding of thick-walled ferromagnetic steels with electromagnetic weld pool support. *Physics Procedia, 83*, 362 - 372.

Frostevarg, J., & Haeussermann, T. (2015). Dropout formation in thick steel plates during laser welding. *The IIW International Conference on High Strength Materials– Challenges and Applications 02/07/2015-03/07/2015.* Helsinki.

Fuhrmann, C. (2007). *Laser-Lichtbogen-Hybridschweißen bis zu Blechdicken von 25 mm.* Aachen: Shaker Verlag.

Giles, C. (1997). Lightwave Applications of Fiber Bragg Gratings. *Journal of Lightwave Technology, 15*(8), 1391 - 1404.

Gloge, D. (1971). Weakly Guiding Fibers. *Applied Optics, 10*, pp. 2252 - 2258.

Goodno, G. D., & Injeyan, H. (2011). *High-Power Laser Handbook.* New York: McGraw Hill.

Gook, S., Gumenyuk, A., & Rethmeier, M. (2009). Orbital Laser-Hybrid Welding of Pipelines Using a 20 kW Fibre Laser. *Proceedings of Lasers in Manufacturing (LiM), World of Photonics Congress.* Munich, Germany: WLT Wissenschaftliche Gesellschaft Lasertechnik e.V.

Gook, S., Gumenyuk, A., & Rethmeier, M. (2014). Hybrid laser arc welding of X80 and X120 steel grade. *19*(1), 15 - 24.

Goussian, J., Becker, A., Chehaibou, A., & P, L. (1997). Heavy Sections Welding with Very Hig Power Laser Beams: The Challenge. *SPIE, 3097*, pp. 118 - 128.

Grubb, S. (2000). *USA Patent No. 6157763.*

Gumenyuk, A., Gook, S., Rethmeier, M., & Kohn, H. (2010). Orbitalschweißen im Pipelinebau - Neue Möglichkeiten durch die Anwendung von Hochleistungslasern. *8. Internationale Konferenz Strahltechnik*, (pp. 74 - 79). Halle.

Guo, W., Crowther, D., Francis, J., Thompson, A., & Li, L. (2016). Process-parameter interactions in ultra-narrow gap laser welding of high strength steels. *Int. J. Adv. Manuf. Technol., 84*, 2457 - 2566.

Hansen, K. P., Olausson, C. B., Broeng, J. N., Maack, M. D., Alkeskjold, T. T., & ... Simonsen, H. (2011). Airclad fiber laser technology. *Optical Engineering, 50*(11), 111609.

Hayashi, I., Panish, M., Foy, P., & Sumski, S. (1970). Junction lasers which operate continuously at room temperature. *Appl. Phys. Lett., 17*(3), 109 - 111.

Hecht, J. (2018). High-Power Fiber Lasers. *Optics & Photonics News, 29*(10), 32 - 37.

Hegarty, J., Broer, M., Golding, B., Simpson, J., & MacChesney, J. (1983). Photon Echoes below 1 K in a Nd3+-Doped Glass Fiber. *Physical Review Letters, 51*(22), 2033 - 2035.

Hill, K., & Meltz, G. (1997). Fiber Bragg Grating Technology Fundamentals and Overview. *Journal of Lightwave Technology, 15*(8), 1263 - 1276.

Howse, D., Scudamore, R., & Booth, G. (2005). YB fibre laser/MAG hybrid processing for welding pipelines. *Proceedings of the IIW2005 Commission IV - Power Beam Processes.* Prague, IV-880-05.

Hübner, A., & Pieschel, J. (2010). Hybridschweißen - Wesensmerkmale, Vorzüge und Anwendungsmöglichkeiten. *DVS Berichte, 266*, 52 - 56.

Hügel, H. (2000). New solid-state lasers and their application potentials. *Optics and Lasers in Engineering, 34*, 213 - 229.

Hügel, H., & Graf, T. (2009). *Laser in der Fertigung.* Wiesbaden: Vieweg und Teubner.

Ion, J. (2005). *Laser Processing of Engineering Materials.* Oxford, MA: Elsevier Butterworth Heinemann.

IPG-Photonics. (2018). *www.ipgphotonics.com.* Retrieved July 19, 2019, from https://www.ipgphotonics.com/en/647/Widget/Industrial+Fiber+Lasers+for+Materials+Processing+2018.pdf

Jasnau, U., & Gaede, R. (2008). Hochleistungsfaserlaser im Schiffbau. *Laser Technik Journal, 2*, 31 - 33.

Jauregui, C., Limpert, J., & Tünnermann, A. (2013). High-power fibre lasers. *Nature Photonics, 7*(11), 861 - 867.

Jauregui, C., Otto, H. J., Breitkopf, S., Limpert, J., & Tünnermann, A. (2016). Optimizing high-power Yb-doped fiber amplifier systems in the presence of transverse mode instabilities. *Optics Express, 24*(8), 7879 - 7892.

Javadimanesh, M., Ghavami Sabouri, S., & Khorsandi, A. (2016). The effect of cladding geometry on the absorption efficiency of double-clad fiber lasers. *XLVI*(2), 277 - 289.

Jeong, Y., Sahu, J., Payne, D., & Nilsson, J. (2004). Ytterbium-doped large-core fiber laser with 1.36 kW continuous-wave output power. *Optics Express, 12*(25), 6088 - 6092.

Jiang, M., Tao, W., Chen, Y., & Li, F. (2019). Comparison of processing window in full penetration laser welding of thick high-strength steel oder atmosphere and sub-atmosphere. *Optics and Laser Technology, 109*, 449 - 455.

Jokinen, T., Karhu, M., & Kujanpää, V. (2003). Narrow Gap Hybrid Welding of Thick Stainless Steel. *Proceedings of the Laser Materials Processing Conference ICALEO 2003.* Laser Institute of America, Section A 309.

Kah, P. (2012). Overview Of The Exploration Status Of Laser-Arc Hybrid Welding Processes. *Rev. Adv. Mater. Sci., 30*, 112 - 132.

Kaplan, A. (2004). *Modellrechnung und numerische Simulation von Absorption, Wärmeleitung und Strömung des Laser-Tiefschweißens.* Dissertation, TU Wien.

Katayama, S. (2013). *Handbook of Laser Welding Technologies.* Cambridge U.K.: Woodhead Publishing Limited.

Katayama, S., Mizutani, M., Kawahito, Y., Ito, S., & Sumimoi, D. (2015). Fundamental Research of 100 kW Fiber Laser Welding Technology. *Proceedings of Lasers in Manufacturing (LiM), World of Photonics Congress.* Munich, Germany: WLT Wissenschaftliche Gesellschaft Lasertechnik e.V.

Katayama, S., Onishi, T., Mizutani, M., & Kawahito, Y. (2010). High-Power Laser Butt Welding of High-Strength Steel Thick-Plate. *IIW Annual Meeting 2010*. Commision IV, Turkey, IV-1031-10.

Katayama, S., Yohei, A., Mizutani, M., & Kawahito, Y. (2011). Development of Deep Penetration Welding Technology with High Brightness Laser under Vacuum. *Physics Procedia*, *12*, 75 - 80.

Kawaguchi, I., Tsukamoto, S., Arakane, G., & Honda, H. (2006). Characteristics of high-power CO2 laser welding. *Welding International*, *20*(2), 100 - 105.

Kawahito, Y., Mizutani, M., & Katayama, S. (2007). Elucidation of high-power fibre laser welding phenomena of stainless steel and effect of factors on weld geometry. *J. Phys. D: Appl. Phys.*, *40*, 5854 - 5859.

Kawahito, Y., Wang, H., Katayama, S., & Sumimori, D. (2018). Ultra high power (100 kW) fiber laser welding of steel. *Optics Letters*, *43*(19), 4667 - 4670.

Kelly, S., Brown, S., Tressler, J., Martukanitz, R., & Ludwig, M. (2009). Using Hybrid Laser-Arc Welding to Reduce Distortion in Ship Panels. *88*(3), 32 - 36.

Kessler, B. (2009). Schweißtechnische Anwendungen der Hochleistungs-Faserlaser. *Laser Technik Journal*, *6*, 42 - 45.

Kim, J., Dupriez, P., Codemard, C., Nilsson, J., & Sahu, J. (2006). Suppression of stimulated Raman scattering in a high power Yb-doped fiber amplifier using a W-type core with fundamental mode cut-off. *OPTICS EXPRESS*, *14*(12), 5103 - 5113.

King, D. (1992). Fluidized catalytic crackers: an engineering review. In O. Potter, & D. Nicklin (Hrsg.), *Proceedings of the Seventh Engineering Conference on Fluidization* (S. 15-26). New York: Engineering Foundation.

Koester, C., & Snitzer, E. (1964). Amplification in a Fiber Laser. *Applied Optics*, *3*(10), 1182 - 1186.

Komizo, Y. (2008). Overview of Recent Welding Technology Relating to Pipeline Construction. *Transaction of JWRI*, *37*(1), 1 - 5.

Kouznetsov, D., & Moloney, J. (2002). Efficiency of pump absorption in double-clad fiber amplifiers. II. Broken circular symmetry. *J. Opt. Soc. Am. B*, *19*(6), 1259 - 1263.

Kouznetsov, D., Moloney, J., & Wright, E. (2001). Efficiency of pump absorption in double-clad fiber amplifiers. I. Fiber with circular symmetry. *J. Opt. Soc. Am. B*, *18*, 743 - 749.

Kristiansen, M., Farrokhi, F., Kristiansen, E., & Villumsen, S. (2017). Application of hybrid laser arc welding for the joining of large offshore steel foundations. *Physics Procedia, 89*, 197 - 204.

Kroos, J. (1993). *Stabilität und Dynamik der Dampfkapillare beim Laserstrahlschweißen von Metallen.* Dissertation, TU Braunschweig.

Krummricht, P., & Akhtari, S. (2014). Selection of energy optimized pump concepts for multi core and multi mode erbium doped fiber amplifiers. *Optics Express, 22*(24), 30267 - 30280.

Laserline. (2019). *www.laserline.com.* Retrieved July 19, 2019, from https://www.laserline.com/fileadmin/Dokumente/Broschueren_DE/Laserline_LDF_Die_Referenzklasse_fuer_Diodenlaser.pdf

Leers, M., & Boucke, K. (2008). Cooling Approaches for High Power Diode Laser Bars. *Proceedings - Electronic Components and Technology Conference* (S. 1011 - 1016). Lake Buena Vista, FL, USA: IEEE.

Lembeck, H. (2002). Laser-Hybrid-Schweißen im Schiffbau. *Aachener Kolloquium für Lasertechnik AKL2002.* Aachen: Fraunhofer-Institut für Lasertechnik ILT.

Levshakov, V., Aleshkin, A., Steshenkova, N., Turichin, G., & Nosyrev, N. (2015). Industrial Laser Technologies for Shipbuilding. *Proceedings of Lasers in Manufacturing (LiM), World of Photonics Congress.* Munich, Germany: WLT Wissenschafltiche Gesellschaft Lasertechnik e.V.

Lezal, D., Pedlikova, J., Kostka, P., Bludska, J., Poulain, M., & Zavadil, J. (2001). Heavy metal oxide glasses: preparation and physical properties. *Journal of Non-Chrystalline Solids, 284*, 288 - 295.

Lezzi, F., & Costa, L. (2013). The development of conventional welding processes in naval construction. *Welding International, 27*(10), 735 - 747.

Li, M.-J., Chen, X., Wang, J., Gray, S., Liu, A., Demeritt, J., . . . Zenteno, L. (2007). Al/Ge co-doped large mode area fiber with high SBS threshold. *Optics Express, 15*(13), 8290 - 8299.

Li, R., Wang, T., Wang, C., Yan, F., Shao, X., Hu, X., & Li, J. (2014). A study of narrow gap laser welding for thick plates using the multi-layer and multi-pass method. *Optics & Laser Technology, 64*, 172 - 183.

Li, Y., Liu, S., Zhan, H., Peng, K., Sun, S., Jiang, J., . . . Lin, A. (2018). Fiber Design and Fabrication of Yb/Ce Codoped Aluminosilicate Laser Fiber With High Laser Stability. *IEEE Photonics Journal, 10*(4), 1943 - 0655.

Limpert, J., Liem, A., Reich, M., Schreiber, T., Nolte, S., Zellmer, H., & Tünnermann, A. (2004). Low-nonlinearity single-transverse-mode ytterbium-doped photonic crystal fiber amplifier. *Optics Express, 12*(7), 1313 - 1319.

Limpert, J., Röser, F., Klingebiel, S., Schreiber, T., Wirth, C., Peschel, T., . . . Tünnermann, A. (2007). The Rising Power of Fiber Lasers and Amplifiers. *IEEE Journal of Selected Topics on Quantum Elektronics, 13*(3), 537 - 545.

Liu, C.-H., Ehlers, B., Doerfel, F., Heinemann, S., Carter, A., Tankala, K., . . . Galvanauskas, A. (2004). 810W continuous-wave and singletransverse-mode fibre laser using 20µm core Yb-doped double-clad fibre. *Electronic Letters, 40*(23).

Lu, K., & Dutta, N. (2002). Spectroscopic properties of Yb-doped silica glass. *Journal of Applied Physics, 91*(2), 576 - 581.

MacChesney, J., & DiGiovanni, D. (1990). Materials Development of Optical Fiber. *J. Am. Ceram. Soc., 73*(12), 3537 - 3556.

Maiman. (1960). Stimulated Optical Radiation in Ruby. *Nature, 187*(4736), 493 - 494.

Mayer, A. (2019). Update on the Global Market for Lasers and Systems in Materials Processing: Vigorous Growth, Will it Last? *14th International Laser Marketplace, Laser World of Photonics 2019.* Munich.

Mears, R., Reekie, L., Jauncey, I., & Payne, D. (1987). Low-noise erbium-doped fibre amplifier operating at 1.54µm. *Electronics Letters, 23*(19), 1026 - 1028.

Midilli, Y., Efunbajo, O., Simsek, B., & Ortac, B. (2017). 1018 nm Yb-doped high power fiber laser pumped by broadband pump sources around 915 nm with output power above 100 W. *Applied Optics, 56*(25), 7225 - 7229.

Miebach, R., & Lembeck, H. (2003). Die neue Fertigung der Meyer-Werft - Laserhybridschweißen als Kerntechnologie. *DVS Berichte, 225*, 187 - 191.

Moore, P., Howse, D., & Wallach, E. (2004). Development of Nd:YAG laser and laser/MAG hybrid welding for land pipeline applications. *Welding and Cutting, 3*(3), 186 - 191.

Moore, P., Howse, D., & Wallach, E. (2004). Microstructures and properties of laser/arc hybrid welds and autogenous laser welds in pipeline steels. *Science and Technology of Welding and Joining*, 314 - 322.

Morasse, B., Gagnon, E., Arsenault-Roy, J., & deSandro, J.-P. (2013). High Peak Power Single-mode Amplification Using Highly Doped Double Cladding Ytterbium

Phosphosilicate Fiber. *Workshop on Specialty Optical Fibers and their Applications* (pp. F2 - F19). Optical Society of America.

Nakazawa, M., Kimura, Y., & Suzuki, K. (1989). Efficient Er3+-Doped Optical Fiber Amplifier Pumped by a 1.48 µm InGaAsP Laser Diode. *Applied Physics Letters, 54*, 295 - 297.

Nielsen, S. (2001). Hybrid Welding of Thick Section Mild Steel. *Proceedings of the 8th Conference on Laser Materials Processing in Nordic Countries (8th NOLAMP). 2*, pp. 167 - 170. Copenhagen, Denmark: Flemming Olsen, Jens Klæstrup Kristensen.

Nielsen, S. (2015). High power laser hybrid welding - challenges and perspectives. *Physics Procedia, 78*, 24 - 34.

Nilsson, J., & Payne, D. N. (2011). High-Power Fiber Lasers. *Science*, S. 921 - 922.

Nodop, D., Jauregui, C., Jansen, F., Limpert, J., & Tünnermann, A. (2010). Suppression of stimulated Raman scattering employing long period gratings in double-clad fibre amplifiers. *Opt. Lett., 35*, 2982 - 2984.

Noordegraaf, D. (2012). *Fused combiners for photonic crystal fibers.* Kgs. Lyngby: Technical University of Denmark (DTU).

Offshore standard DNV-OS-F101: Submarine pipeline systems. (2013). Oslo, Norway: Det Norske Veritas AS.

Okhotnikov, O. (2012). *Fiber Lasers.* Weinheim, Germany: Wiley-VCH Verlag & Co.

Olsen, F. O. (2009). *Hybrid laser-arc welding.* Cambridge, U.K.: Woodhead Publishing Limited.

Overton, G., Nogee, A., Belforte, D. A., & Holton, C. (2013). Laser markets rise above global headwinds. *Laser Focus World, 49*(1), 36 - 68.

Overton, G., Nogee, A., Belforte, D. A., Wallace, J., & Gefvert, B. (2019). Annual Laser Market Review & Forecast 2019: What goes up... *Laser Focus World, 55*(1), 40 - 65.

Pask, H., Carman, R., Hanna, D., Tropper, A., Mackechnie, C., Barber, P., & Dawes, J. (1995). Ytterbium-doped silica fiber lasers: versatile sources for the 1-1.2µm region. *Journal of Selected Topics in Quantum Electronics, 1*(1), 2 - 13.

Pedrotti, F., Pedrotti, L., Bausch, W., & Schmdit, H. (2002). *Optik für Ingenieure.* Heidelberg: Springer-Verlag.

Peng, G.-D. (2019). *Handbook of Optical Fibers.* Singapore: Springer Singapore.

Petring, D., Fuhrmann, C., Wolf, N., & Poprawe, R. (2007). Progress in Laser-MAG Hybrid Welding of High-Strength Steels up to 30 mm Thickness. *Proceedings of the Laser Materials Conference ICALEO 2007.* Laser Institute of America, Paper 604.

Petronis, E., Cerwenka, G., & Emmelmann, C. (2017). Hybrid laser-arc welding of steel S700MC butt joints under different sheet thickness. *Proceedings of Lasers in Manufacturing (LIM).* Munch, Germany: WLT Wissenschaftliche Gesellschaft Lasertechik e.V.

Poole, S., Payne, D., Mears, R., Fermann, M., & Laming, R. (1986). Fabrication and Characterization of Low-Loss Optical Fibers Containing Rare-Earth Ions. *Journal of Lightwave Technology, LT-4*(7), 870 - 876.

Popp, A., Voss, A., Graf, T., Unger, S., Kirchhof, J., & Bartelt, H. (2010). Thin-disk-laser-pumped ytterbium-doped fiber laser with an output power in the kW range. *Solid State Lasers and Amplifiers IV, and High-Power Lasers, 7721*, 772102.

Poprawe, R. (2005). *Lasertechnik für die Fertigung.* Berlin Heidelberg: Springer-Verlag.

Quintino, L., Costa, A., Miranda, R., & Yapp, D. (2007). Welding with high power fiber lasers - a preliminary study. *Materials & Design, 4*, 1231 - 1237.

Reutzel, E., Sullivan, M., & Mikesic, D. (2006). Joining Pipe with the Hybrid Laser-GMAW Process: Weld Test Results and Cost Analysis. *Welding Journal, 85*(6), 66 - 71.

Richardson, D. J., Nilsson, J., & Clarkson, W. (2010). High power fiber lasers: current status and future perspectives. *J. Opt. Soc. Am. B, 27*(11), B63 - B91.

Röhner, M., Wagner, L., Pietrzak, A., & Hülsewede, R. (2013). Fiber-Coupled High-Power Diode-Lasers with Highest Radiance. *High Power Diode Laser and Systems Conference* (pp. 36 - 37). IEEE.

Roland, F., Manzon, L., Kujala, P., Brede, M., & Weitzenböck, J. (2004). Advanced Joining Techniques in European Shipbuilding. *Journal of Ship Production, 20*(3), 200 - 210.

Rominger, V., Koitzscha, M., Kuhnb, V., Gottwaldb, T., Stolzenburg, C., Holzer, M., . . . Rybac, T. (2015). Latest trends in high power disk laser technology. *Proceedings of Lasers in Manufacturing (LiM), World of Photonics Congress.* Munich, Germany: WLT Wissenschaftliche Gesellschaft Lasertechnik e.V.

Ross, T., & Latham, W. (2006). Appropriate Measures and Consistent Standard for High Energy Laser Beam Quality. *Journal of Directed Energy, 2*, 22 - 58.

Rules for classification - Ships - Part 2 Materials and welding - Chapter 4 Fabrication and testing. (2018). Hamburg, Germany: DNVGL AS.

Seffer, O., Lindner, J., Springer, A., Kaierle, S., Wesling, V., & Haferkamp, H. (2012). Laser GMA hybrid welding for thick wall applications of pipeline steel with the grade X70. *Proceedings of the Laser Materials Processing Conference ICALEO 2012.* Laser Institute of America, Paper 1505.

Seyffarth, P., & Krivtsun, I. (2002). *Laser-Arc Processes and their Applications in Welding and Material Treatment.* New York, NY: Tayler & Francis.

Shcheglov, P. (2012). *Study of Vapour-Plasma Plume during High Power Fiber Laser Beam Influence on Metals.* Berlin: BAM Bundesanstalt für Materialforschung und -prüfung.

Shelyagin, V., & Khaskin, V. (2002). Tendencies In Development Of Laser-Arc Welding (Review). *The Paton Welding Journal, 6*, 25 - 28.

Shi, W., Fang, Q., Zhu, X., Norwood, R. A., & & Peyghambarian, N. (2014). Fiber lasers and their applications. *Applied Optics, 53*(28), 6554 - 6568.

Shiner, B. (2006). High-power fiber lasers gain market share. *Industrial Laser Solutions, 21*(2), 1 - 3.

Shiner, B. (2010). Delivering Power. *Nature Photonics, 4*, 290.

Shiner, B. (2016). Fiber Lasers Continue to Gain Market Share in Material Processing Applications. *Manufacturing Engineering, 156*(2), 79 - 85.

Smith, R. (1972). Optical Power Handling Capacity of Low Loss Optical Fibers as Determined by Stimulated Raman and Brillouin Scattering. *Applied Optics, 11*(11), 2489 - 2494.

Snitzer, E. (1961). Cylindrical Dieelectric Waveguide Modes. *J. Opt. Soc. Am., 51*, 491 - 498.

Snitzer, E., Po, H., Hakimi, F., Tumminelli, R., & McCollum, B. C. (1988). Double clad, offset core Nd fiber laser. *Optical Society of America*, PD5.

Snitzer, E., Po, H., Hakimi, F., Tumminelli, R., & McCollum, B. C. (1988). Erbium Fiber Laser Amplifier at 1.55µm with Pump at 1.49µm and Yb Sensitized Er Oscillator. *Optical Fiber Communication, 1*, PD2.

Sokolov, M., & Salminen, A. (2012). Experimental investigation of the influence of edge morphology in high power fiber laser welding. *Physics Procedia, 39*, 33 - 42.

Sokolov, M., Salminen, A., Kuznetsov, M., & Tsibulskiy, I. (2011). Laser welding and weld hardness analysis of thick section S355 structural steel. *Materials and Design, 32*, 5127 - 5131.

Spinelli, C., & Prandi, L. (2012). High Grade Steel Pipeline for Long Distance Projects at Intermediate Pressure. *7th Pipeline Technology Conference 2012.* Hannover.

Stachowiak, D. (2018). High-Power Passive Fiber Components for All-Fiber Lasers and Amplifiers Application—Design and Fabrication. *Photonics, 5*(38).

Stark, J. (1914). Beobachtungen über den Effekt des elektrischen Feldes auf Spektrallinien. *Annalen der Physik, 43*(4), 965 - 982.

Steen, W. (1980). Arc augmented laser processing of materials. *J. Appl. Phys., 51*(11), 5636 - 5641.

Steen, W. (2003). *Laser material processing.* London: Springer-Verlag.

Steen, W., & Eboo, M. (1979). Arc augmented laser welding. *Metal Construction, 11*(7), 332 - 335.

Stiller, B. (2012). *Brillouin scattering in photonic crystalfiber: from fundamentals to fiberoptic sensors.* Doctoral dissertation, Université de Franche-Comté.

Sun, J., Feng, K., & Zhang, K. (2017). Fiber laser welding of thick AISI 304 plate in a horizontal (2G) butt joint configuration. *Materials and Design, 118*, 53 - 65.

Tammela, S., Söderlund, M., Koponen, J., Philippov, V., & Stenius, P. (2006). The Potential of Direct Nanoparticle Deposition for the Next Generation of Optical Fibers. *Proceedings of SPIE Photonics West, 6116*(16).

Tarasawa, S., Zhang, X., & Ashida, E. (2010). Multi-passes narrow gap laser welding process for thick section stainless steels. *Proceedings of the IIW2010 Commission IV - Power Beam Processes.* Istanbul, IV-1016-10.

Taverner, D., Richardson, D., Dong, L., Caplen, J., Williams, K., & Penty, R. (1997). 158-μJ pulses from a single-transverse-mode, large-mode area erbium-doped fiber amplifier. *Opt. Lett., 22*, 378 - 380.

Thomy, C., Seefeld, T., & Vollertsen, F. (2006). Industrial Potential for high power fibre laser welding. *The Industrial Laser User, 42*, 22 - 25.

Träger, F. (2012). *Springer Handbook of Lasers and Optics.* New York: Science+Business Media LLC.

Trumpf. (2019). *www.trumpf.com.* Retrieved July 19, 2019, from https://www.trumpf.com/filestorage/TRUMPF_Master/Products/Lasers/02_Brochures/TRUMPF-TruDisk-Flyer-DE.PDF

Turichin, G., Kuznetsov, M., Tsibulskiy, I., & Firsova, A. (2017). Hybrid Laser-arc Welding of the High-Strength Shipbuilding Steels: Equipment and Technology. *Physics Procedia, 89*, 156 - 163.

Turichin, G., Velichko, O., Kuznetsov, A., Pevzner, J., Grinin, O., & Kuznetsov, M. (2014). Mobile Hybrid system for pipeline welding on the base of 20 kW fiber laser. *8th International Conference on Photonic Technologies LANE 2014.* Bayrisches Laserzentrum GmbH.

Unt, A. (2018). *Fiber laser and hybrid welding of T-joints in structural steels.* Dissertation, Lappeenranta University of Technology.

Unt, A., Poutiainen, I., & Salminen, A. (2014). Effects of sealing run welding with defocused laser beam on the quality of T-joint fillet weld. *Physics Procedia, 56*, 497 - 506.

Unt, A., Poutiainen, I., & Salminen, A. (2015). Influence of Filler Wire Feed Rate on Laser-Arc Hybrid Welding of T-butt Joint in Shipbuilding Steel with different optical setups. *Physics Procedia, 78*, 45 - 52.

Üstündag, Ö., Avilov, V., Gumenyuk, A., & Rethmeier, M. (2018). Full penetration hybrid laser arc welding of up to 28 mm thick S355 plates using electromagnetic weld pool support. *Journal of Physics: Conference Series, 1109*(conference 1), 1 - 7.

van Wachem, B., & Sasic, S. (2008). Derivation, simulation and validation of a cohesive particle flow CFD model. *AIChE Journal, 54*(1), 9-19.

Vänskä, M. (2014). *Defining the keyhole modes – the effects on the weld geometry and the molten pool behaviour in high power laser welding of stainless steels.* Dissertation, Lappeenranta University of Technology.

Vänskä, M., Purtonen, T., & Salminen, A. (2011). Orbital cutting and welding of stainless steel tubes with a fiber laser. *Proceedings of the Laser Materials Processing Conference ICALEO 2011.* Laser Institute of America, Paper 1506.

Vermillac, M., Fneich, H., Lupi, J.-F., Tissot, J.-B., Kucera, C., Vennegues, P., . . . Blanc, W. (2017). Use of thulium-doped LaF3 nanoparticles to lower the phonon energy

of the thulium's environment in silica-based optical fibres. *Optical Materials, 68*, 24 - 28.

Victor, B. (2011). Hybrid Laser Arc Welding. In T. Lienert, T. Siewert, S. Babu, & V. Acoff, *ASM Handbook, Welding Fundamentals and Processes* (Bd. 6A). ASM International.

Vollertsen, F., & Neumann, S. (2009). High brightness solid state laser: Development and application. *Proceedings of LAMP 2009 - 5th International Congress on Laser Advanced Materials Processing, online.*

Vollertsen, F., & Thomy, C. (2005). Welding with fiber lasers from 200 to 17000 W. *Proceedings of the Laser Materials Processing Conference ICALEO 2005.* Laser Institute of America, Paper 506.

Wadsworth, W. J., Percival, R. M., Bouwmans, G., Knight, J. C., & J. Russell, P. S. (2003). High power air-clad photonic crystal fibre laser. *Optics Express, 11*(1), 48 - 53.

Wahba, M., Mizutani, M., & Katayama, S. (2016). Single pass hybrid laser-arc welding of 25 mm thick square groove butt joints. *Materials and Design, 97*, 1 - 6.

Wang, L., He, D., Feng, S., Yu, C., Hu, L., & D., C. (2015). Ytterbium-doped phosphate glass single mode photonic crystal fiber with all solid structure. *Optical Materials Express, 5*(4), 742 - 747.

Wang, P., Sahu, J. K., & Clarkson, W. A. (2007). Power Scaling of Ytterbium-doped Fiber Superfluorescent Sources. *IEEE Journal of Selected Topics in Quantum Electronics, 13*(3), 580 - 587.

Westin, E., Stelling, K., & Gumenyuk, A. (2011). Single-Pass Laser-GMA Hybrid Welding of 13.5 mm thick dupley stainless steel. *Welding in the World, 55*(01-02), 39 - 49.

White, J. O. (2009). Parameters for Quantitative Comparison of Two-, Three-, and Four-Level Laser Media, Operating Wavelengths, and Temperatures. *IEEE Journal of Quantum Electronics, 45*(10), 1213 - 1220.

Wieschemann, A. (2001). *Entwicklung des Hybrid- und Hydraschweißverfahrens am Beispiel des Schiffbaus.* Aachen: Shaker Verlag.

Wirth, C., Schmidt, O., Tsybin, I., Schreiber, T., Eberhardt, R., Limpert, J., . . . M., J. (2011). High average power spectral beam combining of four fiber amplifiers to 8:2kW. *Optics Letters, 36*(16), 3118 - 3120.

Xiao, H., Leng, J., Zhang, H., Huang, L., Xu, J., & Zhou, P. (2015). High-power 1018 nm ytterbium-doped fiber laser and its application in tandem pump. *Applied Optics, 54*, 8166 - 8169.

Yapp, D., & Blackman, S. (2004). Recent Developments in High Productivity Pipeline Welding. *J. of the Braz. Soc. of Mech. Sci. & Eng., 26*(1), 89 - 97.

Yapp, D., & Liratzis, T. (2010). Development of high productivity pipeline girth welding. *Australasian Welding Journal, 55*(4), 26 - 37.

Zervas, M. N., & Codemard, C. A. (2014). High Power Fiber Lasers: A Review. *IEEE Journal of Selected Topics in Quantum Electronics, 20*(5), 0904123.

Zhang, M., Chen, S., Zhang, Y., Chen, G., & Bi, Z. (2018). Mechanisms for Improvement of Weld Appearance in Autogenous Fiber Laser Welding of Thick Stainless Steels. *Metals, 8*(625).

Zhou, P. X., Leng, J., Xu, J., Chen, Z., Zhang, H., & Liu, Z. (2018). High-power fiber lasers based on tandem pumping. *J. Opt. Soc. Am., B34*, A29-A36.

Publications

Publication I

Vollertsen, F., Grünenwald, S., Rethmeier, M., Gumenyuk, A., Olschock, S.
Welding Thick Steel Plates with Fibre Lasers and GMAW

Reprinted with permission from
Welding in the World
Vol. 54, pp. R62 – R70, 2010

WELDING THICK STEEL PLATES WITH FIBRE LASERS AND GMAW






F. Vollertsen **S. Grünenwald** **M. Rethmeier** **A. Gumenyuk** **U. Reisgen** **S. Olschok**

ABSTRACT

The results of a collaborative research project on laser beam weldability of carbon steels of high sheet thickness are presented. That includes single and multiple pass welding of 16 mm and 20 mm thick plates, as well as the investigation of acceptable tolerances i.e. gap bridgeability and edge misalignment. For the welding experiments fibre lasers with 8 kW, 20 kW laser power and different GMAW-techniques were used in various applications. With the 20 kW fibre laser 16 mm plates could be welded with a single pass, 20 mm required a seam preparation or alternatively preheating of the material. For multi pass welding with 8 kW laser power a joint preparation with a single V-butt joint with a broad root face (Y-groove) was applied. The root pass was always welded with a hybrid process, the filler passes with a hybrid process as well as a GMAW process which produced the best results.

IIW-Thesaurus keywords: *Arc welding; Carbon steels; Combined processes; Fibre lasers; Gas shielded arc welding; GMA welding; Multirun welding; Reference lists; Steels; Unalloyed steels.*

1 INTRODUCTION

Joining thick steel plates with conventional GMAW processes used for example in the field of shipbuilding or pipe laying requires a high number of different weld passes. Single pass GMA welding is not a suitable process at a sheet thickness far above 5 mm, as the melt pool becomes very large, which is difficult to control and comes along with a very high heat input into the base material. As a solution processes such as modern hybrid welding systems employing high power lasers are sought-after. Expected benefits are the reduction of required weld passes, the increase of welding speed and the decrease of the heat input, which leads to less distortion and thus less rework for straightening [1, 2]. Following the first ideas of Steen [3] implementations have been made in the past combining CO_2-lasers or Nd:YAG lasers with high powers with a GMAW process to a hybrid process [4]. Fields of application are thick section welding [5-7], e.g. pipe production.

The possibility to transport the laser beam in an optical fibre offers a high degree of freedom for solid state lasers. With the introduction of fibre lasers into welding technology, laser powers of 20 kW and more in cw mode with an excellent beam quality combined with high efficiencies at high laser powers, solid state lasers have become a viable alternative to CO_2 lasers in the above mentioned fields [8], especially due to the additional high degree of mobility for the recent solid state

Prof. Frank VOLLERTSEN (vollertsen@bias.de) and Mr. Stefan GRÜNENWALD (gruenenwald@bias.de), M.Sc., are both with BIAS-Institute of Applied Beam Technology, Bremen (Germany). Prof. Michael RETHMEIER (michael.rethmeier@bam.de) and Dr.-Ing. Andrey GUMENYUK (andrey.gumenyuk@bam.de) are both with BAM – Federal Institute for Material Research and Testing, Berlin (Germany). Prof. Uwe REISGEN (institutsleiter@isf.rwth-aachen.de) and Dr.-Ing Simon OLSCHOK (ol@isf.rwth-aachen.de) are both with ISF – Welding and Joining Institute, RWTH Aachen University, Aachen (Germany).

Doc. IIW-1967-08 (ex-doc. IV-965r1-08), recommended for publication by Commission IV “Power Beam Processes.”

laser concepts. Pipe laying [9] or shipbuilding [10] are examples for applications.

In order to study the potential of fibre lasers together with GMAW-hybrid technique for such kind of applications, a joint project was run with, for example, the purpose of qualifying laser and laser-GMA-hybrid welding processes using lasers of high power and beam quality in the field of heavy industry, shipbuilding, and pipe production for thick materials of plate thickness between 16 mm and 32 mm. The focus in this paper is on 16 mm material which was extensively tested as well as on 20 mm welds. The objectives strived for in particular are the determination of the process boundaries correspondent to the maximum achievable plate thickness for one pass welding as well as acceptable production tolerances (gap and edge misalignment) during welding of low alloyed steels with laser-GMA hybrid welding technique. Further tasks were the determination of a process window for single pass welding providing a good quality of the root pass and developing a strategy for multi pass welding.

2 EXPERIMENTAL WORK

2.1 Material

As a base material for this set of experiments, steel with reduced contents of carbon has been chosen. This steel grade is thermo mechanically rolled and rapidly cooled and has a high yield strength (at least 460 MPa) and a high impact toughness (at least 450 J at -40 °C). It is used for manufacturing large diameter pipes and is specified as X65 according to API 5L standard. The chemical composition of the welded material is given in Table 1. The dimensions of the material used for the experiments were 300 mm × 40 mm with a thickness of 16 mm and 20 mm for single pass welding, as well as 350 mm × 200 mm with a thickness of 16 mm for multi pass welding.

As filler wire electrodes of type G3Si1 and G4Si1 according to DIN EN 440 standard have been used.

The shielding gases for the laser-GMA-hybrid welding process have been chosen according to European standard DIN EN 439, M21. Gas mixtures with 82 % Ar and 18 % CO_2 as well as 90 % Ar and 10 % CO_2 have been used.

Especially for welding multiple passes a joint preparation with a single V-butt joint with a broad root face (Y-groove) was used, Figure 1. Two different included angles were applied, using α = 45° and α = 60°. The root face c varied from 6 mm to 10 mm and the size of the gap b ranged from 0 mm up to 1.2 mm. All experiments were done in flat position.

2.2 Experimental setup 8 kW-laser

The experimental setup for laser-GMA-hybrid welding consisted of a YLR-8000 S fibre laser source with 8 kW output power, a DalexVario MIG 600 l(w)-B power source, an Abicor Binzel APD wire feed unit and a hydraulically operated clamping device. A special feature of the YLR-8000 S fibre laser is the 100 µm feeding fibre coming from the beam combiner and not being interrupted by an optical coupler or a beam switch, thus acting as the processing fibre at the same time. This configuration of the fibre laser allows a very high brightness of the laser beam and consequently a very high beam quality of 4.2 mm*mrad. The fibre was connected to a 160 mm Optoskand collimator mounted on a Trumpf BEO D70 laser welding head with a 280 mm focusing lens. Together with a specially developed GMAW torch, the laser welding head was mounted to a gantry robot work station, Figure 2.

The welding torch was fixed at an angle of 22° and can be used in a trailing as well as a leading position. For the welding experiments, the torch was applied exclusively in the leading position. By using the fine adjustment the position of the torch relative to the laser beam could be changed. Table 2 gives an overview of the parameters used for the experiments.

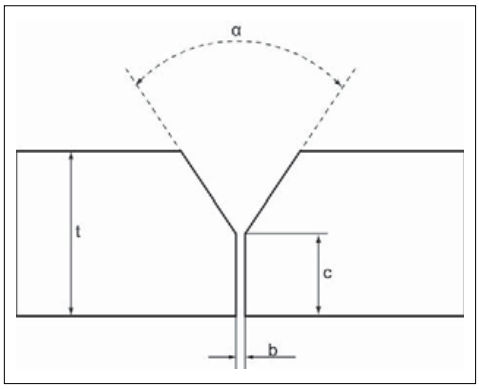

Figure 1 – Joint preparation

Table 1 – Chemical composition of the material used

Chemical Analysis (mass parts in %)													
C	**Si**	**Mn**	**P**	**S**	**Cr**	**Ni**	**Ti**	**Nb**	**Cu**	**Al**	**Mo**	**V**	**B**
X 65, t = 16 mm													
0.04	0.34	1.48	0.006	< 0.001	0.17	0.03	0.012	0.04	0.02	0.03	< 0.01	0.003	< 0.0001
X 65, t = 20 mm													
0.08	0.28	1.67	0.012	< 0.001	< 0.01	< 0.01	0.012	0.05	< 0.01	0.03	< 0.01	0.002	< 0.0001

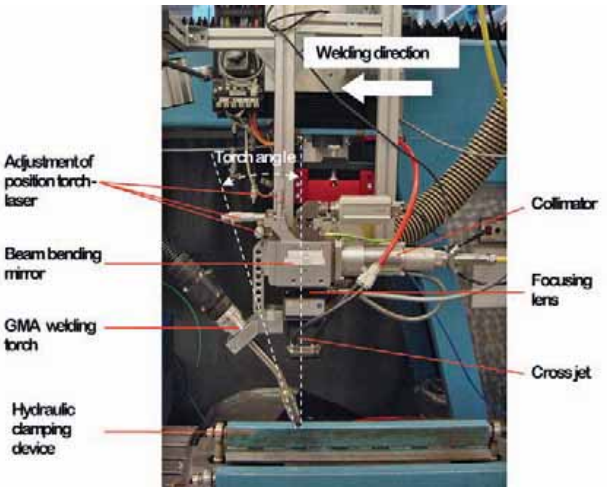

Figure 2 – Experimental setup for laser-GMA-hybrid welding with 8 kW

2.3 Experimental setup 20 kW-laser

A 20 kW Yb fibre laser oscillator from IPG Photonics with a 200 µm optical feeding fibre was used for welding 16 mm and 20 mm thick material using the single laser beam for welding as well as combined with GMAW to a hybrid process. The laser has a BPP of ca. 11.5 mm*mrad. As a focusing optic the optical head of HIGHYAG with a 125 mm collimator and 350 mm focal length was used for this set of experiments. The correspondent theoretical focal spot diameter was 560 µm and the Rayleigh length 5.7 mm. As a GMAW power source digital equipment Quinto QLS 403 has been used. It has an integrated pull-push drive allowing filler wire feed rates up to 30 m/min. The power source allows a welding current up to 400 A at 60 % duty cycle. In this series of experiments the maximum average current of up to 550 A at a maximum welding time of 10 s has been applied. The integrated air cooled GMAW torch has been mounted on the welding optics with a constant inclination angle of 25° to the beam axis, and has the possibility to move its position in 3 directions, Figure 3. Most important for this set of experiments was the possibility to shift the torch in a direction parallel to the beam axis. The relative movement between the laser beam and workpiece was realised by a numerically controlled X-Y coordinate table. For changing the spatial orientation of the optics and control of the height a 6-axis Cloos robot supporting the welding optics and hybrid equipment has been used.

Table 2 – Parameters used for multipass welding experiments

Parameters for setup and material		Process parameters	
Laser type	IPG YLR 8000 S	Joint type	V-butt with broad root face
Laser power	8 kW	Root face size	6-10 mm
Focal length	280 mm	Joint gap size	0-1.2 mm
Focal spot diameter	0.22 mm	Included angle	45°, 60°
Welding torch position and angle	Leading at 22°	Welding position	PA
		Welding speed	0.4-1.8 m/min
Parent metal and thickness	X 65, t = 16 mm,	Filler wire feed rate	6.0 m/min - 13.5 m/min
Filler wire and diameter	Union K56 S (G46 4M G4Si1), Ø 1.2 mm	Wire stick out	12 mm
		Current	210-420 A
		Voltage	22-35 V
		Laser-arc distance	3 mm
		Focal position	-2 mm*, 0 mm**
		Shielding gas and flow rate	90 % Ar + 10 % CO_2 at 20 l/min

** Relating to the top of the root face for the root pass.*
*** Relating to the top of the process for the filler passes.*

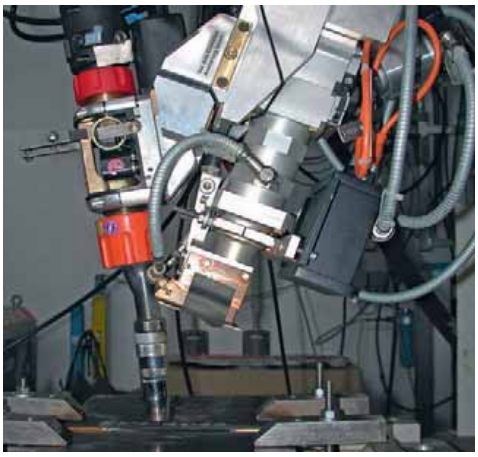

Figure 3 – Hybrid welding head consisting of a 350 mm focal length (right) and a GMAW torch (left) used with 20 kW laser power

3 RESULTS

3.1 Single pass welding

3.1.1 Autogenous laser welding

With 20 kW of laser power it was possible to weld 16 mm and 20 mm in a single pass autogenously. Joining 20 mm thick plates as shown in Figure 4 required 19 kW of laser power at a welding speed of 1.3 m/min with a focal position of -6 mm. A slotted gas nozzle placed above the actual welding process improved the weld seam quality. The top of the weld seam is of acceptable quality, the root side shows a shrinkage groove.

Figure 4 – Single pass welding of 20 mm thick material with an autogenous laser process

3.1.2 Variation of air gap sizes in hybrid welding

With 16 mm thick material, gaps up to a size of 0.35 mm could be successfully bridged, with a laser-GMA-hybrid process, welding a single pass using a square butt joint. However, gaps as large as 0.5 mm were difficult to weld with a single pass at these material thicknesses, Figure 5. The parameters are listed in Table 3.

3.1.3 Variation of edge misalignment in hybrid welding

Hybrid welding 16 mm thick material with vertical misalignment showed results with an acceptable root up to a misalignment of 1 mm. Drops start to form at the root side with a vertical misalignment above 2 mm, see Figure 6 and Table 4 for parameters used. The drop formation could be reduced or fully avoided by using adapted parameters; i. e. increased welding speed or

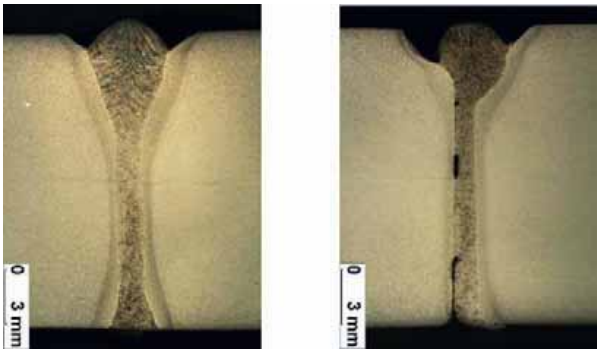

a) 0.35 mm gap **b) 0.5 mm gap**

Figure 5 – Single pass welding of 16 mm material bridging gaps, without joint preparation

Table 3 – Parameters for welded samples with gap in a single pass

Laser power [kW]	Welding speed [m/min]	Wire feed speed [m/min]	Current (mean) [A]	Voltage (mean) [V]	Gap [mm]	Focal position [mm]
17	2.1	15	381	35.8	0.35 / 0.5	-4

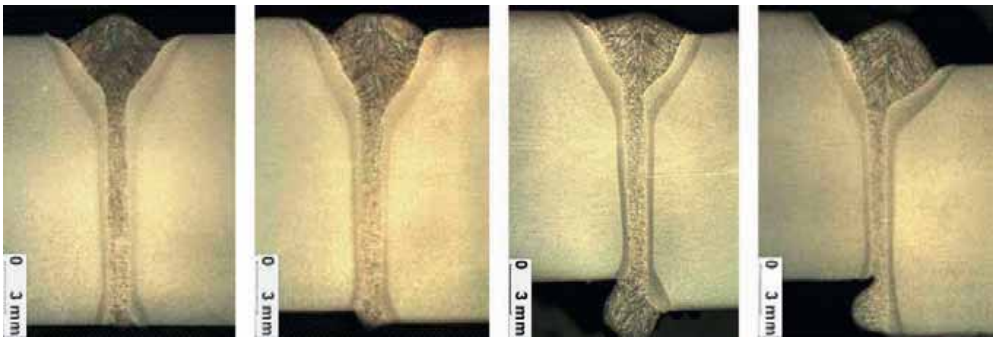

a) Linear misalignment of 0 mm **b) Linear misalignment of 1 mm** **c) Linear misalignment of 2 mm** **d) Linear misalignment of 3 mm**

Figure 6 – Single pass welding of 16 mm material with linear misalignment varying from 0 mm to 3 mm

Table 4 – Parameters for welded samples with linear misalignment in a single pass, Figures 6 and 7

Laser power [kW]	Welding speed [m/min]	Wire feed speed [m/min]	Current (mean) [A]	Voltage (mean) [V]	Gap [mm]	Focal position [mm]
Figure 6						
17	2.3	16	436	37	0	-4
Figure 7a)						
17	2.5	16	443	37.2	0	-4
Figure 7b)						
17	2.5	16	439	37.1	0	0

a variation of the focal position. The best result was achieved using another focal position, Figure 7.

3.1.4 Hybrid welding of 20 mm plates

For welding 20 mm thick plates with a hybrid process, either a joint preparation or preheating the material was necessary to join these plates with a single pass. For the joint preparation a 16 mm root face and a 30° included angle was chosen, Figure 8 a). The preheated material had a temperature of 160 °C when welded and was joined with a square butt joint, figure 8 b). The parameters for the welds are given in Table 5.

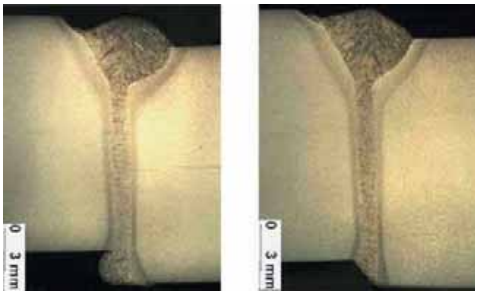

a) Welding speed increased **b) Focus position changed to surface of upper plate**

Figure 7 – Single pass welding with adapted parameters of 16 mm material with linear misalignment of 2 mm

3.2 Multipass welding

3.2.1 Root pass welding

Applying multiple passes with a laser-GMA-hybrid welding process required a different approach to join 16 mm plates or thicker material. With 8 kW laser power available, a joint preparation with root faces between 6 mm and 10 mm and included angles of 45° to 60° was needed for multi pass welding.

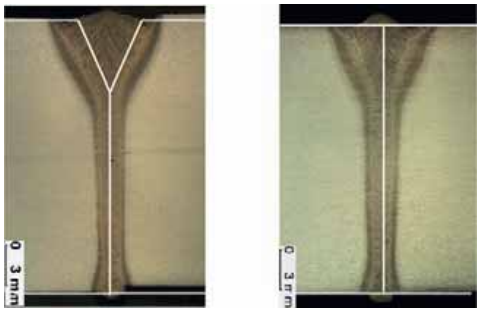

a) with joint preparation **b) with preheating**

Figure 8 – Single pass welding of 20 mm material

Table 5 – Parameters for single pass welding of 20 mm material

Root face [mm]	Included angle [deg.]	Laser power [kW]	Welding speed [m/min]	Wire feed speed [m/min]	Current (mean) [A]	Voltage (mean) [V]	Gap [mm]	Focal position [mm]
Figure 8a (with joint preparation)								
16	30	17	1.8	18	509	38.1	0	-4
Figure 8b (preheated to 160°C)								
-	-	19	1.9	16.5	422	33.7	0	-4

Welding the root pass also with variation of gap and linear misalignment, worked well with a hybrid process. A root face of 6 mm with the joint unchanged as well as 8 mm root face with linear misalignment of 0.5 mm and a root face of 8 mm with a gap of 0.8 mm could be welded, see Figures 9 to 11 and Table 6 for parameters. The crack visible in Figure 11, on the top side of the weld bead, is of minor importance in the root pass. It will be re-melted when welding the second pass and then disappears, or can be easily avoided by preheating the material before welding.

3.2.2 Variation of air gap sizes

When welding 16 mm thick material with a root face of 10 mm and an included angle of 60°, with a laser-GMA-hybrid welding process, it was possible to bridge gaps up to 1.2 mm wide with one root pass. Gaps were successively increased by 0.2 mm starting from 0 mm to 1.2 mm. A second layer, also welded with a hybrid process, was needed to fill the remaining groove. The welding speed for the second layer was gradually reduced to be able to fill the remaining groove properly. For sufficient gap bridging, the wire feed rate for the root pass was increased with the gap becoming wider. Pores occurred in all welded samples, undercuts in those with insufficient filler material fed during welding. Figures 12 to 14 show cross sections with gap sizes 0 mm, 0.6 mm and 1.2 mm. Table 7 shows the parameters used for welding.

3.2.3 Variation of edge misalignment

In addition to variation of the gap in a weld seam, edge misalignment was introduced. The 16 mm material was welded with a V-butt joint, root face of 8 mm, gap 0.5 mm and an included angle of 60°. A sound root with both edges melted properly was achieved with a value for edge misalignment of 0.5 mm. Values

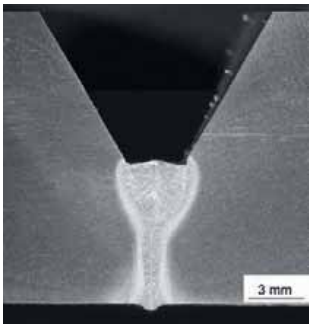

Figure 9 – Cross-section of a root pass of a hybrid welded sample with 0 mm gap

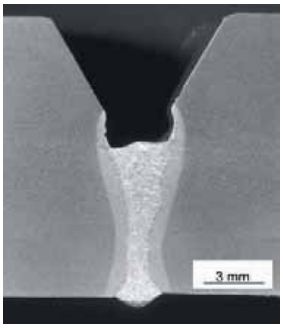

Figure 10 – Cross-section of a root pass of a hybrid welded sample with 0.8 mm gap

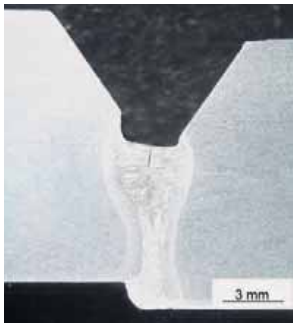

Figure 11 – Cross-section of a root pass of a hybrid welded sample with 0.5 mm gap and linear misalignment of 0.5 mm

Table 6 – Parameters for samples with root pass welded

Layer no.	Root face [mm]	Included angle [deg.]	Laser power [kW]	Welding speed [m/min]	Wire feed speed [m/min]	Current (mean) [A]	Voltage (mean) [V]	Gap [mm]	Focal position [mm]
Figure 9 (0 mm gap)									
1	6	60	7.6	1.8	6.5	229	23.6	0	-2
Figure 10 (0.8 mm gap)									
1	8	60	7.6	1.6	8.5	298	27.3	0.8	-2
Figure 11 (0.5 mm gap, 0.5 mm linear misalignment)									
1	8	60	7.6	1.8	7.5	330	23.7	0.5	-2

Figure 12 – Cross-section of a hybrid welded sample with 0 mm gap

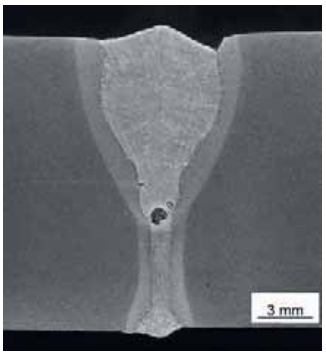

Figure 13 – Cross-section of a hybrid welded sample with 0.6 mm gap

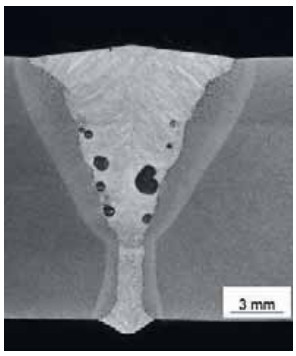

Figure 14 – Cross-section of a hybrid welded sample with 1.2 mm gap

Table 7 – Parameters for welded samples with gap

Layer no.	Root face [mm]	Included angle [deg.]	Laser power [kW]	Welding speed [m/min]	Wire feed speed [m/min]	Current (mean) [A]	Voltage (mean) [V]	Gap [mm]	Focal position [mm]
Figure 12 (0 mm gap)									
1	10	60	7.6	1.4	7.0	210	24.3	0	-2
2	10	60	2.0	1.4	13.5	347	33.6	-	0
Figure 13 (0.6 mm gap)									
1	10	60	7.6	1.4	8.5	232	26.5	0.6	-2
2	10	60	2.0	1.1	13.0	375	35.8	-	0
Figure 14 (1.2 mm gap)									
1	10	60	7.6	1.4	10	277	30.1	1.2	-2
2	10	60	2.0	0.5	12.5	327	32.6	-	0

beyond 0.5 mm produced a root with improper fusion of the melt between the misaligned faces with droplets which started to form on the root side. Pores and cracks occurred only in the filler passes, which were also welded with a hybrid process. Figures 15 to 17 and Table 8 give an overview of welded samples and the parameters used.

3.2.4 Multi pass welding with GMA filler passes

Since acceptable filler passes with a hybrid welding process could not be achieved under the given conditions, it was decided to weld the filler passes with conventional arc welding and use the hybrid process for the root pass only, in order to obtain acceptable

Figure 15 – Cross-section of a hybrid welded sample with 0.5 mm gap and 0.5 mm linear misalignment

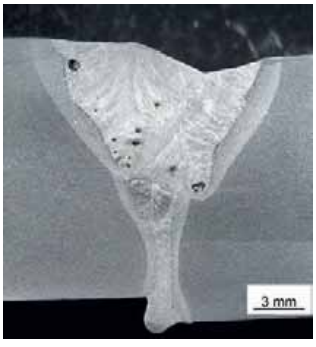

Figure 16 – Cross-section of a hybrid welded sample with 0.5 mm gap and 1.5 mm linear misalignment

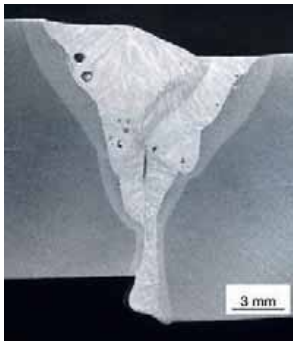

Figure 17 – Cross-section of a hybrid welded sample with 0.5 mm gap and 3 mm linear misalignment

Table 8 – Parameters for welded samples with linear misalignment

Layer no.	Root face [mm]	Included angle [deg.]	Laser power [kW]	Welding speed [m/min]	Wire feed speed [m/min]	Current (mean) [A]	Voltage (mean) [V]	Gap [mm]	Focal position [mm]
Figure 15 (0.5 mm linear misalignment)									
1	8	60	7.6	1.8	8.0	234	26.7	0.5	-2
2	8	60	0	0.4	10.5	-	-	-	0
Figure 16 (1.5 mm linear misalignment)									
1	8	60	7.6	1.8	8.0	339	23.8	0.5	-2
2	8	60	4.0	1.6	11.0	413	31.9	-	0
3	8	60	4.0	0.8	10.0	329	29.3	-	0
4	8	60	4.0	0.8	10.5	334	29.2	-	0
Figure 17 (3.0 mm linear misalignment)									
1	8	60	7.6	1.8	6	231	22.6	0.5	-2
2	8	60	2.0	1.6	12.5	422	30.5	-	0
3	8	60	2.0	0.8	10.0	310	29.7	-	0
4	8	60	2.0	0.8	10.0	318	29.5	-	0

welds. An optimised parameter set was applied for welding 16 mm thick material. Figure 18 shows a cross-section of a sample welded with two passes, the first one with a laser-GMA-hybrid welding process and the second one with a conventional GMAW welding process. The root face was chosen to be 10 mm with an included angle of 45°, to have a groove remaining as small as possible which has to be filled with conventional welding. A gap of 0.5 mm was necessary for full penetration of the material. Parameters for the welded sample shown are given in Table 9.

4 DISCUSSION

Concerning the welding of multiple passes for joining 16 mm thick materials, laser-GMA-hybrid welding for the root passes showed satisfactory up to good results, especially for bridging large gaps. Using a gap also helped to increase the penetration depth of the laser beam as shown in Figures 12 and 13 where it was not possible to fully penetrate a prepared seam with 10 mm root face and 60° included angle when the two plates were joined without a gap. The restrictive feature for the lower penetration depth – compared to autogenous laser welding in this case – is the leading arc process in combination with the chosen seam preparation and the hybrid process. The arc burns above the root face in the groove, the laser beam has to penetrate the melt pool of the arc process and the base material joined with a zero gap. An increase of the gap to 0.2 mm already helped to successfully penetrate the material; a gap size around 0.5 mm as shown above produced the best results in the experiments carried out. Concerning the filler passes, a successive reduction of the welding speed starting from 1.4 m/min down to 0.5 m/min did not help to reduce the formation of pores in the weld seam. The only beneficial effect of reducing the welding speed was a better filling of the remaining groove where undercuts could be avoided.

In contrast to the experiments with no edge misalignment, where a gap of 0.5 mm to 0.6 mm supported the melting of the fusion faces, welding with edge misalignment proved to be difficult. An increase of the wire feed rate added up to the formation of drops on the root side, but did not help in wetting and/or melting both faces of the workpiece. Regarding the multiple passes welded, as shown especially in Figures 16 and

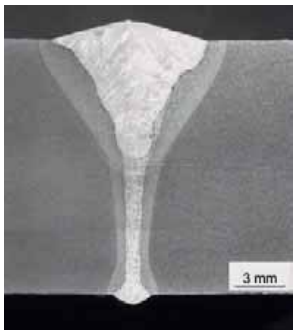

Figure 18 – Cross-section of a hybrid welded sample with optimised parameters for 0.5 mm gap

Table 9 – Parameters for the welded sample shown in Figure 18

Layer no.	Root face [mm]	Included angle [deg.]	Laser power [kW]	Welding speed [m/min]	Wire feed speed [m/min]	Current (mean) [A]	Voltage (mean) [V]	Gap [mm]	Focal position [mm]
1	10	45	7.6	1.6	9	372	25.9	0.5	-2
2	10	45	-	0.4	8.5	290	28.3	-	0

17, where 4 passes were used altogether, altering the parameters did not change the result in terms of pores or cracks. A reduction of the laser power for the filler passes of 50 %, compare parameters for samples depicted in Figures 16 and 17, for example, did not have any effect on the welded seam. Also altering the welding speed from 1.6 m/min to 0.8 m/min within the same weld seam did not benefit the quality.

A successful method to utilise the benefits of a laser-GMA-hybrid welding process as well as the conventional GMAW welding process was to weld the root pass first with the hybrid process and secondly use a GMAW process for filling up the remaining groove. Two passes were needed which produced an acceptable root quality and a pore and crack free weld seam. Despite that successful weld, the big disadvantage of that strategy is the slow welding speed of only 0.4 m/min – the advantages of the laser hybrid process vanishes to a certain extent. Kristensen [11], who also observed pores in the root of the second pass of a multi pass hybrid weld, suggests the low welding speed as the origin of the pores. Due to the much higher speeds used in this investigation (up to 1.4 m/min) compared to that work (0.5 m/min) it is questionable, whether this explanation will hold. Further work has to be done in this field.

5 CONCLUSION

Despite the fact that these are preliminary results of ongoing work, it has shown successful welding within the following limits:

– Autogenous laser welding was used to join plates up to 20 mm thickness with 19 kW at 1.3 m/min without a seam preparation.

– Laser-GMA-hybrid welding of 16 mm thick material was possible with a square butt joint and a single pass at 17 kW and 2.1 m/min.

– 20 mm material welded with a hybrid process required 19 kW and a joint preparation. As an alternative, square butt joint welding was possible when using preheating to 160 °C, which also increased the stability of the process.

– Edge misalignment up to 2 mm and gaps up to 0.35 mm could be bridged when joining 16 mm material with single pass hybrid welding.

– Concerning multi pass welding, gaps up to 1.2 mm and edge misalignment up to 0.5 mm could be bridged with hybrid welding the root pass.

The defects observed in these experiments have been droplet formation at the root, pores in the filler layer and cracks at the top of root passes. It was shown that:

– The permissible edge misalignment is essentially limited by the droplet formation.

– Pores in the filler passes could not be avoided with the parameters used in this investigation when applying hybrid welding for the filler passes. Using the hybrid process for welding the root pass and then applying a GMAW process, yielded a sound weld.

– Some cracks can be observed at the top of root welds, but these disappear during remelting by the first filler pass.

ACKNOWLEDGEMENTS

The authors like to thank the German Federal Ministry of Education and Research (BMBF FK 13N9278) for funding this research work.

REFERENCES

[1] Walz C., Seefeld T., Sepold G.: Hybridschweißen – eine interessante Ergänzung der Laserschweißtechnik, Hybrid welding – an interesting addition to laser welding technology, 2. Sondertagung Schweißen im Schiffbau und Ingenieurbau, Hamburg 2001, pp. 46-55 (in German).

[2] Russell J.D.: Application of laser welding in shipyards, Proceedings of: SPIE, 1997, 3097, pp. 174-183.

[3] Steen W.: Arc augmented laser processing of materials, Journal of Applied Physics, 1980, vol. 51, no. 11, pp. 5636-5641.

[4] Sepold G., Thomy C., Seefeld T., Schilf M., Vollertsen F., Hoffmann R.: CO_2-Laser GMA hybrid welding – aspects of research and industrial application. Proceedings of the 2nd International WLT-Conference LIM 2003, Munich, June 2003, pp. 149-156.

[5] Fuhrmann C., Petring D., Poprawe R.: Recent results on high-power CO_2- and Nd:YAG-laser-arc welding of thick steel plates, Proceedings of the 3rd International WLT-Conference LIM 2005, Munich, June 2005, pp. 185-192.

[6] Thomy C., Seefeld T., Vollertsen F.: Hybrid welding of line pipes, in: Industrial Laser Solutions, September 2003, p. 3.

[7] Walz C., Stiebe-Springer I., Seefeld T., Sepold G.: Hybrid welding of steel for offshore applications. Proceedings of the 11th International Offshore and Polar Engineering Conference ISOPE 2001, vol. IV, pp. 236-240.

[8] Thomy C., Seefeld T., Vollertsen F.: Industrial potential for high power fiber laser welding, in: The Industrial Laser User, 2006, vol. 42, pp. 22-25.

[9] Vollertsen F., Thomy C.: Welding with fiber lasers from 200 to 17000 W, Proceedings of the 24th ICALEO, LIA Publication 598, 2005, Paper 506.

[10] Seyffarth P.: Erfahrungen des Werftausrüsters IMG bei der Einsatzvorbereitung von Lasertechnologien für den Schiffbau, Experiences of shipyard supplier IMG during the preparations for assigning laser technologies to shipbuilding, in: Lasertsrtahlfügen: Prozesse, Systeme, Anwendungen, Trends, eds.: F. Vollertsen, T. Seefeld, Strahltechnik, BIAS Bremen, 2006, vol. 28, pp. 27–38 (in German).

[11] Kristensen J.K.: Thick plate CO_2-Laser/MAG hybrid welding of steels, Doc. IIW-1916-08 (ex-doc. IV-932-07), Welding in the World, 2009, vol. 53, no. 1/2, pp. 48-57.

Publication II

Grünenwald, S., Seefeld, T., Vollertsen, F., Gook, S., Gumenyuk, A., Rethmeier, M.
Laser-MSG-Hybridschweißen dicker Bleche aus Rohrleitungsstahl mit Faserlasern hoher Leistung

Reprinted with permission from
Schweißen und Schneiden
Vol. 62, pp. 338-347, 2010

As addendum to the original publication in German a translation into English will be included.

Laserstrahl-MSG-Hybridschweißen dicker Bleche aus Rohrleitungsstahl mit Faserlasern hoher Leistung

In diesem Beitrag werden die Ergebnisse aus einem gemeinschaftlich durchgeführten Forschungsprojekt zur Schweißeignung unlegierter Stähle mit Laserstrahl- und Lichtbogenschweißverfahren vorgestellt. Es wurden Schweißversuche in Ein- sowie Mehrlagentechnik mit Blechdicken von 16, 20 und 28 mm durchgeführt sowie die Prozessgrenzen für die Spaltüberbrückbarkeit, den Kantenversatz und das Schweißen in Zwangspositionen untersucht. Für die Schweißversuche kamen Faserlaser mit Leistungen von 8, 20 und 30 kW in Verbindung mit einem MAG-Schweißprozess als Laserstrahl-MSG-Hybridschweißen zum Einsatz. Mit dem 30-kW-Faserlaser war es möglich, 28 mm dicke Bleche einlagig zu schweißen, jedoch besteht weiterer Forschungsbedarf, um Aussagen über die erreichbare Qualität treffen zu können. Bei 20 kW Laserstrahlleistung wurde zum einlagigen Schweißen von Blechen mit einer Dicke von 20 mm eine entsprechende Nahtvorbereitung benötigt, 16 mm dicke Bleche konnten dagegen ohne Vorbereitung der Naht im Stumpfstoß geschweißt werden. In der Mehrlagentechnik wurden mit dem 8-kW-Faserlaser 16 mm dicke Bleche vorbereitet mit einer Y-Naht geschweißt. Hierbei wurde die Wurzellage hybrid geschweißt, die Füll- und Decklagen mit einem reinen MAG-Prozess.

M. Sc. Stefan Grünenwald, Dipl.-Ing. Thomas Seefeld, Prof. Dr.-Ing. Frank Vollertsen, Bremen, Dr.-Ing. Sergej Gook, Dr.-Ing. Andrey Gumenyuk, und Prof. Dr.-Ing. Michael Rethmeier, Berlin

1 Einleitung

Beim Schweißen dicker Stahlwerkstoffe mit Lichtbogenverfahren, zum Beispiel im Schiffbau, Stahlbau oder Rohrleitungsbau, ist die Mehrlagentechnik üblich. Einlagiges Schweißen von Blechen über 5 mm Dicke wird wegen der großen, nicht beherrschbaren Schweißbäder und des sehr hohen Wärmeeintrags zumeist vermieden. An Schweißprozessen, wie modernen Laserstrahl- und Laserstrahl-MSG-Hybridschweißverfahren, die über eine hohe Laserstrahlleistung verfügen und dieses Problem lösen können, wird daher sehr intensiv geforscht. Vorteile sind die Reduzierung der Anzahl der Schweißlagen, die Erhöhung der Schweißgeschwindigkeiten sowie ein geringerer Wärmeeintrag in das Bauteil, um damit verbundene Richtarbeiten zu reduzieren [1; 2]. Ein Anwendungsgebiet für solche Hybridschweißverfahren ist das Dickblechschweißen beispielsweise für den Rohrleitungsbau [3...5].

Mit der Weiterentwicklung der Faserlaser wurden der Schweißtechnik unlängst hohe Strahlleistungen bis 50 kW im cw(continuous wave)-Betrieb mit einer hervorragenden Strahlqualität in sehr kompakter Bauweise bereitgestellt [6]. Der Faserlaser zählt zu der Gruppe der Festkörperlaser und emittiert Strahlung mit einer Wellenlänge von etwa 1,07 µm, die mit optischen Fasern flexibel an die Prozesszone geführt werden kann. Gerade die kompakte Bauweise des Faserlasers in Kombination mit der Möglichkeit, optische Fasern einzusetzen, bietet für einen mobilen Einsatz zum Beispiel auf den Werften, bei der Rohrfertigung oder im Feld in der Rohrverlegung damit beste Voraussetzungen [7; 8]. Die Strahlqualität des Faserlasers, welche die Fokussierbarkeit der Strahlung bzw. die Leistungsdichteverteilung entlang der Strahlachse maßgeblich bestimmt, ist deutlich besser als die herkömmlicher Festkörperlaser [9]. Vergleichbare Strahlqualitäten können auch mit einem Scheibenlaser erreicht werden, der heute Strahlleistungen bis maximal 16 kW erzielt

Mitteilung aus dem BIAS – Bremer Institut für angewandte Strahltechnik, Bremen, und der BAM Bundesanstalt für Materialforschung und -prüfung, Berlin.

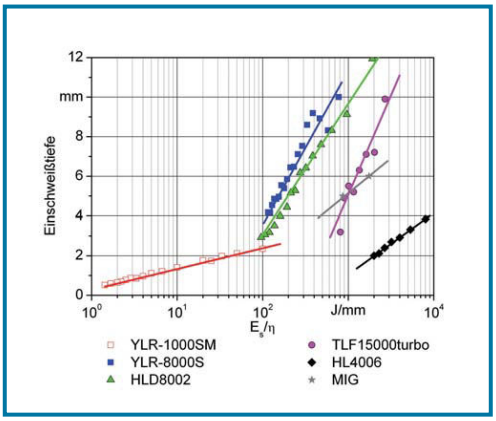

Bild 1. *Einschweißtiefe als Funktion der Streckenenergie dividiert durch den Gesamtwirkungsgrad für verschiedene Laserstrahlquellen (YLR-1000SM: Single Mode Faserlaser, YLR8000S: Multimode Faserlaser, HLD80002: Scheibenlaser, TLF15000turbo: CO_2-Laser, HL4006: Lampengepumpter Nd:YAG-Laser) sowie einen Metall-Schutzgasschweißprozess (MIG) [14].*

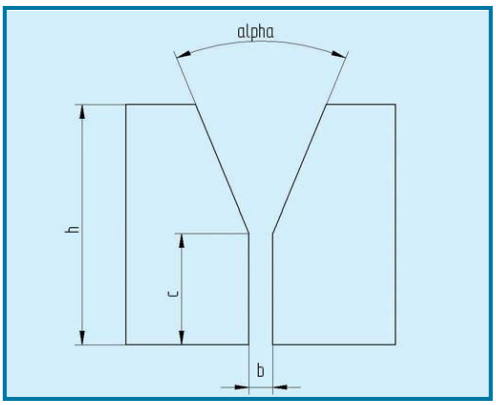

Bild 2. *Nahtvorbereitung.*

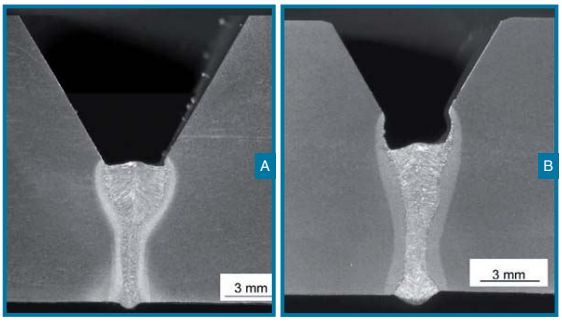

Bild 3. *Hybridgeschweißte Wurzellagen mit unterschiedlichen Spaltweiten;* ***a)*** *0 mm Spalt,* ***b)*** *0,8 mm Spalt.*

[10]. Somit ergibt sich nun erstmalig die Möglichkeit, auch große Bauteildicken bis zu 20 mm in einer Lage zu verschweißen. Die erzielten Schweißnähte ähneln vom Aspektverhältnis her am ehesten Elektronenstrahlschweißnähten. Ein weiterer Vorteil heutiger Festkörperlaser ist eine hohe energetische Effizienz, die mit bis zu 30% weit über den bisher erreichten Wirkungsgraden von CO_2-Lasern mit 10% und Festkörperlasern zwischen 3 und 12% liegt [11]. Bild 1 zeigt die Einschweißtiefe verschiedener Laserstrahlquellen in 5xxx-Aluminiumlegierungen als Funktion der Streckenenergie dividiert durch den Gesamtwirkungsgrad der Strahlquelle. Für den Gesamtwirkungsgrad wurde auch der erste Kühlkreislauf (Wasser/Wasser – Wärmetauscher berücksichtigt). Zum Vergleich wurde zusätzlich ein reiner MIG-Prozess betrachtet. Für die Berechnung der Streckenenergie wurden aus der Literatur beispielhaft Einschweißtiefen von 5 und 6 mm mit den jeweiligen Schweißparametern herangezogen [12]. Der Wirkungsgrad des MIG-Prozesses wurde entsprechend Literaturangaben für verschiedene Stromquellentypen mit 80% angenommen [13]. Die benötigte Gesamtenergie zur Erzielung einer bestimmten Einschweißtiefe ist bei Faser- und Scheibenlasern um fast eine Größenordnung besser als bei CO_2-Lasern und dem reinen MIG-Prozess. Im Vergleich dazu benötigen lampengepumpte Nd:YAG-Laser, die den geringsten Gesamtwirkungsgrad aufweisen, sogar fast das 20-Fache mehr an Energie, um eine vergleichbare Einschweißtiefe zu erreichen [14].

2 Versuchsdurchführung

2.1 Werkstoffe

Als Grundwerkstoff für die Versuche wurde ein thermomechanisch gewalzter und beschleunigt gekühlter Rohrleitungsstahl mit reduziertem Kohlenstoffanteil ausgewählt. Dieser Werkstoff wird nach API 5L als X65 bezeichnet, hat eine Zugfestigkeit von mindestens 460 MPa und eine Kerbschlagarbeit von 47 J bei −40° C. Die chemische Zusammensetzung der geschweißten Bleche mit den verschiedenen Dicken ist in Tabelle 1 aufgeführt. Die Abmessungen des Versuchswerkstoffs waren 300 mm × 40 mm für die Blechdicken 16 mm für Versuche mit 20 kW Laserstrahlleistung, für alle weiteren Versuche wurden Proben mit 350 mm × 200 mm mit den Dicken 16 mm und 28 mm für 8 kW bzw. 30 kW Laserstrahlleistung verwendet. Als Zusatzwerkstoff wurden Drahtelektroden vom Typ G3Si1 und G4Si1 nach DIN EN 440 verwendet. Die Schutzgase für den Schweißprozess waren die Gasmischungen M21 nach DIN EN 439 mit 82% Ar und 18% CO_2, bzw. 90% Ar und 10% CO_2.

Für die Schweißversuche mit 8 kW Laserstrahlleistung wurde zum Fügen der Bleche zwingend eine Nahtvorbereitung benötigt. Zum Einsatz kam eine Y-Nahtvorbereitung, wobei variierende Öffnungswinkel α und Steghöhen c untersucht wurden, Bild 2. Schweißversuche mit 20 kW Laserstrahlleistung wurden im I-Stoß und mit einer Y-Nahtvorbereitung (α = 30°, c = 16 mm) durchgeführt. Ausschließlich im I-Stoß wurden die Schweißversuche mit 30 kW Laserstrahlleistung durchgeführt.

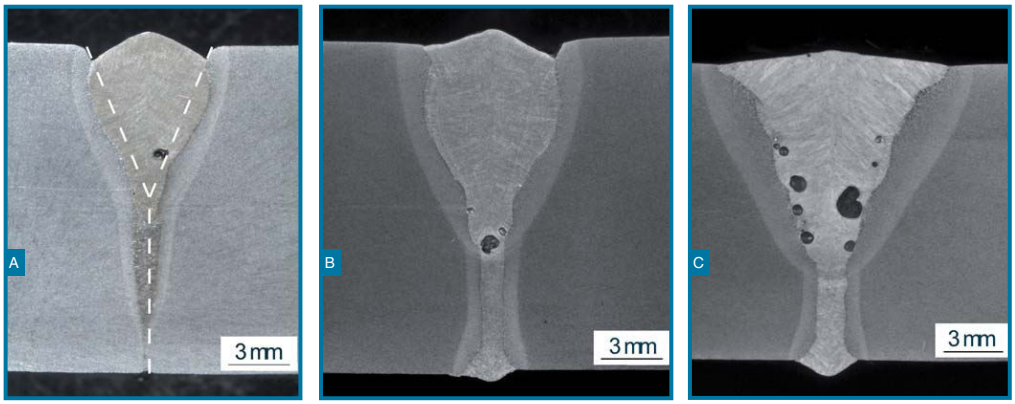

Bild 4. *Querschliffe von Proben mit verschiedenen Spaltweiten, die in PA-Position mit einem hybriden Prozess geschweißt wurden;* ***a)*** *0 mm Spalt,* ***b)*** *0,6 mm Spalt,* ***c)*** *1,2 mm Spalt.*

2.2 Experimenteller Aufbau

Der Versuchsaufbau für das Laserstrahl- und Laserstrahl-MSG-Hybridschweißen bestand jeweils aus drei verschiedenen Strahlquellen mit 8 kW, 20 kW und 30 kW Laserstrahlleistung. Jeder Laser war mit einem MSG-Brenner und entsprechender Schweißausrüstung ausgestattet, Tabelle 2.

3 Ergebnisse

3.1 Hybridschweißen von 16 mm Blechdicke

3.1.1 Mehrlagentechnik mit 8 kW Laserstrahlleistung

Bei maximal 8 kW Laserstrahlleistung konnten 16 mm dicke Werkstoffe nicht in einer Lage gefügt werden. Daher wurde in diesem Fall die Mehrlagentechnik angewendet. Um diese Blechdicke in mehreren Lagen fügen zu können, war eine Nahtvorbereitung mit Öffnungswinkeln von 45° und 60° sowie Steghöhen zwischen 6 und 8 mm für das Schweißen mehrerer Lagen notwendig. Das Schweißen der Wurzellage, auch mit Spalt oder geringem Kantenversatz, war mit dem eingesetzten hybriden Prozess ohne Probleme möglich. Steghöhen von 6 mm konnten mit Nullspalt fehlerfrei gefügt werden, ebenso wie 8 mm Steghöhe mit einem Spalt von 0,8 mm, Bild 3a) und b) sowie Tabelle 3. Ein Einfluss des Spalts auf die Qualität der Wurzellage in Bezug auf Poren oder Risse wurde nicht beobachtet.

Wurde bei der Nahtvorbereitung die Steghöhe c von 8 mm auf 10 mm erhöht, so war es bei technischem Nullspalt nicht möglich, für die Wurzellage eine vollständige Durchschweißung bei gleichbleibender Schweißgeschwindigkeit zu erreichen, Bild 4a). Bereits ab einem Spalt von 0,2 mm konnte eine ausgeprägte Wurzel erzielt werden, deren Qualität (beurteilt nach dem äußerlichen Erscheinungsbild) sich mit größer werdendem Spalt verbesserte. Spalte bis 1,2 mm wurden erfolgreich überbrückt, Bild 4b) und c), wobei die Drahtvorschubgeschwindigkeit entsprechend angepasst wurde, Tabelle 4. Als optimale Spaltweite in Bezug auf Einschweißtiefe, Aussehen und benötigtes Drahtvolumen haben sich 0,5 bzw. 0,6 mm herausgestellt. Begrenzende Faktoren für die maximal erreichbare Einschweißtiefe sind die Nahtvorbereitung und der vorlaufende Lichtbogen. Der Laserstrahl muss das Schmelzbad des Lichtbogens und den Grundwerkstoff (Höhe des Stegs) durchdringen, um eine vollständige Durchschweißung zu erzielen. Zusätzlich zur Wurzellage wurde eine weitere Schweißlage benötigt, um die verbleibende Fuge zu füllen. Diese wurde zunächst mit einem hybriden Prozess geschweißt, wobei in jeder Lage Poren auftraten, typischerweise im unteren Bereich der Naht. Die Einbrandkerben, erkennbar vor allem in Bild 4a) und b), können auf eine zu hohe Schweißgeschwindigkeit zurückgeführt werden.

Da beim Schweißen von Rohren auf der Baustelle neben unterschiedlichen Spaltweiten auch Kantenversatz auftreten kann, wurde dieser im Rahmen der Versuche mit der Mehrlagentechnik

Tabelle 1. *Chemische Zusammensetzung der verwendeten Werkstoffdicken.*

Chemische Zusammensetzung (Massenanteile in %)														
C	Si	Mn	P	S	Cr	Ni	Ti	Nb	Cu	Al	Mo	V	B	Fe
X 65, t = 16 mm														
0,04	0,34	1,48	0,006	<0,001	0,17	0,03	0,012	0,04	0,02	0,03	<0,01	0,003	<0,0001	Rest
X 65, t = 20 mm														
0,08	0,28	1,67	0,012	<0,001	<0,01	<0,01	0,012	0,05	<0,01	0,03	<0,01	0,002	<0,0001	Rest
X 65, t = 28 mm														
0,04	0,24	1,32	0,009	<0,001	0,06	0,24	0,005	0,04	0,19	0,04	<0,01	0,004	<0,0001	Rest

Tabelle 2. *Parameter für den Versuchsaufbau mit unterschiedlichen Laserstrahlleistungen.*

	Laserstrahlquelle		
	YLR-8000 S BIAS	YLR-20000 BAM	YLR-30000 IPG
Leistung	8 kW	20 kW	30 kW
Schweißstromquelle	Dalex Vario MIG 600	Cloos GLC 403 Qunito	Cloos GLC 403 Qunito
Brennerwinkel [°]	22	25	25
Brennerposition	schleppend		
Transportfaser ∅ [µm]	100	200	200
Schweißkopf	Trumpf BEO D70	HIGHYAG Bimo-HP	HIGHYAG Bimo-HP
Brennweite [mm]	280	350	300
Fokus- ∅ [µm]	220	560	420
Nahtvorbereitung Y-Naht			
Öffnungswinkel [°]	45-60	30/-	-
Steghöhe [mm]	6-10	16/-	-

Tabelle 3. *Parameter für das Schweißen der Wurzellage.*

Lage Nr.	Steg-höhe [mm]	Öffnungs-winkel [Grad]	Laserstrahl-leistung [kW]	Schweiß-geschw. [m/min]	Draht-vorschub [m/min]	Strom (Mittel) [A]	Spannung (Mittel) [V]	Spalt [mm]
0 mm Spalt								
1	6	60	7,6	1,8	6,5	229	23,6	0
0,8 mm Spalt								
1	8	60	7,6	1,6	8,5	298	27,3	0,8

Tabelle 4. *Parameter für hybridgeschweißte Proben mit Spalt.*

Lage Nr.	Steg-höhe [mm]	Öffnungs-winkel [Grad]	Laserstrahl-leistung [kW]	Schweiß-geschw. [m/min]	Draht-vorschub [m/min]	Strom (Mittel) [A]	Spannung (Mittel) [V]	Spalt [mm]
0 mm Spalt (Bild 12 a)								
1	10	60	7,6	1,4	7,0	210	24,3	0
2	10	60	2,0	1,4	13,5	347	33,6	-
0,6 mm Spalt (Bild 12 b)								
1	10	60	7,6	1,4	8,5	232	26,5	0,6
2	10	60	2,0	1,1	13,0	375	35,8	-
1,2 mm Spalt (Bild 12 c)								
1	10	60	7,6	1,4	10	277	30,1	1,2
2	10	60	2,0	0,5	12,5	327	32,6	-

bis auf maximal 3 mm variiert. Verwendet wurde eine Nahtvorbereitung mit 8 mm Steghöhe und 60° Öffnungswinkel. Bis zu einem Versatz von 0,5 mm konnte eine gute Wurzellage geschweißt werden, bei Werten über 0,5 mm konnten die versetzten Kanten nicht vollständig angebunden werden und es bildeten sich Tropfen an der Wurzelseite aus. In Bild 5 sind Querschnitte von Proben dargestellt, die mit Kantenversatz geschweißt wurden. Die dazugehörigen Schweißparameter sind in Tabelle 5 aufgeführt. Poren und Risse kamen ausschließlich in den Fülllagen vor, die ebenfalls mit einem hybriden Prozess geschweißt wurden, Bild 5b) und c). Ohne Risse und Poren ist die Fülllage der Schweißnaht in Bild 5a). Hier wurde die Strategie für die Mehrlagentechnik geändert, da unter den gegebenen Voraussetzungen die Fülllagen mit einem hybriden Prozess nicht fehlerfrei geschweißt werden konnten. Der hybride Schweißprozess wurde nur noch für die Wurzellage verwendet, welche mit einer möglichst großen Steghöhe geschweißt werden soll. Die Fülllagen wurden nicht mehr hybrid, sondern mit einem reinen MAG-Prozess geschweißt.

Der Querschnitt einer Probe in Bild 6 zeigt die erfolgreiche

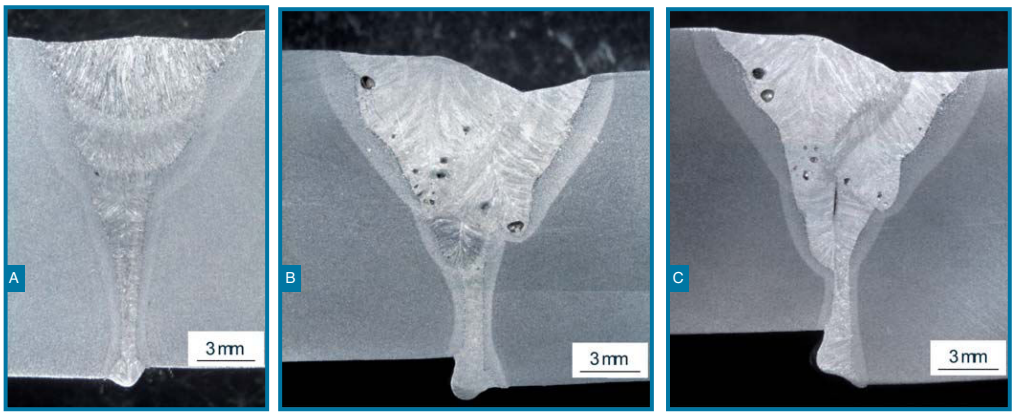

Bild 5. *Querschnitte geschweißter Proben mit 0,5 mm Spalt und unterschiedlichem Kantenversatz;* ***a)*** *0,5 mm,* ***b)*** *1,5 mm,* ***c)*** *3,0 mm.*

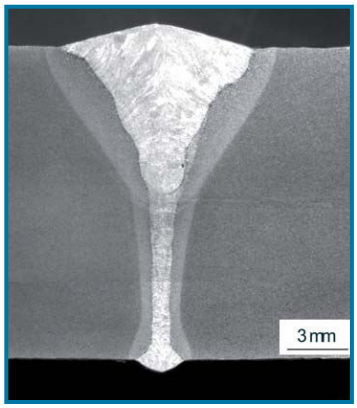

Bild 6. Querschnitt einer Probe mit hybrid geschweißter Wurzellage und MAG-geschweißter Fülllage.

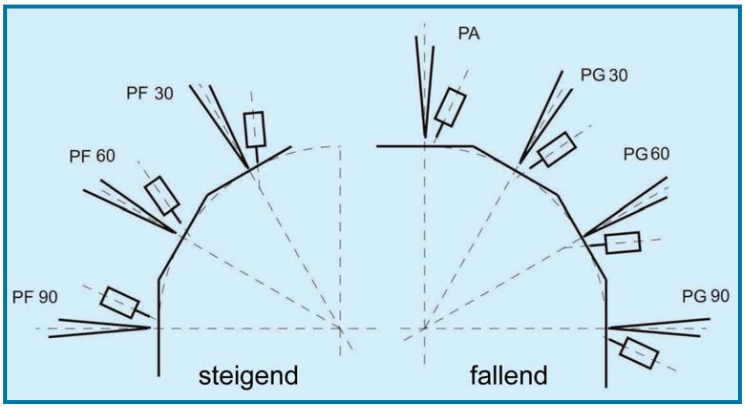

Bild 7. Schweißversuche in Zwangslagen: schematische Darstellung der untersuchten Schweißpositionen.

Anwendung dieser Strategie, bei der die Vorteile des Laserstrahl-MSG-Hybridverfahrens und des konventionellen MIG/MAG-Schweißprozesses genutzt werden konnten. Die Wurzellage als erste Lage wurde mit einem hybriden Prozess geschweißt, die Fülllage als zweite Lage mit einem konventionellen MAG-Prozess. Die Steghöhe wurde mit 10 mm so hoch wie möglich gewählt und der Öffnungswinkel mit 45° so klein wie möglich, um für das Schweißen der Fülllage das aufzufüllende Volumen der Fuge zu minimieren. Für eine vollständige Durchschweißung des 10 mm hohen Stegs war ein Spalt von 0,5 mm erforderlich. Die Parameter der geschweißten Probe sind in Tabelle 6 abgebildet. Für ein 16 mm dickes Blech wurden zwei Schweißlagen benötigt, die mit akzeptabler Qualität hergestellt werden konnten, das heißt ohne Poren oder Risse. Jedoch wirkt sich trotz der hohen Qualität der Schweißnaht die langsame Schweißgeschwindigkeit der zweiten Lage auf die Hauptzeit des Gesamtprozesses aus, was insgesamt betrachtet für die Hauptzeit einen verringerten Vorteil bringt. Hier erscheint es sinnvoll, nach Alternativen für den eingesetzten MAG-Prozess zu suchen, zum Beispiel MSG-Tandemverfahren.

3.1.2 Einlagentechnik mit 20 kW

Mit Laserstrahlleistungen bis 20 kW konnten 16 mm dicke Werkstoffe in einer Lage ohne Nahtvorbereitung gefügt werden. Neben Schweißversuchen in Wannenposition (PA) wurde ein großer Teil der Versuche in Zwangspositionen durchgeführt. Der eingesetzte Versuchsaufbau ermöglichte es, Versuche in fallender

Tabelle 5. Parameter für hybridgeschweißte Proben mit Kantenversatz.

Lage Nr.	Steg-höhe [mm]	Öffnungs-winkel [Grad]	Laserstrahl-leistung [kW]	Schweiß-geschw. [m/min]	Draht-vorschub [m/min]	Strom (Mittel) [A]	Spannung (Mittel) [V]	Spalt [mm]
0,5 mm Kantenversatz (Bild 5a)								
1	8	60	7,6	1,8	8,0	234	26,7	0,5
2	8	60	0	0,4	10,5	von Hand gependelt		-
1,5 mm Kantenversatz (Bild 5b)								
1	8	60	7,6	1,8	8,0	339	23,8	0,5
2	8	60	4,0	1,6	11,0	413	31,9	-
3	8	60	4,0	0,8	10,0	329	29,3	-
4	8	60	4,0	0,8	10,5	334	29,2	-
3,0 mm Kantenversatz (Bild 5c)								
1	8	60	7,6	1,8	6	231	22,6	0,5
2	8	60	2,0	1,6	12,5	422	30,5	-
3	8	60	2,0	0,8	10,0	310	29,7	-
4	8	60	2,0	0,8	10,0	318	29,5	-

Tabelle 6. *Parameter für die Schweißnaht in Bild 6.*

Lage Nr.	Steg-höhe [mm]	Öffnungs-winkel [Grad]	Laserstrahl-leistung [kW]	Schweiß-geschw. [m/min]	Draht-vorschub [m/min]	Strom (Mittel) [A]	Spannung (Mittel) [V]	Spalt [mm]
1	10	45	7,6	1,6	9	372	25,9	0,5
2	10	45	-	0,4	8,5	290	28,3	-

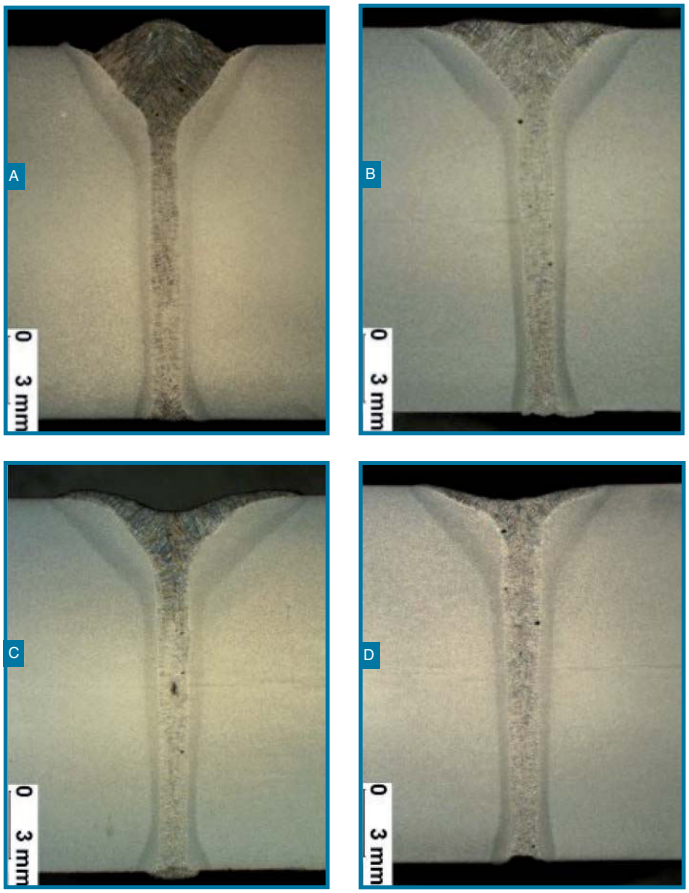

Bild 8. *Schweißversuche in Fallpositionen: Anpassung der Drahtvorschubgeschwindigkeit bei konstanten Parametern P_L = 17 kW, v_s = 2 m/min, $\Delta z_f = -4$ mm;* ***a)*** *PA,* ***b)*** *PG 30°,* ***c)*** *PG 60°,* ***d)*** *PG 90°.*

(PG) und steigender (PF) Position bei 30°, 60° und 90° durchzuführen, Bild 7. Der X-Y-Tisch wurde der Schweißposition entsprechend gekippt und der Laserstrahl-Hybrid-Bearbeitungskopf senkrecht zur Schweißprobe ausgerichtet.

Der Laserstrahl-MSG-Hybridprozess war beim fallenden Schweißen bis zur Neigung der Schweißprobe von 90° sehr gut beherrschbar. Die verwendeten Parameter zum Schweißen in PA-Position konnten auf die PG-Position 30° übertragen werden. Zusätzlich wurde ein stabileres Prozessverhalten als in PA-Position beobachtet, was zu einer gleichmäßigeren Wurzel mit wenig bis keinen Tropfen an der Wurzelseite führte. Um den Schweißprozess auch in den PG-Positionen 60° und 90° zu beherrschen, wurden die Parameter des Schweißprozesses angepasst und die Drahtvorschubgeschwindigkeit verringert. Dabei wurde eine typische Ausbildung der Schweißnaht – leicht abgesenkt in der Mitte der Nahtoberraupe – beobachtet, Bild 8. Die bessere Beherrschung des Schmelzbads beim Schweißen mit einem hybriden Prozess in fallender Position ist wahrscheinlich auf die Umverteilung der Kräfte im Schmelzbad zurückzuführen.

Bei Schweißversuchen in steigender Position hat sich gezeigt, dass der Prozess nur bei einer Neigung der Probe bis 30° beherrschbar war. Im Vergleich zur fallenden Schweißposition 30° wurde die Nahtoberraupe nicht flacher, sondern es bildete sich in der Mitte eine ausgeprägte Nahtüberhöhung aus, Bild 9. Bei weiterer Steigerung des Neigungswinkels bis 60° und darüber hinaus wurde der Prozess instabil, Schmelze sammelte sich in der Mitte und bildete Tropfen aus, die in regelmäßigem Abstand erstarrten, Bild 10.

Hier zeigte sich der Einfluss der Schwerkraft vor allem auf das durch den

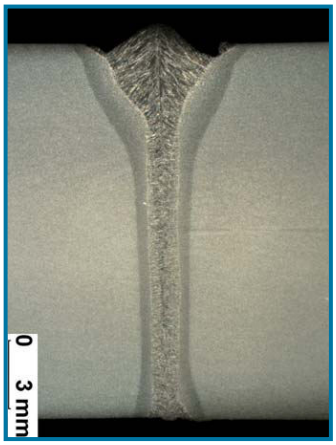

Bild 9. *Hybridgeschweißte Naht in steigender Position PF 30°.*

Bild 10. *Oberraupe einer hybridgeschweißten Naht, steigende Schweißposition PF 60°.*

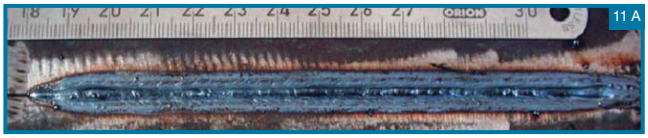

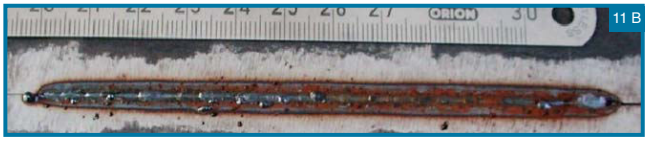

Lichtbogen erzeugte Schmelzbad. Die damit verbundene Gefahr ist, dass flüssiger Werkstoff aus der Prozesszone ausfließt, der Schweißprozess nicht mehr kontrollierbar ist und das Schweißergebnis mangelnde Qualität aufweist. Der durch den Laserstrahlschweißprozess dominierte Teil der Schweißnaht wies bei der Variation der Schweißposition keine Veränderung auf, was frühere Versuche zum Orbitalschweißen mit autogenem Laserstrahl bestätigten [4]. Durch den Einsatz einer aktiven Schmelzbadkühlung mittels einer zusätzlich zur Brennerdüse nachlaufenden Schutzgasdüse wurde eine bessere Beherrschbarkeit des Schmelzbads in steigender Schweißposition 60° erzielt. Gekühlt wurde mit reinem Argon, das direkt auf das Schmelzbad geleitet wurde. Die Tropfenbildung in der Mitte der Schweißnaht konnte erheblich reduziert werden, die Ausbildung der Wurzelseite

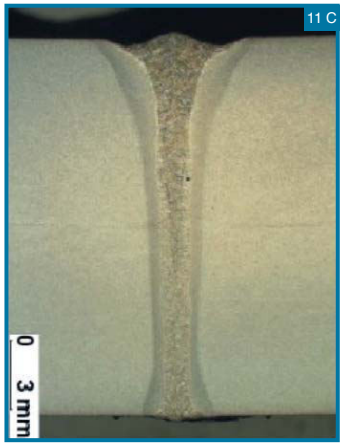

Bild 11. *Hybridschweißnaht mit Schmelzbadkühlung, steigende Schweißposition PF 60°; **a)** Querschliff, **b)** Schweißnahtoberraupe und **c)** Schweißnahtwurzel*

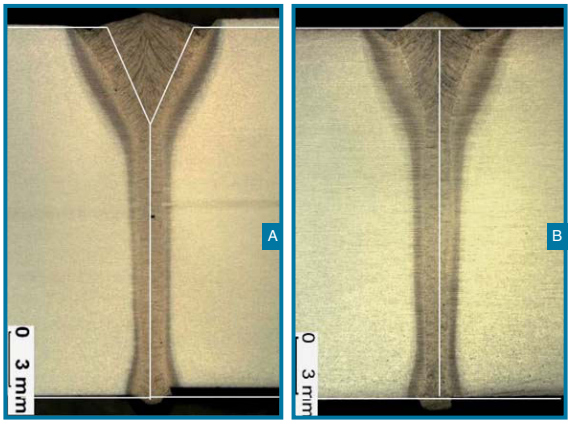

Bild 12. *Einlagenschweißen von 20 mm dickem Werkstoff; **a)** mit Nahtvorbereitung und **b)** mit Vorwärmen.*

wurde ebenfalls verbessert, Bild 11, im Vergleich zu den Versuchen ohne aktive Kühlung.

3.2 Hybridschweißen von 20 mm Blechdicke

Für das Schweißen von 20 mm dicken Blechen mit einem 20-kW-Faserlaser in einer Lage war entweder eine Nahtvorbereitung oder Vorwärmen des Werkstoffs notwendig. Die Nahtvorbereitung bestand aus einer Y-Naht mit 16 mm Steghöhe und 30° Öffnungs-

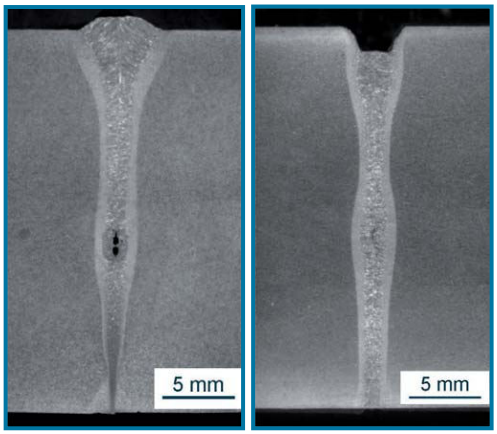

Bild 13. *Einlagenschweißen von 28 mm dickem Werkstoff;* ***a)*** *mit 0,15 mm Spalt und* ***b)*** *mit 0,35 mm Spalt.*

winkel, Bild 12a). Beim Vorwärmen auf 160°C konnte ohne Nahtvorbereitung im I-Stoß geschweißt werden, Bild 12b). Die Parameter für beide Schweißungen sind in Tabelle 9 angegeben.

Während des Schweißens der Bleche mit Nahtvorbereitung lag die Prozessstabilität im Grenzbereich. Diese konnte aber durch die Vorwärmung auf 160°C verbessert werden, was sich in einer besseren Nahtausbildung mit weniger Einbrandkerben zeigte. Zusätzlich konnte auf eine Nahtvorbereitung verzichtet werden. In der Praxis soll die entsprechende Vorwärmtemperatur sowohl auf die mechanisch-technologischen Eigenschaften wie zum Beispiel Härte und Kerbschlagzähigkeit als auch auf die Korrosionseigenschaften abgestimmt werden.

3.3 Potenzial der Anwendung des Laserstrahl-MSG-Hybridschweißens für größere Blechdicken

Mit 30 kW Laserstrahlleistung wurden 28 mm dicke Werkstoffe mit einem I-Stoß in der Einlagentechnik gefügt. Schweißversuche wurden jeweils mit Spaltweiten von 0,15 und 0,35 mm durchgeführt. Bild 13a) zeigt eine entsprechende Nahtausbildung bei 0,15 mm Spalt. Die Nahtform ist in der oberen Hälfte sehr regelmäßig, verjüngt sich aber zur Wurzel stark, was eine sehr schmale Nahtwurzel, teilweise nicht vollends durchgeschweißt, zur Folge hat. Die Schweißnahtoberfläche hingegen ist von guter Qualität, Einbrandkerben oder Nahteinfall sind nicht zu erkennen. Röntgenaufnahmen zeigen, dass Poren und Bindefehler über die gesamte Nahtlänge zu finden sind. Mit 0,35 mm Spaltweite war die Naht vollständig durchgeschweißt, Bild 13b). Die Schweißnahtoberfläche zeigt jedoch deutlichen Nahteinfall, was auf den Drahtvorschub zurückzuführen ist, der auf 24 m/min begrenzt war, was wiederum bei der verwendeten Schweißgeschwindigkeit von 2,5 m/min zum Füllen des Spalts nicht ausreichend war. Röntgenaufnahmen zeigen einige Poren am Nahtende und deutlich weniger Bindefehler. Die zugehörigen Parameter sind in Tabelle 10 aufgeführt. Um zuverlässige Aussagen über die erreichbare Qualität einlagig geschweißter Verbindungen im Blechdickenbereich größer 20 mm treffen zu können, sind weitere Untersuchungen notwendig.

4 Ausblick

Die Arbeiten haben gezeigt, dass Blechdicken von 16, 20 und 28 mm mit einem Laserstrahl-MSG-Hybridschweißprozess gefügt werden konnten. Insgesamt zeigen diese Ergebnisse das Potenzial des hybriden Schweißprozesses mit hohen Laserstrahlleistungen

Tabelle 7. *Parameter zum Schweißen in Fallposition (Bild 8).*

Schweiß-position	Laserstrahl-leistung [kW]	Schweiß-geschw. [m/min]	Drahtvor-schub [m/min]	Strom (Mittel) [A]	Spannung (Mittel) [V]	Spalt [mm]
PA	17	2	15	364	35,6	0
PG 30°	17	2	15	364	35,6	0
PG 60°	17	2	12	339	34,2	0
PG 90°	17	2	8	245	29,9	0

Tabelle 8. *Parameter der Schweißungen in Steigposition.*

Schweiß-position	Laser leistung [kW]	Schweiß-geschw. [m/min]	Drahtvor-schub [m/min]	Strom (Mittel) [A]	Spannung (Mittel) [V]
Bild 9					
PF 30°	17	2	10	272	29,5
Bild 10					
PF 60°	17	2	10	272	29,5
Bild 11					
PF 60°	19	2,2	7	206	30,2

Tabelle 9. *Parameter Einlagenschweißen von 20 mm Werkstoff (Bild 7).*

Laserstrahl-leistung [kW]	Schweiß-geschw. [m/min]	Drahtvor-schub [m/min]	Strom (Mittel) [A]	Spannung (Mittel) [V]	Spalt [mm]
Bild 13 (links)					
30	2,5	15	357	25,7	0,15
Bild 13 (rechts)					
30	2,5	24	340	25,9	0,35

Tabelle 10. *Parameter für Einlagenschweißen von 28 mm dicken Blechen.*

Steg-höhe [mm]	Öffnungs-winkel [Grad]	Laserstrahl-leistung [kW]	Schweiß-geschw. [m/min]	Drahtvor-schub [m/min]	Strom (Mittel) [A]	Spannung (Mittel) [V]	Spalt [mm]
Bild 12a) (mit Nahtvorbereitung)							
16	30	17	1,8	18	509	38,1	0
Bild 12b) (vorgewärmt auf 160°C)							
-	-	19	1,9	16,5	422	33,7	0

auf. Mögliche Anwendungsgebiete sind neben dem Rohrleitungsbau auch im Schiff-, Behälter- und Schienenfahrzeugbau zu finden. Für die Umsetzung der Forschungsergebnisse in die industrielle Produktion besteht jedoch noch weiterer Forschungsbedarf.

Diese Arbeiten wurden im Rahmen eines durch das Bundesministerium für Bildung und Forschung (BMBF) geförderten Projekts „HyBright" (BMBF FK 13N9278) durchgeführt. Schweißversuche mit 8 kW Laserstrahlleistung wurden am BIAS – Bremer Institut für angewandte Strahltechnik und mit 20 kW Laserstrahlleistung von der BAM Bundesanstalt für Materialforschung und -prüfung in Berlin durchgeführt. Die Schweißversuche mit 30 kW wurden bei der IPG Laser GmbH in Burbach durchgeführt.

Literatur

[1] Walz, C., u. a.: Hybridschweißen – eine interessante Ergänzung der Laserschweißtechnik. 2. Sondertagung Schweißen im Schiffbau und Ingenieurbau, Hamburg 2001, S. 46/55.
[2] Russell, J. D.: Application of laser welding in shipyards. Proc. of: SPIE, 3097, 1997, S. 174/83.
[3] Fuhrmann, C., u. a.: Recent results on high-power CO_2- and Nd:YAG-laser-arc welding of thick steel plates. Proc. of the 3rd Int. WLT-Conference LIM 2005, Munich, June 2005, S. 185/92.
[4] Thomy, C., u. a.: Hybrid welding of line pipes. Industrial Laser Solutions, 18, 3 (2003), S. 3.
[5] Walz, C., u. a.: Hybrid welding of steel for offshore applications. Proc. 11th International Offshore and Polar Engineering Conference (ISOPE '01), Vol. IV, S. 236/40.
[6] IPG Photonics [online]. www.igpphotonics.com/index.htm, Zugriff am 25.11.2009.
[7] Jasnau, U., u. R. Gaede: Hochleistungsfaserlaser im Schiffbau. Laser Technik Journal, 2 (2009), S. 30/33.
[8] Gook, S., u. a.: Orbital laser hybrid welding of pipelines using a 20 kW fibre laser. Proc. of 5th Int. WLT-Conference on Lasers in Manufacturing (LIM'09). Eds.: A. Ostendorf, T. Graf, D. Petring, A. Otto. AT Fachverlag Stuttgart (2009), S. 65/70.
[9] Vollertsen, F., u. S. Neumann: High brightness solid state laser: Development and Application. Proc. of 5th Int. Congress on Laser Advanced Materials Processing (LAMP'09), paper 317.
[10] Brockmann, R.: The new benchmark of industrial lasers: TruDisk (4C). Proc. of 10th European Automotive Laser Application (EALA'08). CD.
[11] O'Neill, W., u. a.: High power high brightness industrial fiber laser technology. Proc. of 23rd Int. Congress on Applications of Lasers and Electro-Optics (ICALEO'04), paper 301.
[12] Aichele, G.: Leistungskennwerte für das Schweißen und Schneiden. DVS-Verlag GmbH Düsseldorf (1994), 72.
[13] Matthes, K-J., u. E. Richter (Hrsg.): Schweißtechnik. Fachbuchverlag Leipzig (2002), 71.
[14] Vollertsen, F.: Properties and Prospects of High Brightness Solid State Lasers. Laser Technik Journal, 5 (2009), S. 27/31.

English translation of

Publication II

as addendum to the original publication

Laser-GMA Hybrid Welding of Thick Section Pipe Steel with High-Power Fiber Lasers

S. Grünenwald[1], T. Seefeld[1], F. Vollertsen[1], S. Gook[2], A. Gumenyuk[2], M. Rethmeier[2]

[1] BIAS – Bremer Institut für angewandte Strahltechnik GmbH, Klagenfurter Straße 2, 28359 Bremen
[2] BAM Bundesanstalt für Materialforschung und –prüfung, Unter den Eichen 87, 12205 Berlin

Abstract

This paper presents the results of a joint research project on the weldability of carbon steel in hybrid laser-GMA welding processes.

The welding tests were carried out with single-pass and multi-pass welding to join material thicknesses of 16 mm and 20 mm, and the process limits for gap bridging, linear misalignment and welding in different positions were investigated. Fiber lasers with powers of 8, 20 and 30 kW, in combination with a GMAW process, were used for the GMA hybrid welding tests. Using a 30 kW fiber laser, it was possible to weld 28 mm-thick plates in a single pass. With 20 kW fiber laser power, a joint preparation was needed to weld 20 mm thick plates in a single pass, whereas 16 mm plates could be welded as a butt joint without a joint preparation. Multiple passes were performed to join 16 mm thick plates with an 8 kW fiber laser and a Y-butt joint preparation. In the latter case, the root pass was welded with a hybrid process and the fill and cap passes with a GMAW process.

1 Introduction

When welding thick section steel material with arc welding processes, for example in shipbuilding, steel construction or pipeline construction, multi-pass welding is commonly used. Single-pass welding of plate thicknesses greater than 5 mm is mostly avoided because of the large melt pool, which is difficult to control, and due to the high heat input. Welding processes such as modern laser welding and laser-GMA hybrid welding processes, which deliver a high laser power and could solve these problems, are currently being intensively researched. The advantages are the reduced number of weld passes, the increase in welding speed and the decrease in heat input into the workpiece, thus reducing the need for straightening work [1], [2]. One field of application for such hybrid welding processes is pipeline construction, for example [3], [4], [5].

With the further development of fiber laser technology, beam powers up to 50 kW in cw (continuous wave) mode with an excellent beam quality and a compact design have been made available [6]. Fiber laser belongs to the group of solid-state lasers and emits radiation at a wavelength of around 1.07 µm, which can be guided to the process area with a flexible optical fiber. The compact design of the fiber laser, combined with the possibility of using optical fibers, offers ideal conditions for mobile applications in shipyards, pipe manufacturing or pipe laying [7], [8]. The beam quality of a fiber laser, which is significantly defined by the focusability of the radiation and the power density along the beam axis, is better than that of other solid-state lasers [9]. Comparable beam qualities can also be

achieved with disk lasers, which now generate output powers of up to max. 16 kW [10]. This opens up the possibility of welding up to 20 mm-thick material in a single pass. As regards the aspect ratio, the weld seams produced are most similar to those produced by electron beam welding. Another advantage of current solid-state lasers is their high energy efficiency of up to 30%, which is far greater than the efficiency of CO_2 lasers (10%) and solid-state lasers (between 3 and 12%) [11].

Figure 1 shows the penetration depth of different laser sources in 5xxx aluminum alloys as a function of the line energy divided by the overall efficiency of the laser source. For the overall efficiency, the primary cooling circle (water/water heat exchanger) was also taken into account. A MIG process was taken for comparison. To calculate the line energy, results for penetration depths of 5 mm and 6 mm, including the welding parameters, were taken by way of example from the literature [12]. The efficiency of the MIG process was assumed to be 80%; see [13], for example, for different welding power sources. The overall efficiency required to achieve a certain penetration depth for fiber lasers or disk lasers is one magnitude better than for CO_2 lasers and the MIG process. By comparison, lamp pumped Nd:YAG lasers show the lowest overall efficiency and consume 20 times more energy to achieve a similar penetration depth [14].

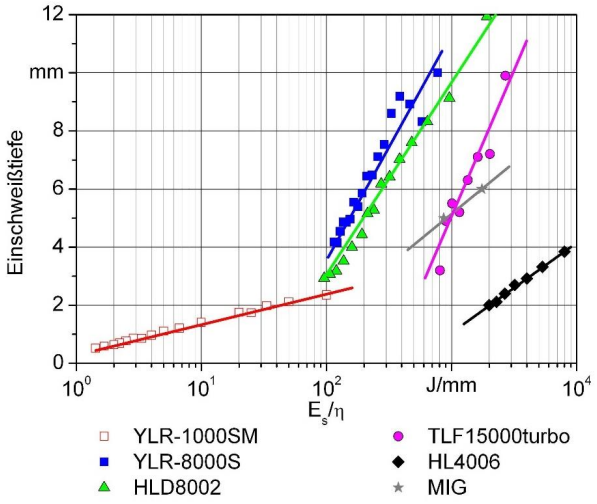

Figure 1: Penetration depth as a function of the line energy divided by the overall efficiency for different laser beam sources (YLR-1000SM: single mode fiber laser, YLR8000S: multimode fiber laser, HLD80002: disk laser, TLF15000turbo: CO_2 laser, HL4006: lamp pumped Nd:YAG-laser) and a gas metal arc welding process (MIG) [14]
(y-axis: penetration depth)

2 Experimental Procedure

2.1 Material

The base material for the experiments was a thermomechanically rolled and rapidly cooled pipe steel with a reduced amount of carbon content. This material is classified as X65 in accordance with API 5L, has a tensile strength of at least 460 MPa and a notch impact value of 47 J at -40°C. The chemical composition of the welded plates with different thicknesses is shown in Table 1. The dimensions of the plate material used for the experiments were 300 mm x 40 mm for the 16 mm thickness welded with 20 kW of laser power; all other experiments were carried out with samples measuring 350 mm x 200 mm and with thicknesses of 16 mm and 28 mm, using 8 kW and 30 kW of laser power. The filler metal used was a G3Si1 and G4Si1 wire in accordance with DIN EN 440. Shielding gases for the welding process were gas mixtures M21 in accordance with DIN EN 439, consisting of 82% Ar with 18% CO_2 and 90% Ar with 10% CO_2.

Table 1: Chemical composition of the materials used

Composition in wt-%														
C	Si	Mn	P	S	Cr	Ni	Ti	Nb	Cu	Al	Mo	V	B	Fe
X 65, t = 16 mm														
0.04	0.34	1.48	0.006	<0.001	0.17	0.03	0.012	0.04	0.02	0.03	<0.01	0.003	<0.0001	Rest
X 65, t = 20 mm														
0.08	0.28	1.67	0.012	<0.001	<0.01	<0.01	0.012	0.05	<0.01	0.03	<0.01	0.002	<0.0001	Rest
X 65, t = 28 mm														
0.04	0.24	1.32	0.009	<0.001	0.06	0.24	0.005	0.04	0.19	0.04	<0.01	0.004	<0.0001	Rest

Joint preparation was required for the welding experiments with 8 kW laser power. A Y-butt joint preparation with varying opening angles α and root faces c was used (see Figure 2). Welding experiments with 20 kW laser power were carried out with an I-butt joint and a Y-butt joint preparation ($\alpha = 30°$, $c = 16$ mm). For the welding experiments with 30 kW of laser power, an I-butt joint was used exclusively.

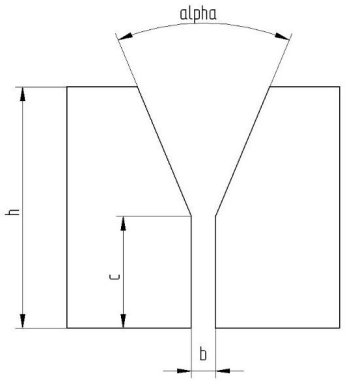

Figure 2: Joint preparation

2.2 Experimental set-up

The experimental set-up for laser and laser-GMA-hybrid welding consisted of three different laser sources with 8 kW, 20 kW und 30 kW laser power. Each laser was equipped with a GMAW torch and further equipment for welding, see Table 2.

Table 2: Parameter for the experimental set-up with different laser powers

	Laser beam sources		
	YLR-8000 S BIAS	YLR-20000 BAM	YLR-30000 IPG
Power	8 kW	20 kW	30 kW
Welding power source	Dalex Vario MIG 600	Cloos GLC 403 Qunito	Cloos GLC 403 Qunito
Torch angle [°]	22	25	25
Torch position	trailing		
Transport fiber ∅ [µm]	100	200	200
Welding head	Trumpf BEO D70	HIGHYAG Bimo-HP	HIGHYAG Bimo-HP
Focal length [mm]	280	350	300
Focal- ∅ [µm]	220	560	420
Joint preparation Y-butt			
Opening angle [°]	45-60	30/-	-
Root face [mm]	6-10	16/-	-

3 Results

3.1 Hybrid welding of 16 mm thick plates

3.1.1 **Multi-pass welding with 8 kW laser power**

With a maximum of 8 kW laser power, 16 mm-thick material cannot be joined in a single pass. Hence, multiple passes were welded. To join this thickness in several passes, a joint preparation with opening angles of 45° and 60° and root faces from 6 mm to 8 mm was required. Welding the root pass, even with a gap or linear misalignment, could be done without difficulty using a hybrid process. Root faces of 6 mm could be joined defect-free, as could root faces of 8 mm with a gap of 0.8 mm; see Figure 3 a) and b) as well as Table 3. No influence of the gap on the quality of the root pass, in terms of porosity or cracks, was seen.

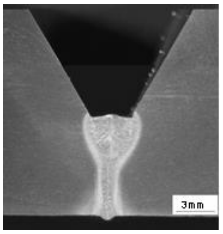

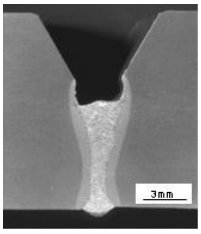

a) 0 mm gap b) 0,8 mm gap

Figure 3: Hybrid welded root pass with different gap sizes.

Table 3: Parameter for welding the root pass

Pass No.	Root face [mm]	Opening angle [deg.]	Laser power [kW]	Welding speed [m/min]	Wire feed rate [m/min]	Current (mean) [A]	Voltage (mean) [V]	Gap [mm]
0 mm gap								
1	6	60	7.6	1.8	6.5	229	23.6	0
0,8 mm gap								
1	8	60	7.6	1.6	8.5	298	27.3	0.8

When the root face was increased from 8 mm to 10 mm in the joint preparation, it was not possible to achieve full penetration with a technical zero gap at a constant welding speed; see Figure 4 a). Starting at a gap of 0.2 mm, full penetration with a sound root was possible, achieving a quality that improved with increasing gap size (according to visual inspection). Gap sizes up to 1.2 mm could be bridged successfully (see Figures 4 b) and c)), whereby the wire feed rate needed to be adjusted. With regard to penetration depth, visual appearance and required filler metal volume, it was found that ideal gap sizes ranged between 0.5 mm and 0.6 mm. The joint preparation and the leading arc are limiting factors for the maximum achievable penetration depth. The laser beam has to penetrate the melt pool of the arc and the base material (root face) to achieve full penetration. In addition to the root face, one further weld pass was needed to fill the remaining groove. This pass was welded with a hybrid process first, with pores typically occurring in the lower part of the seam. Undercuts visible in Figures 4 a) and 4 b), especially, can be explained by the high welding speed used.

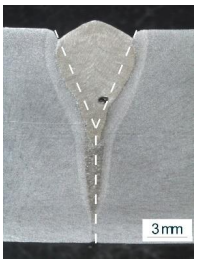

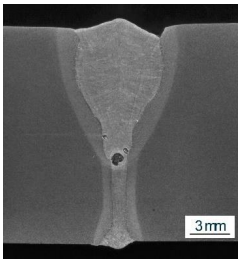

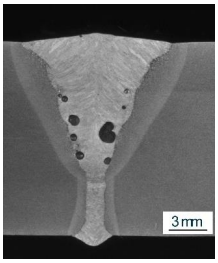

a) 0 mm gap b) 0.6 mm gap c) 1.2 mm gap

Figure 4: Cross-sections of samples with different gap sizes welded in PA position with a hybrid process.

Table 4: Parameter for hybrid welded samples with gap

Pass No.	Root face [mm]	Opening angle [deg.]	Laser power [kW]	Welding speed [m/min]	Wire feed rate [m/min]	Current (mean) [A]	Voltage (mean) [V]	Gap [mm]
0 mm gap (Figure 12 a)								
1	10	60	7.6	1.4	7.0	210	24.3	0
2	10	60	2.0	1.4	13.5	347	33.6	-
0,6 mm gap (Figure 12 b)								
1	10	60	7.6	1.4	8.5	232	26.5	0.6
2	10	60	2.0	1.1	13.0	375	35.8	-
1,2 mm gap (Figure 12 c)								
1	10	60	7.6	1.4	10	277	30.1	1.2
2	10	60	2.0	0.5	12.5	327	32.6	-

Due to the fact that linear misalignment can also occur, in addition to different gap sizes, when welding pipes in field applications, the linear misalignment was varied up to a maximum of 3 mm in the experimental test series. A joint preparation with a root face of 8 mm and an opening angle of 60° was used. Linear misalignment up to 0.5 mm could be welded successfully, but above that value the edges could not be bridged completely, and droplets formed on the root side. Figure 5 shows cross-sections of samples welded with linear misalignment and the respective parameters shown in Table 5. Cracks and pores occurred exclusively in the fill passes (see Figures 5 b) and c)), which were also welded with a hybrid process. The fill pass shown in Figure 5 a) is free of pores and cracks. The strategy for multi-pass welding was changed here, since the fill passes could not be welded defect-free with a hybrid process under the given conditions. The hybrid process was used for the root pass only, welding the highest possible root face. For the fill passes, a MAG process was used instead of a hybrid one.

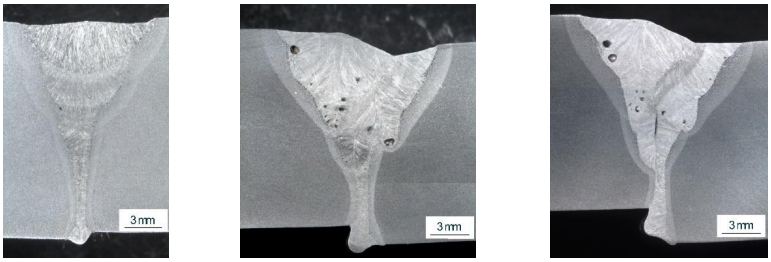

a) 0,5 mm b) 1,5 mm c) 3,0 mm

Figure 5: Cross-sections of samples welded with a 0.5 mm gap and different linear misalignments.

Table 5: Parameter for hybrid welded samples with linear misalignment

Pass No.	Root face [mm]	Opening angle [deg.]	Laser power [kW]	Welding speed [m/min]	Wire feed rate [m/min]	Current (mean) [A]	Voltage (mean) [V]	Gap [mm]
0.5 mm linear misalignment (Figure 5a)								
1	8	60	7.6	1.8	8.0	234	26.7	0.5
2	8	60	0	0.4	10.5	manual weaving		-
1.5 mm linear misalignment (Figure 5b)								
1	8	60	7.6	1.8	8.0	339	23.8	0.5
2	8	60	4.0	1.6	11.0	413	31.9	-
3	8	60	4.0	0.8	10.0	329	29.3	-
4	8	60	4.0	0.8	10.5	334	29.2	-
3.0 mm linear misalignment (Figure 5c)								
1	8	60	7.6	1.8	6	231	22.6	0.5
2	8	60	2.0	1.6	12.5	422	30.5	-
3	8	60	2.0	0.8	10.0	310	29.7	-
4	8	60	2.0	0.8	10.0	318	29.5	-

The cross-section in Figure 6 shows the successful application of this strategy, combining the advantages of laser-GMA hybrid welding and conventional MIG/MAG welding processes. The root pass was welded with a hybrid process, the fill pass with a conventional MAG process. The root face with 10 mm was chosen to be as high as possible, the opening angle with 45 as small as possible to minimize the volume of the groove to be filled. To achieve full penetration of the 10 mm root face a gap of 0.5 mm was needed. The parameters of the welded sample are shown in Table 6. Two passes were needed to join 16 mm-thick plate material, resulting in an acceptable level of quality without porosity or cracks. However, despite the high quality of the welded seam, the low welding speed of the second pass impacts on the main welding time, thus reducing the overall advantage. It is recommended that an alternative be found for the MAG welding process, for example GMA-tandem welding.

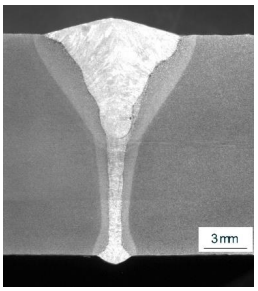

Bild 6: Cross-section of a sample with hybrid welded root pass and MAG welded fill pass.

Table 6: Parameter welded seam in Figure 6

Pass No.	Root face [mm]	Opening angle [deg.]	Laser power [kW]	Welding speed [m/min]	Wire feed rate [m/min]	Current (mean) [A]	Voltage (mean) [V]	Gap [mm]
1	10	45	7.6	1.6	9	372	25.9	0.5
2	10	45	-	0.4	8.5	290	28.3	-

3.1.2 **Single-pass welding with 20 kW**

Using laser powers up to 20 kW, 16 mm-thick material could be joined in a single pass without a joint preparation. Besides welding experiments in flat position, a large proportion of the experiments were performed for out-of-position welding. The experimental set-up allowed experiments to be executed in vertical up and vertical down position at 30°, 60° and 90° (Figure 7). A x-y positioning table was tilted to the respective degree and the laser-hybrid welding head was oriented perpendicular to the weld sample.

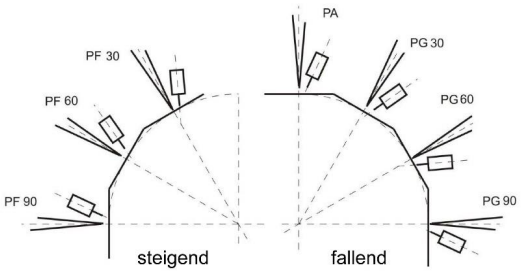

Figure 1: Weld tests in different welding positions: schematic illustration of the investigated welding positions (left: vertical up, right: vertical down).

The laser-GMA hybrid welding process could be controlled up to a vertical down position of 90°. The parameter sets used in PA position could be transferred to the PG position of 30°. In addition, the process was observed to be more stable than in PA position, which led to a smooth root side, showing only a few to no droplets. To control the welding process for PG 60° and PG 90° positions, the parameters of the welding process were adapted and the welding speed reduced. A typical formation of the weld seam can be observed in Figure 8 with slight sagging in the middle of the top part. It can be assumed that the improved control of the melt pool when welding with a hybrid process in vertical down position is related to a change of forces in the melt pool.

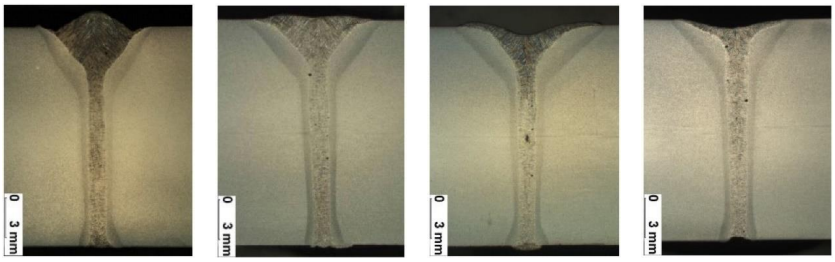

a) PA b) PG 30° c) PG 60° d) PG 90°

Figure 8: Welding tests in vertical down position: adapting the wire feed rate with constant parameters P_L = 17 kW, v_s = 2 m/min, Δz_f = -4 mm

Table 7: Parameter for welding in vertical down position (Figure 8)

Welding position	Laser power [kW]	Welding speed [m/min]	Wire feed rate [m/min]	Current (mean) [A]	Voltage (mean) [V]	Gap [mm]
PA	17	2	15	364	35,6	0
PG 30°	17	2	15	364	35,6	0
PG 60°	17	2	12	339	34,2	0
PG 90°	17	2	8	245	29,9	0

Vertical up welding experiments have shown that the process could be controlled only up to a sample position of 30°. In comparison to the vertical down position of 30°, the welded seam was not flat, but formed excessive weld metal on the top part (Figure 9). Increasing the angle up to 60° and further resulted in an unstable process in which melt accumulated in the middle and formed droplets which solidified at a uniform, periodic distance (Figure 10). The influence of gravitation, above all on the melt pool formed by the arc, can be seen here. The difficulty is to control the welding process and the liquid material flowing out of the process zone, which produces a weld of poor quality. The laser-dominated part did not show any changes during the variation of the welding position, which has been confirmed by earlier orbital welding experiments with an autogenous laser process [4]. By using argon as an active cooling medium directly on the melt pool through a nozzle of a trailing torch, control of the melt pool in vertical up welding position of 60° could be improved. The droplet formation in the middle of the weld seam was reduced significantly and the formation of the root was improved compared to experiments without active cooling (Figure 11).

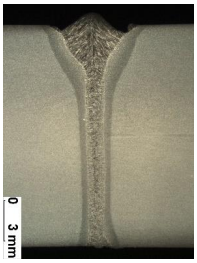

Figure 9: Hybrid welded seam in vertical up position PF 30°.

Figure 10: Top bead of a hybrid welded seam, vertical up position PF 60°.

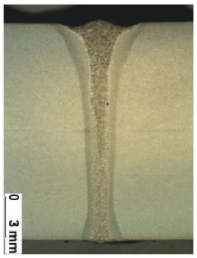

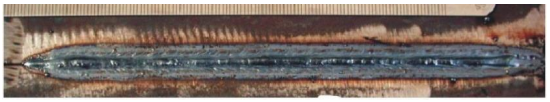
Top bead of weld seam
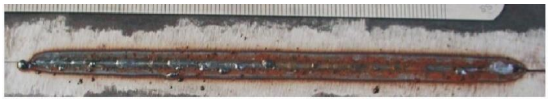
Root side of weld seam
Figure 11: Hybrid weld seam with melt pool cooling, vertical up position PF 60°.

Table 8: Parameter for weld in vertical up position

Welding position	Laser power [kW]	Welding speed [m/min]	Wire feed rate [m/min]	Current (mean) [A]	Voltage (mean) [V]
Figure 9					
PF 30°	17	2	10	272	29.5
Figure 10					
PF 60°	17	2	10	272	29.5
Figure 11					
PF 60°	19	2,2	7	206	30.2

3.2 Hybrid welding of 20 mm-thick material

When welding 20 mm-thick material with a 20 kW fiber laser in a single pass, either a joint preparation or pre-heating of the material was required. A Y-butt joint preparation with 16 mm root face and an opening angle of 30° was used (Figure 12 a)). Pre-heating up to 160°C allowed an I-butt joint without any further preparation to be welded (Figure 12 b)). The parameters for welding are listed in Table 9. When welding the plate material with the joint preparation, the stability of the process was at its limit. This could be improved by pre-heating to 160°C, as indicated by a better weld seam formation with fewer undercuts. In addition, a joint preparation was not necessary.

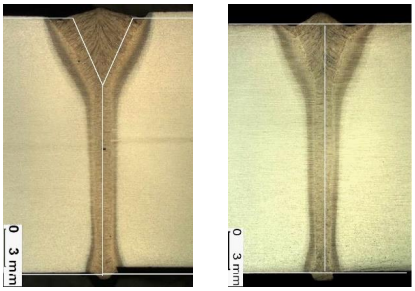

a) b)

Figure 12: Single-pass welding of 20 mm material a) with joint preparation and b) with pre-heating.

For practical applications, the pre-heating temperature needs to be matched with the mechanical-technological properties, for example, hardness and toughness as well as the corrosion properties.

Table 9: Parameter for single-pass welding of 20 mm material (Figure 12)

Root face [mm]	Opening angle [deg.]	Laser power [kW]	Welding speed [m/min]	Wire feed rate [m/min]	Current (mean) [A]	Voltage (mean) [V]	Gap [mm]
Figure 12a (with joint preparation)							
16	30	17	1.8	18	509	38.1	0
Figure 12b (pre-heated to 160°C)							
-	-	19	1.9	16.5	422	33.7	0

3.3 Application potential of laser-GMA hybrid welding for thicker plate material

Using 30 kW of laser power, 28 mm thick material could be welded in a single pass with an I-butt joint. The welding tests were carried out with gap sizes of 0.15 mm and 0.35 mm. Figure 13 a) shows a weld seam with a gap of 0.15 mm. The weld seam is of regular formation, but tapered towards the root side, which results in a very thin root which is partially lacking full penetration. The top side of the weld seam is of good quality; undercuts or sagging of the top were not found. X-ray photographs show porosity and lack of fusion along the full length of the welded seam. With a gap of 0.35 mm, full

penetration was achieved. However, the top part shows distinctive sagging which can be explained by the wire feed speed, which was limited to 24 m/min and was not sufficient for a welding speed of 2.5 m/min. X-ray photographs show some porosity at the end of the weld seam and a significantly reduced lack of fusion. The parameters are listed in Table 10.

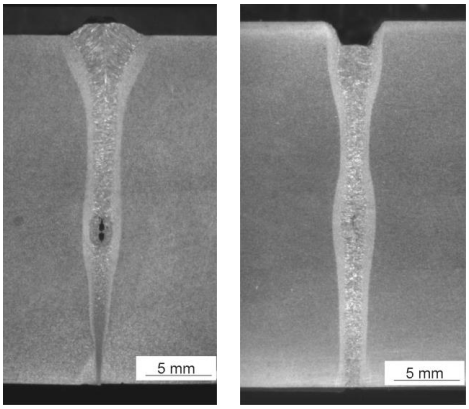

a) b)

Figure 13: Single-pass welding of 28 mm Material, left with a 0.15 mm gap and right with a 0.35 mm gap.

Table 10: Parameter for single-pass welding of 28 mm material

Laser power [kW]	Welding speed [m/min]	Wire feed rate [m/min]	Current (mean) [A]	Voltage (mean) [V]	Gap [mm]
Figure 13 (left)					
30	2.5	15	357	25.7	0.15
Figure 13 (right)					
30	2.5	24	340	25.9	0.35

4 Outlook

This research work has shown that 16 mm, 20 mm and 28 mm-thick material can be joined with a laser-GMA hybrid welding process. Overall, the results show the potential of the hybrid welding process with high laser powers. Possible fields of applications in addition to pipeline welding are shipbuilding, container construction and railway vehicle manufacturing. However, further research is needed to transfer these research results to industrial production.

Acknowledgements

This research work was carried out as part of the 'HyBright' project funded by the Federal Ministry for Education and Research (BMBF, FK 13N9278). Welding experiments with 8 kW laser power were carried out at the Bremen Institute of Applied Beam Technology (BIAS - Bremer Institut für angewandte Strahltechnik), experiments with 20 kW laser power were carried out at the Federal Institute for Materials Research and Testing (BAM – Bundesanstalt für Materialforschung und –prüfung) in Berlin. Welding experiments with 30 kW laser power were carried out at IPG in Burbach.

References

[1] Walz, C.; Seefeld, T.; Sepold, G.: Hybridschweißen – eine interessante Ergänzung der Laserschweißtechnik. 2. Sondertagung Schweißen im Schiffbau und Ingenieurbau, Hamburg 2001, pp. 46-55.

[2] Russell, J.D.: Application of laser welding in shipyards. Proc. of: SPIE, 3097, 1997, pp. 174-183.

[3] Fuhrmann, C.; Petring, D.; Poprawe, R.: Recent results on high-power CO2- and Nd:YAG-laser-arc welding of thick steel plates. Proc. of the 3rd Int. WLT-Conference LIM 2005, Munich, June 2005, pp.185-192.

[4] Thomy, C.; Seefeld, T.; Vollertsen, F.: Hybrid Welding of Line Pipes. Industrial Laser Solutions, 18, 3 (2003), p 3.

[5] Walz, C.; Stiebe-Springer, I.; Seefeld, T.; Sepold, G.: Hybrid Welding of Steel for Offshore Applications. Proc. 11th International Offshore and Polar Engineering Conference (ISOPE '01), Vol. IV, 236-240.

[6] IPG Photonics [online]. www.igpphotonics.com/index.htm, Zugriff am 25.11.2009

[7] Jasnau, U., Gaede, R.: Hochleistungsfaserlaser im Schiffbau. Laser Technik Journal, 2 (2009), pp 30-33.

[8] Gook, S., Gumenyuk, A., Rethmeier, M.: Orbital Laser Hybrid Welding of Pipelines using a 20 kW Fibre Laser. Proc. of 5th Int. WLT-Conference on Lasers in Manufacturing (LIM'09). Eds.: A. Ostendorf, T. Graf, D. Petring, A. Otto. AT Fachverlag Stuttgart (2009), pp 65-70.

[9] Vollertsen, F.; Neumann, S.: High Brightness solid state laser: Development and Application. Proc. of 5th Int. Congress on Laser Advanced Materials Processing (LAMP'09), paper 317.

[10] Brockmann, R.: The new benchmark of industrial lasers: TruDisk (4C). Proc. of 10th European Automotive Laser Application (EALA'08). CD.

[11] O'Neill, W.; Sparkes, M.; Varnham. M.; Horley, R.; Birch, M.; Woods, S.; Harker, A.: High Power High Brightness Industrial Fiber Laser Technology. Proc. of 23rd Int. Congress on Applications of Lasers and Electro-Optics (ICALEO'04), paper 301.

[12] Aichele, G.: Leistungskennwerte für das Schweißen und Schneiden. DVS-Verlag GmBH Düsseldorf (1994), 72.

[13] Matthes, K-J.; Richter, E. (Hrsg.): Schweißtechnik. Fachbuchverlag Leipzig (2002), 71.

[14] Vollertsen, F.: Properties and Prospects of High Brightness Solid State Lasers. Laser Technik Journal, 5 (2009), pp 27-31.

Publication III

Grünenwald, S., Seefeld, T., Vollertsen, F., Kocak, M.
Solutions for joining pipe steels using laser-GMA-hybrid welding processes

Reprinted with permission from
Physics Procedia
Vol. 5, pp. 77-87, 2010

Available online at www.sciencedirect.com

ScienceDirect

Physics Procedia 5 (2010) 77–87

Physics Procedia

www.elsevier.com/locate/procedia

LANE 2010

Solutions for joining pipe steels using laser-GMA-hybrid welding processes

S. Grünenwald[a*], T. Seefeld[a], F. Vollertsen[a], M. Kocak[b]

[a] *BIAS – Bremer Institut für angewandte Strahltechnik, Klagenfurter Straße 2, 28359 Bremen, Germany*
[b] *GKSS Research Center, Geesthacht, GERMANY. Currently at the GEDIK Welding Inc., Ankara Cad. No. 306 Seyhli 34913 Pendik – ISTANBUL / TURKEY*

Abstract

This paper focuses on high power fiber laser welding of steel material for the field of pipe production. X65 and X70 steel plate material in thicknesses of 9.5 mm and 14 mm was welded with laser-GMA-hybrid welding processes with a maximum laser power of 8 kW. Two different filler wires and joint preparations were tested for their weldability. Relating to these welding procedures and thicknesses, characterisation of welded samples such as hardness, tensile testing and Charpy V-notch testing were carried out and the results will be reported in this paper.

Keywords: Laser welding; laser-GMA-hybrid-welding; pipe steels; X65; X70

1. Introduction

During the last few years, the application of laser beam welding technologies for joining thick section steels has found its way into several different industrial fields such as shipbuilding [1], pipe production [2;3], or pipelaying [4;5]. Considering shipbuilding, it was shown [1] that the application of CO_2-laser beam welding in panel production allows an improvement of economic competitiveness whilst improving quality e.g. by reducing distortion and obtaining strength overmatched weld zone while satisfying required weld properties. However, earlier CO_2-laser systems are characterised by low energetic efficiency and high efforts needed to deliver the beam to the workpiece. Besides the CO_2-laser, high-power fibre lasers have been successfully applied for shipbuilding showing their specific advantages such as fiber delivery, high powers up to 20 kW and more in cw mode and its excellent beam quality also at higher powers [6].

Pipelaying, meaning girth welding of pipelines, was hardly accessible to laser welding up to now. Especially for onshore pipelaying under field conditions, the laser systems previously available were missing such qualities as

* Corresponding author. Tel.:+49-421-218-01; fax:+49-421-218-5063.
E-mail address: gruenenwald@bias.de.

1875-3892 © 2010 Published by Elsevier B.V.
doi:10.1016/j.phpro.2010.08.032

robustness, mobility and the high degree of freedom needed for welding around the pipe. Howse et al. have successfully applied fibre delivered lasers for welding to show their potential for the application of pipeline welding [7].

In pipe production e.g. longitudinal welding or spiral welding, conventional laser welding techniques such as CO_2-laser-GMA-hybrid welding have been investigated for the production of a variety of steel grades [2], [3]. Fiber lasers have not yet been widely applied in this field, yet with the advantages over CO_2-lasers as described above, it would be a viable alternative. In this paper the main focus is set on presenting research work done for process development and weld characterization of pipe steels. Process development was carried out firstly in the field of single pass welding of X65 pipe steel to demonstrate the feasibility of laser welding/laser hybrid welding to reduce bottle-neck situations in production. Secondly, welding 14 mm X70 using a hybrid process for the root pass and a GMAW process for the fill or cap pass with as little passes as possible, is presented.

2. Materials, Experimental Set-up and Test Methods used

2.1. Material

Two different grades of base material were used for laser-hybrid welding processes. The X65 steel in 9.5 mm thickness and X70 steel in 14 mm thickness were used in the form of flat plates with dimensions of 450-500 mm long and 150-200 mm wide. The chemical compositions of these two steels are given in Table 1. For the hybrid welding experiments, two different welding wires of 1.2 mm diameter were used: a solid one, Nertalic 70S (T46 4 M M 1 H5 according to EN 758) and a metal cored wire, SAF DUAL 200 (G2 Si according to EN440), Table 2.

Shielding gases for the laser-GMA-hybrid welding process have been chosen in accordance with European standard DIN EN 439, M21. Gas mixtures with 82 % Ar and 18 % CO_2 as well as 90 % Ar and 10 % CO_2 have been used. Several different joint preparations were applied for welding the plate material. For the X65 material, an I-butt joint configuration was used. In order to weld the 14 mm X70 with 8 kW of laser power, a specific joint preparation was necessary. Thus, a single V-butt joint with root faces of 6 mm and 8 mm and an included angle of 45° was used for this welding task.

Table 1. Chemical compositions of the X65 and X70 steels

Chemical analysis (wt %)													
C	Si	Mn	P	S	Al	Cr	Cu	Mo	N	Nb	Ni	Ti	V
X65, t = 9.5 mm													
0.05	0.18	1.07	0.012	0.0015	0.03	0.03	0.01	-	0.006	0.057	0.02	0.002	0.035
X70, t = 14 mm													
0.083	0.228	1.73	0.013	0.0028	0.049	0.031	0.047	0.002	0.0054	0.051	0.055	0.005	0.082

Table 2. Chemical composition of welding consumables used

Chemical analysis (wt %)				
C	Mn	Si	S	P
Nertalic 70S Solid wire – on deposited metal with gas M21				
0.06	0.9	0.45	0.015	0.015
SAF DUAL 200 Metal cored wire – on deposited metal with gas M21				
0.04	1.7	0.5	0.014	0.01

2.2. Experimental set-up

For the experiments carried out, an YLR-8000 S fibre laser set-up with 8 kW output power was used for laser-GMA-hybrid welding. A DalexVario MIG 600 l(w)-B power source and an Abicor Binzel APD wire feed unit were employed for the hybrid welding process. A hydraulically operated clamping device was used to ensure correct fixation of the work piece during welding. A special feature of the YLR-8000S fibre laser is the 100 µm feeding fibre coming from the beam combiner and not being interrupted by an optical coupler or a beam switch, thus acting as the processing fibre at the same time. This configuration of the fibre laser allows a very high brightness of the laser beam and consequently a very high beam quality of 4.2 mm*mrad. The fibre was connected to a 160 mm Optoskand collimator mounted on a Trumpf BEO D70 laser welding head with a 280 mm focusing lens producing a focal spot of 0.22 mm in diameter. For the hybrid welding process, the laser welding head was mounted together with a specially developed GMAW torch to a gantry robot work station, Fig. 1. By using the fine adjustments, the position of the torch relative to the laser beam could be changed. The welding experiments were carried out with the torch in leading position. Concerning the X70 material with the single V-butt joint preparation, the weld was made in two separate steps. First, the root pass was welded with the hybrid process and second the fill pass was made using the same torch, but without the laser beam.

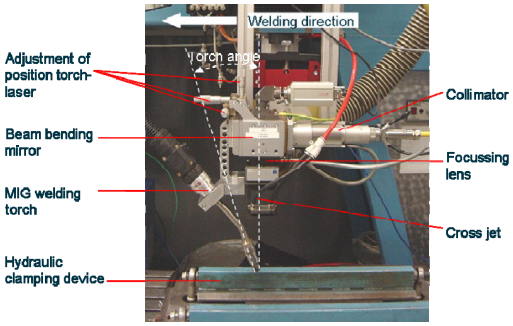

Fig. 1. Experimental set-up for laser-GMA-hybrid welding with 8 kW

2.3. Test methods

The following methods were used to characterize the welded specimen and determine the properties of the weld seams. Non-destructive testing as a visual inspection was carried out to check on the visual appearance of root and fill pass as well as X-raying of the welded samples. Several destructive testing methods were carried out. First, macrographs of polished and etched cross-sections were prepared to allow an evaluation of possible imperfections and determination of the microstructure as well as conducting hardness measurements. Mechanical testing was

carried out by conducting tensile testing, micro tensile testing and Charpy V-notch testing. All three methods comprised testing of base materials and welded seams.

3. Results

3.1. Welding X65 material with I-butt joint

In the first set of experiments, X65 material with a thickness of 9.5 mm was welded as butt joint in a single welding pass using a hybrid laser welding process. Experiments were carried out with welding speeds between 1 m/min and 2 m/min with solid wire and metal cored wire, specified above. For all welding speeds and both wire electrodes used, acceptable up to good weld seams according to visual inspection and requirements of DIN 13919 for laser welded joints were achieved. Fig. 2 shows cross-sections of the weld joints welded with solid wire and Fig. 3 those welded with metal cored wire.

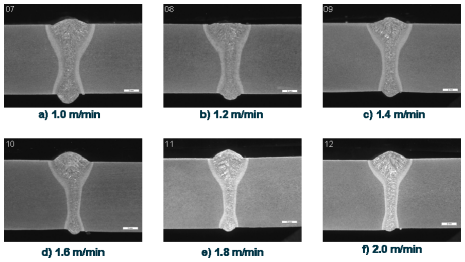

Fig. 2. Welding of 9.5 mm thick X65 plate material with solid wire

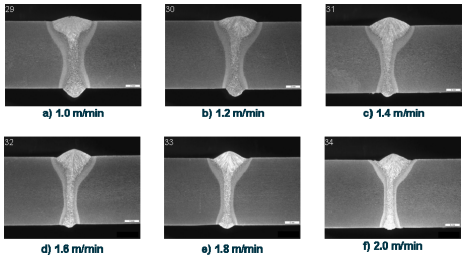

Fig. 3. Welding of 9.5 mm thick X65 plate material with metal cored wire

Regarding the experiments made with the solid wire, increasing the weld speeds lead to a narrower shape of the weld seams, excess weld metal protruding through the root decreased with increasing welding speed. As for the welds made with the metal cored wire, the weld beads had a relatively uniform width at all welding speeds, the cap part was wider than compared to the weld beads with the solid wire. On the root side of the seams welded with both wires, excessive penetration is visible with a tendency to form drops at a welding speed of 1 m/min. Weld seam characterization was carried out for the laser-GMA-hybrid welded X65 plates according to API 5L. The mechanical analysis comprised hardness measurement, tensile testing and Charpy V-notch testing. Samples for testing purposes were welded at 1.8 m/min welding speed with the solid wire exclusively, for parameters see Table 3. X-ray analysis of the samples showed some incomplete fusion at the beginning of two weld beads. All other tested samples passed this test without defects. Hardness testing results for the base material ranged from 187 to 220 HV10, the HAZ and weld metal had hardnesses between 207 to 245 and 215 to 256 HV10 respectively. The yield strength achieved lay between 518 to 543 MPa, the tensile strength between 610 to 623 MPa. For Charpy V-notch testing, out of 10 test series tested with the notch location in the weld, only two produced values in the range of 25 to 40 J at temperatures of 0 °C and -20 °C which did not meet the requirements of the API 5L standard. Yet values achieved with the notch location in the HAZ for the same samples were around 180 J to 220 J. Full testing range and average values of the results of all tested specimen are presented in Table 3 and 4.

Table 3. Welding parameters for welded X65 material for testing purposes

Laser power [kW]	Welding speed [m/min]	Wire feed speed [m/min]	Current (range) [A]	Voltage(range) [V]	Gap [mm]	Focal position [mm]
8	1.8	7.5	313-312	23.6-23.8	0	-2

Table 4. Hardness testing of welded samples

Hardness testing [HV10]					
Base metal		HAZ		Weld metal	
range	average	range	average	range	average
187-220	198.9	207-245	215.8	215-256	234

Table 5. Tensile and Charpy V-notch testing of welded samples

Tensile testing		Charpy V-notch testing			
R_m [MPa]		Notch location	Temp. [°C]	range [J]	average [J]
range	average	Weld	0	25-342	171
610-623	617		-20	25-307	175
		HAZ	0	174-323	210

3.2. Welding X70 material with 6 mm root face

Fig. 4 shows the cross-sections of a root pass and fully welded seam. The joint preparation was 6 mm root face and 45° included angle welded with 0 mm gap. Both weld passes welded with solid wire have no indications of visible defects. The root has a straight, uniform shape with little excess penetration. Due to the zero gap used, the width of the weld seam is narrow in the middle and bottom part. The cap height of the fill pass is acceptable, the weld bead itself free of undercuts. Parameters for the welded sample are listed in Table 6.

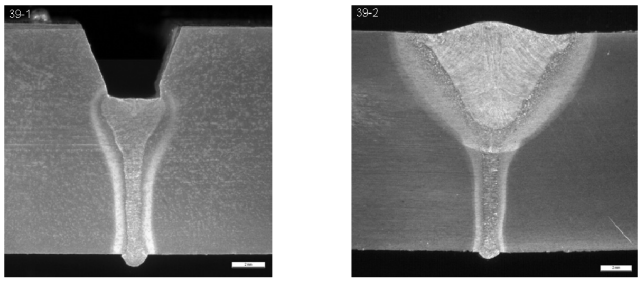

Fig. 4. Cross-sections of 14 mm thick X70 material, single V-butt joint preparation, 6 mm root face and 45° included angle

Table 6. Parameters for welded samples shown in, Figures 4, 5 and 6

Layer	Root face [mm]	Included angle [deg.]	Laser power [kW]	Welding speed [m/min]	Wire feed speed [m/min]	Current (mean) [A]	Voltage (mean) [V]	Gap [mm]	Focal position [mm]
Figure 4, single V-butt joint preparation, 6 mm root face and 45° included angle									
root pass	6	45	8	1.6	6.5	257	24.2	0	-2
fill pass	-	45	-	0.4	9	294	28.4	-	-
Figure 5, single V-butt joint preparation, 8 mm root face and 45° included angle welded with solid wire									
root pass	8	45	8	1.6	7.6	296	24	0.5	-2
fill pass	-	45	-	0.4	7.1	259	24	-	-
Figure 6, single V-butt joint preparation, 8 mm root face and 45° included angle welded with metal cored wire									
root pass	8	45	8	1.6	7.5	297	25.9	0.5	-2
fill pass	-	45	-	0.4	8	246	26.4	-	-

3.3. Welding X70 material with 8 mm root face

Prepared joints with 45° included angle and 8 mm root face were welded the same way as described above, but a 0.5 mm gap was additionally introduced. Two different wire electrodes were used for the welding experiments, a solid wire and a metal cored one. Depicted in Fig. 5 and Fig. 6 are cross-sections of the root pass and the fill pass of a sample welded with the solid wire and metal cored wire respectively. The sample welded with the solid wire has a root pass of regular shape with a nicely formed root side, Fig. 5. The fill pass shows a pore on the bottom side and the cap part is slightly excessive compared to the sample welded with metal cored wire. This sample, Fig. 6, shows excessive penetration on the bottom side. The upper side of the root pass shows an inclination of the weld seam towards the right groove face. The fill pass melted both sides of the groove face uniformly and the asymmetry of the upper part of the root pass has disappeared. Slight undercut can be seen on the top right side. Parameters for both welded samples are given in Table 6. Concerning the use of a 0.5 mm gap, both samples showed a broad, nicely developed root bead and a root seam in the cross-sections which was wider than compared to the root with 0 mm gap shown in Fig. 4. Samples with this joint preparation as welded with parameters given in Table 6 were extensively tested.

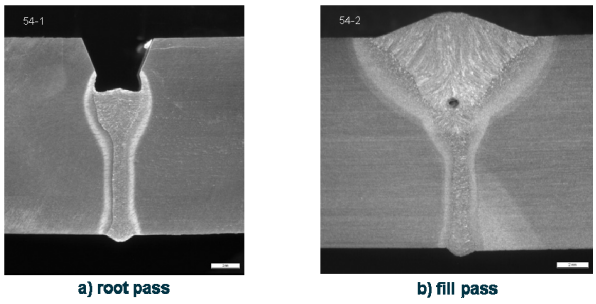

Fig. 5. Cross-sections of 14 mm thick X70 material, single V-butt joint preparation, 8 mm root face and 45° included angle welded with solid wire

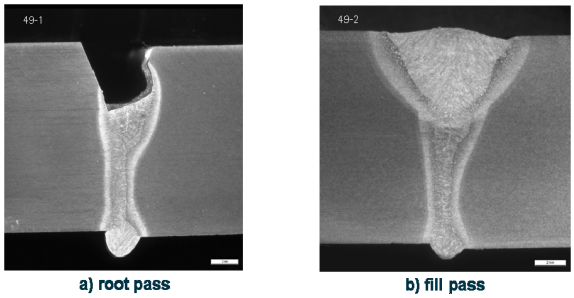

Fig. 6. Cross-sections of 14 mm thick X70 material, single V-butt joint preparation, 8 mm root face and 45° included angle welded with metal cored wire

3.3.1. Hardness testing

The hardness of the welded joints, in accordance with EN 1043-1, was measured across the weld beads in two lines. The first line was situated 2 mm below the upper surface and the second line 2 mm above the lower surface. Shown below are exemplary hardness measurements for samples welded with solid wire, and metal cored wire, Fig. 7. Both samples had identical joint preparationsm, a single V-butt joint with 8 mm root face. The highest hardness was measured on both samples for the HAZ and the weld metal of the root pass. For the fill pass or cap, the hardness dropped down to around 250 HV5 while it kept the level of the root pass in the HAZ.

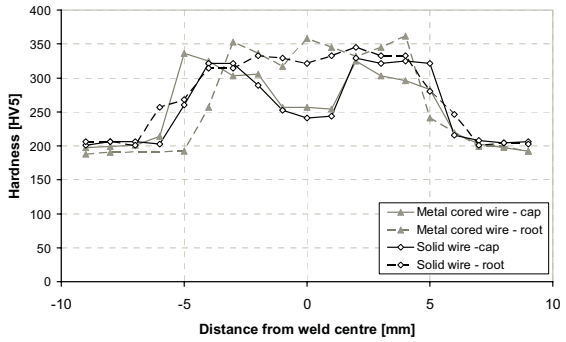

Fig. 7. Hardness measurements of a sample from 14 mm thick X70 material welded with solid and metal cored wire

3.3.2. Charpy V-notch impact testing

Altogether, three series of Charpy V-notch tests were carried out from specimen welded with solid wire and metal cored wire according to EN 10045-1 and EN 875 at temperatures of -20 C. Notches were prepared in the base metal, weld metal and the HAZ 50/50. The values obtained from testing are shown in Table 7. Those obtained from testing the base material were expectedly the highest ones. Test results of the weld metal and HAZ showed that values obtained from specimens welded with solid wire, were - on average - above the ones welded with metal cored wire. However, all specimens tested exhibited ductile fracture.

3.3.3. Tensile testing

The tensile properties of the tested specimen are presented in Table 7. Testing was carried out at 20 °C according to EN 10002-1 and EN 895. Along with the base metal, specimens welded with solid wire and metal cored wire were tensile tested. In the case of the welded specimens tested, the position of fracture was located in the base material. The test results obtained for the welded specimens showed only little deviation from those made of the base material. Values for tensile strength were about in the same range for all tested specimen; results for solid wire and metal cored wire did not show any significant differences.

Table 7. Results of mechanical testing

Tensile Testing at 20°C					
Base Metal		Solid wire		Metal cored wire	
$R_{p0,2}$ [MPa]	R_m [MPa]	R_m [MPa]		R_m [MPa]	
521	633	625		623	
529	635	618		620	
543	639				
Charpy V-Notch testing at -20°C					
Base Metal		Solid wire		Metal cored wire	
[J]		Weld Metal [J]	HAZ 50/50 [J]	Weld Metal [J]	HAZ 50/50 [J]
280		152	246	105	206
250		124	189	126	214
297		130	215	92	146

3.3.4. Micro Tensile Testing

A special micro tensile testing technique [8] was used to determine the local tensile properties of the welds. The specimens 2 mm wide and 0.5 mm thick were cut out longitudinally from the weld at two positions, root pass and fill pass using spark erosion. Test results were obtained for the base material, the HAZ and the weld metal. Samples welded with solid wire and metal cored wire were tested accordingly. Fig. 8 shows the obtained results from altogether 24 tested specimens, 15 from the fill pass and 9 from the root pass. For the fill pass, the values for yield strength and ultimate tensile strength correspond to each other quite well, the values of the test results from the solid wire were on average 20 MPa lower for the yield strength and 46 MPa for the ultimate tensile strength. Clearly visible is the influence of the HAZ (specimen no. 4 and 13) on the tensile strength of the fill pass which produced the highest values. Within the weld metal (specimen no. 5 to 12) the values are close to the yield strength and ultimate tensile strength of the base material. This trend is not clearly reproduced by the elongation values of the solid wire specimens, the values are in the range of the elongation of the base material, merely the value from specimen 14 responds to the higher tensile strength. The values of the elongation obtained from samples welded with metal cored wire perform according to the pattern of yield strength and ultimate tensile strength. At the peak values of the tensile strength in the HAZ the elongation is lowest, approximating the elongation value of the base material in the weld metal except specimen no. 8 and 9 which are significantly lower.

On the root pass tested, the weld metal of the samples welded with solid wire can be easily distinguished by the prominent peak (specimen no. 19). Adjacent to it are two samples (no. 18 and 20) representing the HAZ, in Fig. 8 b. Less distinctive is the difference between HAZ and weld metal for the specimen taken from the sample welded with metal cored wire. The transition from HAZ to weld metal is rather smooth, the tensile strength for the weld metal can be expected at specimens no. 20 and 21 and the transition to the HAZ for specimen no. 19 on the left and no. 22 on the right side. Regarding the elongation measured for the solid wire, the values show as can be expected, a contrary behaviour to the tensile strength, having the lowest value at around 10 % and approaching the elongation of the base material on specimens no. 16 and 17 and from specimen no. 21 onwards. The elongation of the metal cored wire shows a similar trend, however, with a larger scatter band over the whole test series.

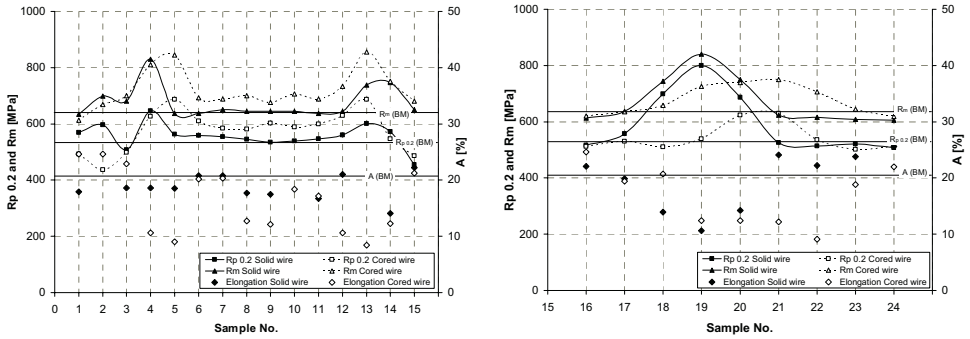

a) b)

Fig. 8. Micro tensile testing of X70 specimens welded with solid wire and metal cored wire, a) fill pass and b) root pass

4. Discussion

By using a laser-GMA-hybrid welding process with a maximum of 8 kW laser power, it was possible to join 9.5 mm thick plates for the task of welding a pipe in a single weld pass. Furthermore, it was shown that this process was feasible within a wide process window applying welding speeds ranging from 1.0 m/min up to 2.0 m/min without an significant loss of weld quality. The two different filler wires used, a solid one and a metal cored one, did not affect on the quality of the weld, merely the MAG dominated top part of the weld seam varies a little bit in shape comparing the two wires. Concerning the results from mechanical testing, especially the hardness achieved for the X65 samples tested and presented in this paper having a range of 215-256 HV10 would comply with recognised standards like the DNV, for example, where for this material with the respective value for yield strength a maximum hardness of 270 HV10 is permitted according to DNV-OS-F101 (table 6-3) for linepipe. The values presented for tensile testing were in a range that can match those achieved with conventional welding. Even though two values obtained from two different Charpy V-notch test series at 0°C and -20 °C were below the admissible minimum, the average of all tested samples was in a range comparable to values achieved with arc welding processes.

Altogether, this hybrid process has two apparent advantages over conventional methods used for longitudinal welding in pipe production. First, a specific joint preparation for tack welding and the subsequent e.g. submerged arc welding is not needed, an I-butt joint is sufficient. Second, with the employed hybrid welding process this thickness of 9.5 mm can be welded in one pass from one side, whereas using conventional methods two passes are usually required. The application of a single pass hybrid welding process for pipe production would save production time, considerable amounts of filler wire and the preparation of a more or less complex and costly joint in a production environment that uses sequential multi pass welding today.

Welding 14 mm thick X70 material with a hybrid process in one pass was not possible with a maximum of 8 kW laser power available. At least two weld passes and a suitable joint preparation were needed to weld this thickness successfully. The material was prepared with a single V-butt joint with an included angle of 45° and root faces of 6 mm and 8 mm. Previously published results have shown that a laser-GMA-hybrid welding process was not suitable for welding fill passes so far since pores and occasional hot cracking appeared in the welds [9]. Hence, the fill passes for the welds presented in this section are done with a conventional arc welding process. A root face of 6 mm could be welded successfully with the given laser power. Up to a root face of 8 mm full penetration was achieved. Higher root faces, however, led to incomplete penetration and were thus not used as joint preparation. The positive effect of a higher root face is that less wire is needed for the fill pass. The amount of wire used to fill the groove left for the second pass was 9 m/min for the sample with 6 mm root face and 7.1 m/min for the sample with 8 mm root face which is a saving of about 20 % of wire electrodes. Concerning the use of a gap for welding the

14 mm thick material with a zero gap, the hybrid welded root of the weld seam was very thin and the surface of the visible part of the root on the welded plate was slightly irregular in shape and height. With a gap (in this case 0.5 mm was chosen), the root pass became thicker and opened up a little towards the bottom of the root side. The visible part of the root was wider and more regular in shape. A difference between the two wires also used for the X70 material during the process concerning hybrid welding was not observed. For the fill passes carried out with arc welding about 10-12 % more metal cored wire was needed to fill the groove.

Comparing the test results obtained from mechanical testing in general, the results for Charpy V-notch testing and tensile testing achieved with this welding process and material were comparable to those achieved with other welding processes and the same or slightly higher grade material presented in [10], for example. As expected, the highest hardness with values well over 300 HV5 were measured in the weld metal of the laser-GMA-hybrid welded root pass as well as in the HAZ region of both weld passes. These characteristics are also reflected by the local tensile properties measured by micro tensile test specimen. In the region with the highest hardness, the yield strength and tensile strength are the highest while the measured elongation is low. Furthermore, the micro tensile tests results revealed that there is no excessive overmatching or undermatching which can be seen especially in the weld metal of the fill pass where the achieved tensile strengths are close to the ones of the base material. This behaviour would have not been observed with ordinary tensile testing alone. Regarding the two different wires used, a significant difference of the mechanical properties from the mechanical testing results could not be found. Concerning the application of pipe welding, the hardness particularly in the laser-GMA-hybrid welded root pass, is higher than those normally expected and exceed the maximum acceptable requirement by standards. However, in order to reduce the hardness, additional measures such as pre-heating prior to welding, can be considered [11].

5. Conclusion

Welding experiments with X65 and X70 pipe steels carried out as part of the FIBLAS project have shown that laser-GMA-hybrid welding can be regarded as potential welding processes to be employed among conventional welding processes for the field of pipe production. In order to join 9.5 mm X65 material, it was demonstrated that a laser-GMA-hybrid welding process with max. 8 kW of laser power was able to weld the given sheet thickness in a single pass. The mechanical properties such as hardness and tensile strength as well as impact toughness obtained from the hybrid welded samples were comparable to those achieved with conventional arc welding. Welding 14 mm thick X70 grade material also with a maximum of 8 kW laser power and a hybrid process showed that:

- two weld passes and a proper joint preparation was needed to join this thickness.
- the use of a 0.5 mm gap brought better quality of the root than a zero gap.
- test results achieved for tensile testing and Charpy V-notch testing were comparable to those of other arc welding processes.
- hardness values of the tested samples were above the average values accepted in standards, thus further measures need to be undertaken to reduce it.

For the first time local tensile properties were investigated for samples welded with the combination of hybrid process and GMAW process by micro tensile testing. The achieved results show a good correspondence to those of the standard mechanical testing methods and point out trends of the hardness testing on the investigated welds.
The advantages of the two approaches presented are saving of filler material as well as a reduced number of welding passes. These advantages contribute to a higher productivity and lower production costs.

Acknowledgements

We gratefully acknowledge funding from the EU within the Research Fund for Coal and Steel Programme for the FIBLAS project, reference number RFSR-CT-2006-00029.

References

[1] F. Roland, H. Lembeck: Laserschweißen im Schiffbau – Erfahrungen und Perspektiven auf der Meyer Werft. Proc. 7. Internationales Aachener Schweißtechnik Kolloquium, Aachen (2001), 463-475.
[2] C. Thomy, G. Sepold, T. Seefeld, C. Walz, R. Hoffmann, I. Stiebe-Springer, M. Koçak, R. Segar: Industrial Implementation of Laser/GMA Welding and Mechanical Properties of the Welds. Proc. Supermartensitic Stainless Steels 2002 Conference. Brüssel, KCI Publishing BV, Zutphen (2002), 147-155.
[3] G. Sepold, C. Thomy, T. Seefeld, M. Schilf, F. Vollertsen, R. Hoffmann: CO2-Laser GMA Hybrid Welding - Aspects of Research and Industrial Application. Proc. Lasers in Manufacturing (2003), AT-Fachverlag, Stuttgart, 149-156.
[4] C. Bonigen, C. Geertsen: Orbital laser Welding: A Major Advanve on Offshore Pipelaying. Proc. Conf. Deep Offshore Technology (1998), paper 10-2.
[5] G. Booth: Laser Welding of Land Pipelines. Proc. Int. Conf. New Developments in Onshore Pipeline Technology, Loughborough (2001).
[6] U. Jasnau, R. Gaede: Hochleistungsfaserlaser im Schiffbau. LTJ, 2 (2008), 30-33.
[7] D.S. Howse, R.J. Scudanore, G.S. Booth: The evolution of Yb fibre laser/MAG hybrid processing for welding of pipelines, Proc. of 15th Int. Offshore and Polar Engineering Conference Seoul, Korea (2005), 90-95.
[8] M. Kocak, G. Cam, S. Riekehr, F. Torster, J.F. dos Santos: Microtensile Test Technique for Weldments. IIW-Doc. SC X-F-079-98, 1998.
[9] F. Vollertsen, S. Grünenwald, M. Rethmeier, A. Gumenyuk, U. Reisgen, S. Olschock: Welding Thick Steel Plates with Fibre Lasers and GMAW. IIW Commission IV Annual Assembly, Austria (2008), IIW Doc.Nr.: IV-965-08.
[10] S. Velbert: Mechanical-technological and fracture mechanical properties of the high grade pipeline-steel X80 with results of different pipeline projects. Welding in the World. 52, 5/6 (2008), 42-50.
[11] A. Gumenyuk, S. Gook, M. Rethmeier, H. Kohn: Orbitalschweißen im Pipelinebau – Neue Möglichkeiten durch die Anwendung von Hochleistungslasern (in German). Proc. of the 8th int. Conference on Beam Technology (2010), 74-79.

Publication IV

Unt, A., Poutiainen, I., Grünenwald, S., Sokolov, M., Salminen, A.
High Power Fiber Laser Welding of Single Sided T-joint on Shipbuilding Steel with Different Processing Setups

Reprinted with permission from
Appl. Sci.
Vol. 7, pp. 1276, 2017

applied sciences

MDPI

Article

High Power Fiber Laser Welding of Single Sided T-Joint on Shipbuilding Steel with Different Processing Setups

Anna Unt *, Ilkka Poutiainen, Stefan Grünenwald, Mikhail Sokolov and Antti Salminen

Laboratory of Laser Materials Processing, Lappeenranta University of Technology, Skinnarilankatu 34, Lappeenranta 53850, Finland; Ilkka.Poutiainen@lut.fi (I.P.); Gruenenwald@gmx.net (S.G.); mikhail.sokolov@gef.fi (M.S.); antti.salminen@lut.fi (A.S.)

* Correspondence: anna.unt@student.lut.fi; Tel.: +358-40-668-8343

Received: 2 November 2017; Accepted: 4 December 2017; Published: 8 December 2017

Abstract: Laser welding of thick plates in production environments is one of the main applications of high power lasers; however, the process has certain limitations. The small spot size of the focused beam produces welds with high depth-to-width aspect ratio but at times fails to provide sufficient reinforcement in certain applications because of poor gap bridging ability. The results of welding shipbuilding steel AH36 with thickness of 8 mm as a single-sided T-joint using a 10 kW fiber laser are presented and discussed in this research paper. Three optical setups with process fibers of 200 µm, 300 µm and 600 µm core diameters were used to study the possibilities and limitations set by the beam delivery system. The main parameters studied were beam inclination angle, beam offset from the joint plane and focal point position. Full penetration joints were produced and the geometry of the welds was examined. It was found that process fibers with smaller core diameter produce deeper penetration but suffer from sensitivity to beam positioning deviation. Larger fibers are less sensitive and produce wider welds but have, in turn, lower penetration at equivalent power levels.

Keywords: shipbuilding steel; fiber laser; laser keyhole welding; T-joint; fillet joint

1. Introduction

Laser welding with multi-kilowatt fiber lasers is fast becoming a highly advantageous joining technology in manufacturing industries such as shipbuilding, where it saves production time and cost compared to conventional arc based welding processes [1]. The growing acceptance and adoption of laser technology can be seen, for example, in sales statistics, which show an annual growth rate of over 10% for the last few years [2,3]. Modern high power fiber lasers are low maintenance, easy to integrate with production robots, and produce welds with deep penetration and low heat input at high throughput rates [4,5]. High beam quality at high power levels and the decreasing price per kilowatt of laser power are enabling previous limitations to be overcome and opening up new possibilities, especially in keyhole welding. The main limiting factor hindering more extensive utilization of laser welding is its demand for high accuracy in joint fit-up tolerances. A common way to compensate gap fluctuations and ensure welds of acceptable quality is to add an arc process working in synergy with the laser. While such hybrid laser-arc welding allows control of weld bead formation through adjustment of the arc parameters and extends the gap bridging ability of the welding system, it increases process complexity and production costs.

One of the most important characteristics of a laser welding system is the beam quality that the lasers deliver. The beam quality affects the power density of the beam, which has a direct effect on the penetration depth and geometry of the weld [6,7]. High power density of the beam means deeper penetration for the same level of power and welding speed. Single-sided welding of T-joints with fiber

lasers is not an entirely novel concept, and its applicability and key parameters have been studied, for example, for aluminum welding in the aircraft industry [4]. The high depth-to-width aspect ratio of typical fiber laser welds can be a drawback in medium and thick section welding of T- and fillet joints. Space and maneuverability restrictions on the welding head can cause the laser beam to cross the joint plane at a certain angle, and a narrow melt pool may easily partially miss the joint plane and produce incomplete fusion. In addition, T-joint welds can be several meters long and heat-induced distortions during welding can thus cause variations in joint fit-up regardless of the accuracy of the original setup.

Classification societies such as DNV (Det Norske Veritas) and IIW (International Institute of Welding) suggest avoiding fillet welds in parts of a construction that are subjected to fatigue, because partial penetration creates a possible crack initiation point at the root of the weld [8,9]. Nevertheless, more than 80% of welded joints are fillet welds, because one of the plates serves as backing during the welding process and less post-welding correction is required. Figure 1 illustrates the principal differences in the geometry and location of the stress concentration of arc, laser and hybrid welded joints.

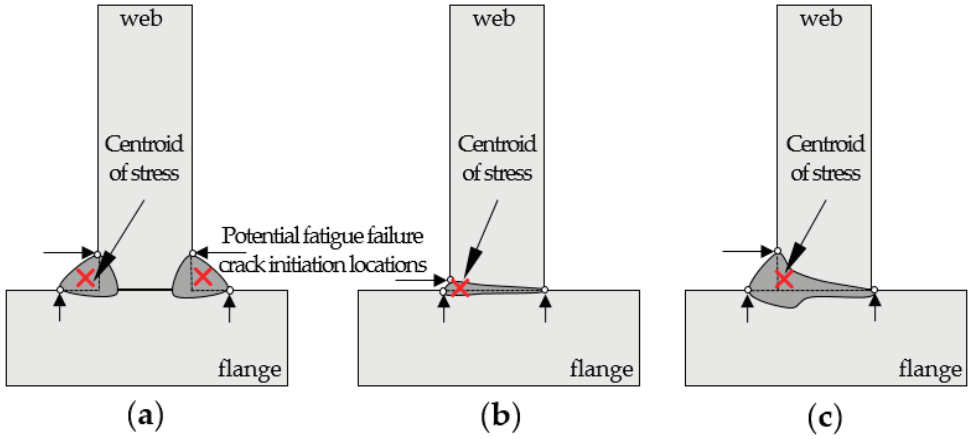

Figure 1. Comparison of weld joint geometries produced with: (**a**) arc welding; (**b**) autogenous laser welding; and (**c**) laser-arc hybrid welding, and stress concentration locations.

The key problem with T-joints is ensuring fusion throughout the whole joint plane, preferably with single-sided welding. In autogenous laser welding, avoidance of the possible occurrence of underfill or undercut due to an absence of filler material is important, because throat thickness and shape of the weld toe influence the fatigue performance of the joint. In thin materials and flat assembly joints, this problem can be addressed by increasing weld width through wider distribution of the beam energy. Approaches used include but are not limited to: manipulation of the focal point position [10], and usage of dual focal point setups [11–13] and beam oscillation techniques [14–17]. Scanning is also beneficial for bringing more heat into the material, which decreases the cooling rate and keeps the hardness of the weld at acceptable levels. Unfortunately, this procedure is not applicable in thick section welding, where the typical weld length is several meters, because scanning mirrors are unable to handle the power levels needed [14,18]. Large components such as scanning optics also limit the degree of freedom and flexibility of the welding process as regards positioning.

Determining the operational window for a good quality weld accounts for three main process parameters: laser power, welding speed and focal point position. These three easily adjustable parameters affect the power density at the top of workpiece, and therefore melt flow and distribution of the energy inside the keyhole, which have a major influence on the geometry of the weld. A certain threshold value of power density must be reached in order to be able to form the keyhole [19].

The threshold is typically defined as 10^6 W/cm^2, or more commonly 10^3 W/mm^2, with typical dimensions of laser beam focal point. The power density is calculated as follows:

$$E = \frac{P}{\pi r^2}, \quad (1)$$

where P is laser power and r radius of the beam on the surface of the workpiece. The above-mentioned power density threshold is valid for CO_2 laser welding, whereas when using solid state lasers with wavelengths around 1000 nm the threshold is lower [20,21]. The lower threshold is a result of higher absorption of shorter wavelengths, and it gives extra flexibility to parameter selection and greater freedom to tailor parameters to specific applications, for example, with static or dynamic beam formation.

Suder and Williams et al. [22] developed the concept of Specific Point Energy (E_{SP}). In addition to energy density (power density × interaction time), E_{SP} includes also beam diameter on the surface:

$$E_{SP} = \rho_P T_i A = P_L T_i = \frac{Pd}{v}, \quad (2)$$

where ρ_P is average power density of the beam (mW/cm^2), T_i is interaction time (s), A is area of the beam on the surface (mm^2), P_L is laser power (W), d is beam diameter on the surface (mm), and v is welding speed (mm/s). Experiments performed with bead-on-plate joints have shown that power density and E_{SP} control the depth of penetration and interaction time controls the bead width [22–24]. E_{SP} has also been shown to be suitable for evaluating the efficiency of laser cutting [25,26].

The relationship between spot size and welding performance in steel and aluminum welding has been addressed in several studies [27–30], and it has been found that small spot size produces deeper welds yet is accompanied by defects such as undercut and porosity. A study by Vänskä [14] showed that in some cases the keyhole welding mode changes between selected parameter values, resulting in different weld cross section shape in butt joint welding of stainless steel with a disk laser. Lap and butt joints produced with CO_2 and solid-state laser sources have been characterized and compared [20]; for example, Kawahito et al. [28] addressed the effect of focal spot size on weld defects and showed that, of the four sizes studied, welds with highest quality were obtained using the two larger spot sizes.

The effect of focal point diameter on beam intensity on surface is much stronger than the effect via laser power. A simple way to manipulate the focal point diameter is to change the focal length of the focusing lens. A problem with this approach is that the focusing angle, i.e., the angle at which the beam enters the keyhole, changes as the focal length is changed, and the effect of focal point diameter is influenced by the effect of focusing angle and changes in the shielding gas arrangement. Change in the beam feeding fiber can only increase the diameter of the raw beam and the beam parameter product. This paper addresses the issue of weld quality of high power fiber laser welded T-joints of shipbuilding steel AH36 by comparing welds produced with three optical set-ups having beam transfer fibers of different diameters.

2. Materials and Methods

Shipbuilding steel AH36 is commonly used for shipbuilding and offshore structures. Hot rolled steel plates of AH36 have excellent weldability with a CEV (carbon equivalent value) of 0.248, calculated based on the chemical composition presented in Table 1. The yield strength of AH36 is 355 MPa.

Table 1. Chemical composition of AH36 steel (wt %).

Material	C	Si	Mn	P	S	Cr	Mo	Ni	Cu	Al	V
AH36	0.111	0.149	0.711	0.035	0.150	0.051	0.01	0.041	0.031	0.030	0.008

Test specimens (100 mm × 350 mm × 8 mm) were cut with a CO_2 laser using oxygen-assisted cutting. The edges were grid blasted with aluminum oxide and cleaned with acetone to remove possible contaminants. The plates were tack welded from the root side from the ends and the middle using gas metal arc welding. The workpiece was fixed in the flat (1F) position using stiff fixtures to avoid heat-induced air gap fluctuations during the welding. Single-sided welds with a length of 165 mm were performed. The experimental setup is shown in Figure 2.

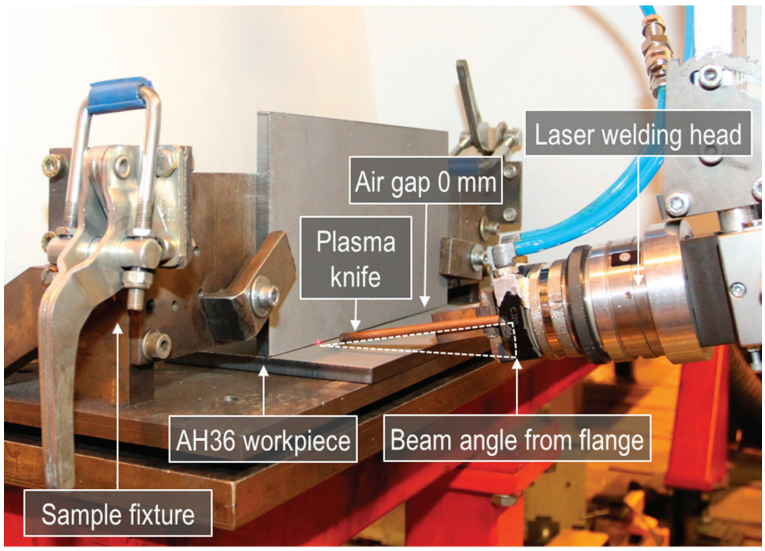

Figure 2. Experimental setup for laser welding of T-joints. Beam is positioned at the joint plane (offset 0 mm).

All welding experiments were made with a continuous wave fiber laser IPG YLS-10000 having wavelength of 1070 nm and a top-hat focused beam profile. A Kugler LK190 mirror optics laser welding head was used. An air knife protected the focusing system from contamination with fumes and spatter, and no additional shielding gas was used. When comparing a T-joint with a butt joint, a further parameter, called offset, describing the distance of the beam center from the joint at the flange front edge, must be added. This parameter has a crucial effect on weld quality and must be considered for thick section joints of the type studied in this work. The experimental parameters of the welding process are presented in Table 2.

Table 2. Welding process parameters.

Parameter	Unit	Parameter Range
Fiber diameter	[µm]	200; 300; 600
Laser power, P_L	[kW]	6.0; 8.0; 10.0
Welding speed, v_w	[m/min]	0.75; 1.0; 1.25; 1.5; 1.75
Focal point position, F_{PP}	[mm]	−2.0; −4.0; −6.0
Beam angle from flange α	[°]	6; 10; 15
Beam offset from flange	[mm]	0.5; 1.0; 1.2; 1.5; 2.0

The beam was delivered by a system consisting of a beam transfer fiber (with core diameters of either 200, 300 or 600 µm), 120 mm collimating length optics, and a 300 mm focal length mirror. The properties of the laser beam emitted from each transport fiber were measured using a laser beam analyzer from Primes GmbH and are shown in Table 3.

Table 3. Beam properties.

Delivery Fiber Diameter (μm)	200	300	600
Beam profile	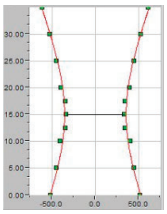	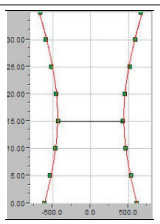	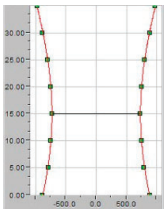
Nominal beam waist (mm)	0.50	0.75	1.50
Measured beam waist (86% pts) (mm)	0.710	0.882	1.460
BPP (mm·mrad)	9.079	12.000	23.800
Rayleigh length (mm)	13.86	16.18	22.38
P_L at workpiece (kW)	6.0	6.0	6.0
Beam area at surface (mm^2)	0.396	0.611	1.674

The bead surface and root of each weld were visually evaluated based on standard EN ISO 13919-1, which classifies welds into three quality levels based on the type and severity of the imperfections that are present. The categories from best to worst are: B, stringent; C, intermediate; and D, moderate [31]. Metallographic preparation of the samples was carried out according to SFS-EN ISO 17639 [32]. The welds were transversely sectioned at the middle of the joint length, and polished and etched using a 2% Nital solution. Macrographs of the weld cross sections were taken for inspection of penetration, defects, and dimensions and shape of the fusion zone and HAZ (heat affected zone).

3. Results

3.1. Effect of Beam Inclination Angle α

To study the effect of beam inclination angle α on the morphology/geometry of the weld, all other process parameters were kept constant. The beam was positioned 0.5 mm above the joint plane on the flange and focused 2 mm below the surface of the material. Focal point diameters on the surface were 0.82 mm, 1.00 mm and 1.61 mm for the 200 μm, 300 μm and 600 μm process fibers, respectively. The cross sections of the welds are shown in Figure 3.

It can be seen in Figure 3 that the penetration depth (measured from top of the weld) and the length of the joint fusion along the intersection decreased as the inclination angle increased. It can also be noticed that the penetration depth and area of the fusion zone correlate with the energy density of the beam. A full penetration weld was obtained only with the 200 μm process fiber and 6° inclination angle. All of the joints followed the axis of beam propagation. Averaged dimensions from three welds produced with each inclination angle are shown in Table 4.

Table 4. Effect of fiber diameter on the weld dimensions.

Fiber Diameter [μm]	Penetration Depth [mm]	Bead Width [mm]	Fusion Zone [mm^2]	HAZ Area [mm^2]	Depth to Width Ratio	Max Hardness HV5 [FZ [1]/HAZ]
200	8.7	2.3	13.2	6.5	4.0	386/373
300	7.8	2.4	12.6	6.0	3.3	392/359
600	5.6	2.7	12.0	5.5	2.0	393/365

[1] FZ = fusion zone.

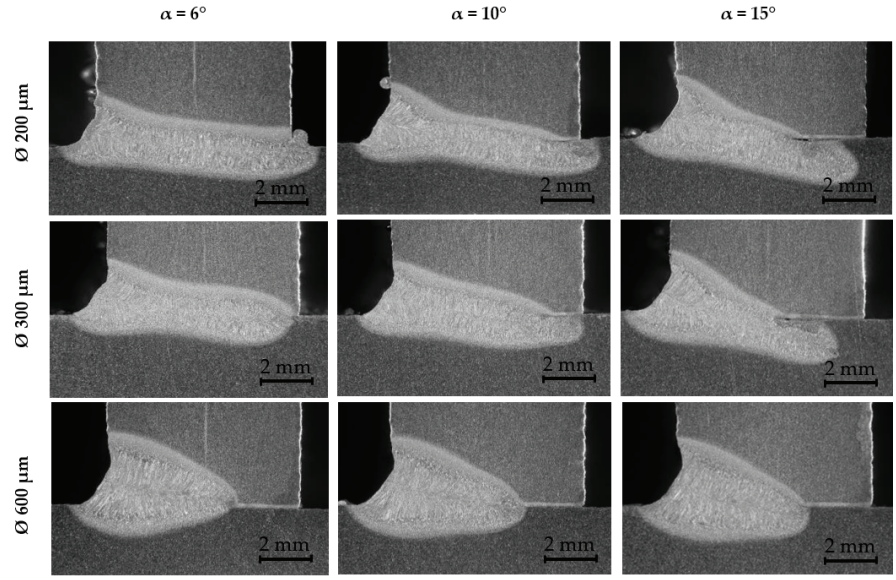

Figure 3. Macrographs of weld samples at different beam inclination angles: AH36, t = 8 mm, P_L = 6 kW, v_w = 1.25 m/min, beam offset from flange 0.5 mm, F_{PP} = −2 mm.

3.2. Effect of Beam Offset from the Flange

The effect of the beam offset from the flange was studied only with 300 µm and 600 µm process fibers. Based on the very narrow bead width produced earlier with the 200 µm process fiber and an assumption that the weld width largely determines the tolerance limits, the 200 µm process fiber was not included in the experiments. The laser power needed for full penetration was first calculated using the Power Factor Model developed by Suder et al. [23] and subsequently determined experimentally. The calculated values exceeded the real power requirement by at least 30% (less than 8 kW vs. 9.7 kW, F_{PP} −2 mm, beam Ø on surface 1.0 mm; 10 kW vs. 13 kW, F_{PP} −2 mm, beam Ø on surface 1.6 mm). Macrographs showing beam offsets from 0.5 mm to 2.0 mm are presented in Figure 4.

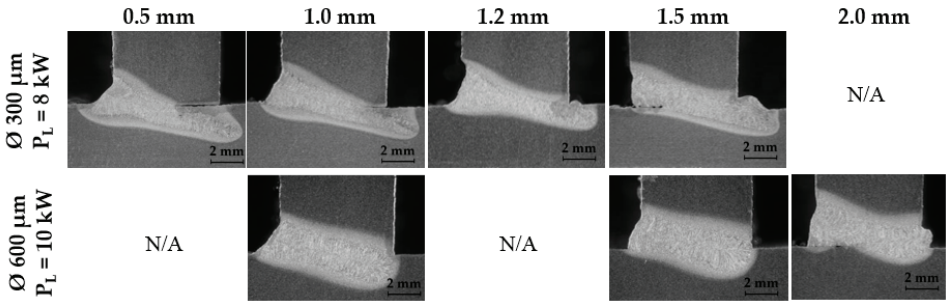

Figure 4. Macrographs of weld cross-sections when beam position from the flange was varied: material = AH36, t = 8 mm, v_w = 1.25 m/min, F_{PP} = −2 mm, α = 15°.

As shown in Figure 4, despite similar width of weld bead, there was a significant difference in the geometry of the fusion area. Welds produced with the 300 µm process fiber had a deep and narrow profile with a slightly wider top typical of high power laser welds. The setup with the 600 µm process

fiber produced welds that were wide throughout the whole fusion area, resulting in a more acceptable weld profile for a T-joint.

3.3. Effect of Focal Point Position

Negative defocusing was used to study whether decrease in beam density at the workpiece surface has a favorable effect on the formation of the weld bead. The influence of focal point position on the weld profile was investigated by changing the defocusing distance in steps of 2 mm. Beam offset from the flange was selected as 1 mm and 1.5 mm (for the 300 µm and 600 µm setups, respectively) to increase the likelihood of full penetration. The focal point was moved along the beam propagation direction inside the material in 2 mm steps. Figure 5 shows cross-sectional macrographs of the welds produced.

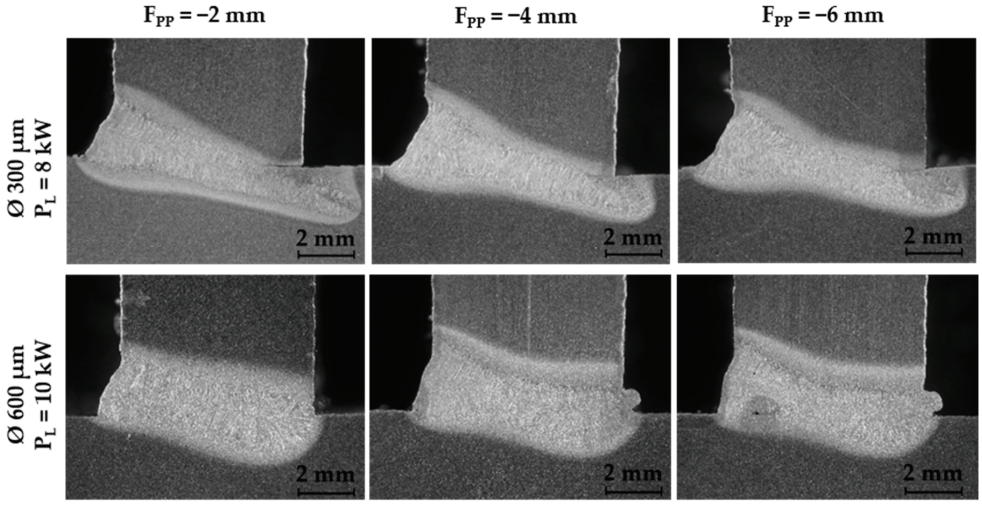

Figure 5. Weld profiles at various focal point positions: AH36, t = 8 mm, v_w = 1.25 m/min, beam offset from flange 1.0 mm (up) and 1.5 mm (down), α = 15°.

It can be seen from the images presented in Figure 5 that decreasing the focal point position leads to a slight decrease in penetration. F_{PP} −4 mm resulted in full penetration in the set-up with the 600 µm process fiber, while none of the welds produced with the 300 µm fiber had complete penetration at the weld root.

4. Discussion

4.1. Geometry of the Welds

The purpose of this study was to investigate geometrical differences in welds produced with three different beam delivery fibers and to determine the effect of process parameters on T-joint welds. Thirty welds were produced, evaluated, and their cross-sections analyzed. The acceptance criteria in visual inspection were smooth and plain face and root sides of the weld seam, lack of spatter, cracks or other defects listed in the Standard EN ISO 13919-1, and full visible penetration on the root side. Cracks or porosity were not present, qualifying the welds for class C of ISO 13919-1. Obvious undercut and lack of fusion produced by an inappropriately positioned beam or a lack of laser power were causes of rejection.

The width of the weld fusion zone determines the largest acceptable inclination angle for producing full penetration at a given web thickness. It can be seen in Figure 3 that compared to

the other set-ups studied, the process fiber with a core diameter 600 µm was least sensitive to increase of α. However, at given thickness of 8 mm, $\alpha = 6°$ produced the largest weld throat in all set-ups, regardless of the diameter of the beam, since the keyhole formed strictly along the axis of beam propagation. Figure 6 illustrates the effect of beam inclination angle on melt distribution relative to the middle axis of the joint.

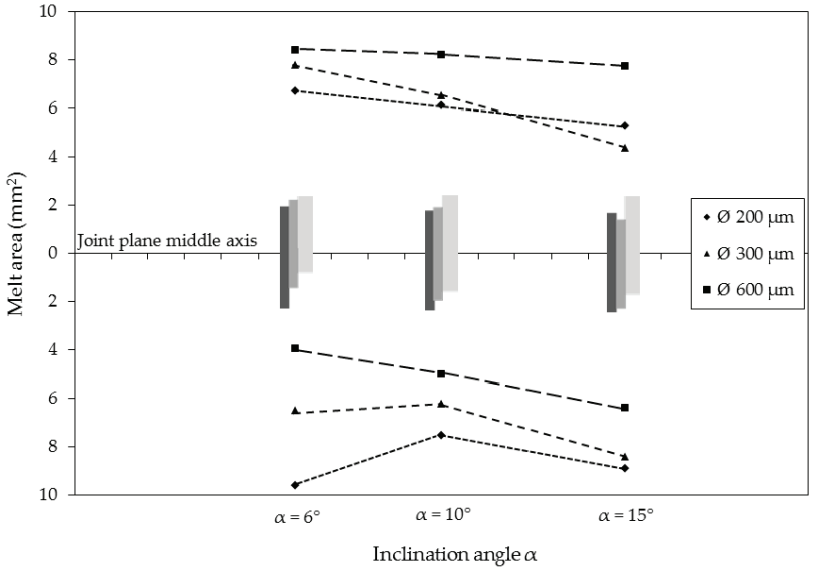

Figure 6. Proportions of the weld and melt area distribution differences at three inclination angles tested. AH36, $t = 8$ mm, $P_L = 6$ kW, $v_w = 1.25$ m/min, $F_{PP} = -2$ mm.

Figure 6 shows the size of the melt area above and below the middle axis of the joint of the welds presented earlier in Figure 3. The bars illustrate the proportions of the melt area above (web) and below (flange) the joint plane, and the lines show the area of the melt. Process fibers with core diameters of 200 µm and 300 µm produced welds with similar properties: the melt area decreased with increase of inclination angle. The 600 µm diameter process fiber produced welds in which the melt area increased while simultaneously keeping the same proportions of the fusion zone above and below the joint axis. The fiber producing the largest focal point diameter was least sensitive to change of inclination angle.

From an engineering point of view, beam offset is an important parameter affecting the weld quality of fillet welds, where joint bridging ability and ensuring complete fusion are more important than the penetration depth itself. As can be observed in Figure 4, tolerance to beam offset is also determined by the width of the weld. An inclination angle of 15° was chosen over two smaller angles tested based on the width of the weld bead and possible accessibility restrictions of the welding head. Optimal offsets for acceptable top bead and full fusion at the root are: 1.0 mm with the 300 µm transfer fiber, and, 1.0 mm and 1.5 mm with the 600 µm transfer fiber. The diameters of the beams on the surface were 1.0 mm and 1.6 mm, respectively.

When the 300 µm fiber was used, deviation to either side from the 1.0 mm offset produced either lack of fusion at the root or undercut and lack of penetration at the face of the weld. Due to the small width of the weld/fusion zone, higher offset resulted in formation of severe undercut on the top of the weld, while part of the melt was pushed through the weld root. The transfer fiber with 600 µm core diameter had a wider positioning tolerance window because the width of the weld throughout the fusion area is also wider. All of the welds produced with the 600 µm process fiber had a smooth bead and root sides, complete penetration, and class B quality according to EN-ISO 13919-1. It seems

that a change in the keyhole process, noticed earlier by [14], can be seen in the case of fillet welds in low alloyed steel. It is logical that power density has an effect on the process mechanism while still producing weld shape that is similar but wider than in the case of higher power density.

The focal point position has the same effect on T-joints as any other weld. Comparing the setups studied, an insignificant increase in bead width in correlation with an increase in beam dimension on the surface of material was noticed. F_{PP} of −2 mm produced welds with a larger weld toe radius than F_{PP} −6 mm. When F_{PP} was positioned at −4 mm, that is, at half of the thickness of the web, the setup produced fully fused welds lacking porosity or other defects on both sides of the joint.

4.2. Application of Specific Point Energy to Welding of T-Joints

Traditionally, the depth of penetration has been characterized through the concept of heat input, also called line energy, which describes the energy available for producing the weld through the relationship of available laser power and welding speed. E_{SP} also considers the diameter of the beam on the surface of the specimen and therefore provides higher accuracy in definition of the penetration depth and weld geometry [23]. Suder and Williams [22] have shown that, in the case of bead-on-plate welds, the penetration depth is defined by power density and specific point energy, and the width of the weld by interaction time, regardless of the optical setup used. T-joint fillet welds follow the same analytical model regarding the penetration depth as bead-on-plate welds; in this work, however, there was a deviation at larger beam diameters produced with the 600 µm process fiber. The relationship between E_{SP} and penetration depth for all three setups is summarized in Figure 7.

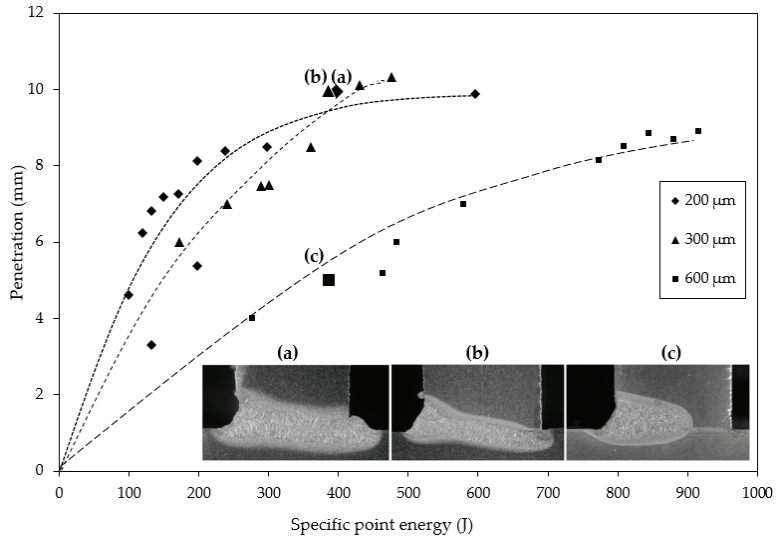

Figure 7. Penetration depth plotted as a function of specific point energy. E_{SP} values of the three welds shown: (▲a) 396 J; (♦b) 384 J; and (■c) 386 J.

Figure 7 shows curves for penetration depth produced with each of the process fibers and macrographs of three welds obtained at similar E_{SP} using different process fibers. Beam diameters on the surface of the welds shown in Figure 7 were 0.82 mm, 1.00 mm and 1.61 mm (F_{PP} −2 mm). The following laser power and welding speed combinations were used: (a) P_L = 6 kW, v_w = 0.75 m/min; (b) P_L = 8 kW, v_w = 1.25 m/min; and (c) P_L = 4 kW, v_w = 1 m/min. Welds (a) and (b) both had penetration depths close to 10 mm, when measured from the top of the bead, thus exceeding the thickness of the material, while weld (c) had only partial penetration. At similar E_{SP}, the 200 µm process fiber produced the weld with the deepest penetration and largest melt area (a). Full penetration was not

obtained with the 300 μm process fiber despite sufficient penetration depth, and the weld produced with the 600 μm fiber was noticeably shallower.

It is known that the diameter of the beam governs the dimensions of the keyhole, which in turn define the depth and width of the weld. As expected, beams with smaller diameters produced deeper penetrations at any given E_{SP}. Within each setup, it can be seen that an increase in E_{SP} also increases the penetration depth, but comparison of all three setups shows that the power density of the beam has a more pronounced effect on the morphology of the weld than E_{SP}. A possible explanation for this might be that the heat conduction in T-joints is different than in butt joints or bead on plate joints. Distribution of energy over a larger area leads to a slight decrease in molten area and reduced penetration depth. The power density of the beam determines the depth of the weld, while the width of the weld is determined by the diameter of the focused beam on the surface of the specimen.

4.3. Optimal Welding Conditions for T-Joint

The effects of beam inclination angle, beam offset from the flange and the focal point position relative to the surface of the material were studied to gain insight into the applicability of each setup under industrial conditions. Table 5 summarizes the findings.

Table 5. Acceptable limits for beam positioning for producing full penetration.

Parameter	200 μm Process Fiber	300 μm Process Fiber	600 μm Process Fiber
α	6°	6°	6°; 10°
Beam offset	1 mm	1 mm	1−1.5 mm
F_{PP}	−4 mm	−4 mm	−2–−6 mm

The optimal parameters for all set-ups were inclination angle 6°, beam offset from the flange 1 mm, and focal point position −4 mm below the surface of the material. In all of the setups, the axis of the weld was aligned along the direction of the beam propagation. For this reason, when the beam was aimed past the root of the joint, the formed molten pool did not follow the joint plane, resulting in a lack of fusion at the back of the weld. However, the applicability of a beam inclination angle of 6° in industrial applications may be limited because of a danger of collision of the laser welding head while maneuvering in restricted space, especially in situations where the incident beam side of the flange exceeds the focal length of the laser.

From the industrial point of view, the most versatile solution for T-joints of the three process fibers tested would be the fiber with a core diameter of 600 μm. This setup produced top beads superior in quality to the two other setups studied. The welds made with the 200 μm and 300 μm process fibers were deep yet extremely narrow at the deepest section of the weld and prone to undercut at the surface. A setup with a 600 μm fiber results in a more stable process that has a greater tolerance for beam displacement and smaller probability for seam imperfections.

5. Conclusions

The present work reported welding of single-sided T-joints of 8 mm thick AH36 shipbuilding steel with three optical setups using process fibers with core diameters of 200 μm, 300 μm and 600 μm. The current study found that:

(1) Full fusion in one welding pass was produced with all three process fibers studied.
(2) Penetration depth and width of the weld both primarily depend on the beam diameter. The parameter with the greatest influence on the depth of the weld is the power density of the beam, while the width of the weld is determined by the diameter of the focused beam. The width of the weld bead only has a minor correlation to the diameter of the beam on the surface.

(3) Smaller spot sizes provide an advantage in penetration depth at the same welding speed and power but are prone to producing undercuts. Due to the narrowness of the weld, the positioning of the beam has to be extremely accurate to avoid the weld missing the root of the joint.
(4) Welds produced with 600 μm process fiber were less prone to undercut formation and had more favorable shape of the weld toe than welds produced with 200 μm and 300 μm process fibers.
(5) Process fiber with core diameter 600 μm produced welds with the highest quality and was least sensitive to changes in beam positioning.
(6) Using beam delivery fibers with larger core diameters has a favorable effect on achieving full fusion in T-joints. Reduced energy density on surface increases the width of the weld throughout the penetration and produces smoother junctions of weld bead and base material.

Acknowledgments: Authors gratefully acknowledge Pertti Kokko for assistance with the experiments and Antti Heikkinen for the help with the metallography. Authors would like to thank the project PAMOWE of Academy of Finland for financial support.

Author Contributions: Anna Unt, Ilkka Poutiainen and Antti Salminen conceived and designed the experiments; Anna Unt and Ilkka Poutiainen performed the experiments; Anna Unt, Stefan Grünenwald, Mikhail Sokolov and Antti Salminen analyzed the data; Antti Salminen and Ilkka Poutiainen contributed materials/analysis tools; and Anna Unt and Antti Salminen wrote the paper.

Conflicts of Interest: The authors declare no conflicts of interest.

References

1. Grupp, M.; Klinker, K.; Cattaneo, S. Welding of high thicknesses using a fibre optic laser up to 30 kW. *Weld. Int.* **2013**, *27*, 109–112. [CrossRef]
2. Belforte, D. Laser Market Results Confound the Experts. Available online: http://www.industrial-lasers.com/articles/2017/01/laser-market-results-confound-the-experts.html (accessed on 16 August 2017).
3. Thoss, A.F. Four laser companies to exceed $1 billion revenue in 2016. *Adv. Opt. Technol.* **2017**, *6*, 13–16. [CrossRef]
4. Enz, J.; Khomenko, V.; Riekehr, S.; Ventzke, V.; Huber, N.; Kashaev, N. Single-sided laser beam welding of a dissimilar AA2024–AA7050 T-joint. *Mater. Des.* **2015**, *76*, 110–116. [CrossRef]
5. Liu, S.; Mi, G.; Yan, F.; Wang, C.; Jiang, P. Correlation of high power laser welding parameters with real weld geometry and microstructure. *Opt. Laser Technol.* **2017**, *94*, 59–67. [CrossRef]
6. Sokolov, M.; Salminen, A. Improving laser beam welding efficiency. *Engineering* **2014**, *6*, 559–571. [CrossRef]
7. Kuryntsev, S.V.; Gilmutdinov, A.K. Welding of stainless steel using defocused laser beam. *J. Constr. Steel Res.* **2015**, *114*, 305–313. [CrossRef]
8. Hobbacher, A. *Recommendations for Fatigue Design of Welded Joints and Components*; Springer: Berlin, Germany, 2015.
9. Det Norske Veritas. *Fatigue Design of Offshore steel Structures, Recommended Practice*; DNV-RP-C203; DNV GL: Oslo, Norway, 2008.
10. Matsumoto, N.; Kawahito, Y.; Nishimoto, K.; Katayama, S. Effects of laser focusing properties on weldability in high-power fiber laser welding of thick high-strength steel plate. *J. Laser Appl.* **2017**, *29*, 012003. [CrossRef]
11. Grajcar, A.; Morawiec, M.; Różański, M.; Stano, S. Twin-spot laser welding of advanced high-strength multiphase microstructure steel. *Opt. Laser Technol.* **2017**, *92*, 52–61. [CrossRef]
12. Morawiec, M.; Różański, M.; Grajcar, A.; Stano, S. Effect of dual beam laser welding on microstructure–property relationships of hot-rolled complex phase steel sheets. *Arch. Civ. Mech. Eng.* **2017**, *17*, 145–153. [CrossRef]
13. Shen, J.; Li, B.; Hu, S.; Zhang, H.; Bu, X. Comparison of single-beam and dual-beam laser welding of Ti–22Al–25Nb/TA15 dissimilar titanium alloys. *Opt. Laser Technol.* **2017**, *93*, 118–126. [CrossRef]
14. Vänskä, M. Defining the Keyhole Modes—The Effects on the Weld Geometry and the Molten Pool Behaviour in High Power Laser Welding of Stainless Steels. Ph.D. Thesis, Lappeenranta University of Technology, Lappeenranta, Finland, 2014.
15. Müller, A.; Goecke, S.F.; Sievi, P.; Albert, F.; Rethmeier, M. Laser beam oscillation strategies for fillet welds in lap joints. *Phys. Proc.* **2014**, *56*, 458–466. [CrossRef]
16. Wang, L.; Gao, M.; Zhang, C.; Zeng, X. Effect of beam oscillating pattern on weld characterization of laser welding of AA6061-T6 aluminum alloy. *Mater. Des.* **2016**, *108*, 707–717. [CrossRef]

17. Hao, K.; Li, G.; Gao, M.; Zeng, X. Weld formation mechanism of fiber laser oscillating welding of austenitic stainless steel. *J. Mater. Process. Technol.* **2015**, *225*, 77–83. [CrossRef]
18. Zhang, M.; Chen, G.; Zhou, Y.; Liao, S. Optimization of deep penetration laser welding of thick stainless steel with a 10 kW fiber laser. *Mater. Des.* **2014**, *53*, 568–576. [CrossRef]
19. Ion, J. *Laser Processing of Engineering Materials: Principles, Procedure and Industrial Application*; Butterworth-Heinemann: Oxford, UK, 2005; p. 179. ISBN 0-7506-6079-1.
20. Zou, J.L.; He, Y.; Wu, S.K.; Huang, T.; Xiao, R.S. Experimental and theoretical characterization of deep penetration welding threshold induced by 1-μm laser. *Appl. Surf. Sci.* **2015**, *57*, 1522–1527. [CrossRef]
21. Courtois, M.; Carin, M.; Le Masson, P.; Gaied, S.; Balabane, M. A new approach to compute multi-reflections of laser beam in a keyhole for heat transfer and fluid flow modelling in laser welding. *J. Phys. D Appl. Phys.* **2013**, *46*, 505305. [CrossRef]
22. Suder, W.J.; Williams, S.W. Investigation of the effects of basic laser material interaction parameters in laser welding. *J. Laser Appl.* **2012**, *24*, 032009. [CrossRef]
23. Suder, W.J.; Williams, S. Power factor model for selection of welding parameters in CW laser welding. *Opt. Laser Technol.* **2014**, *56*, 223–229. [CrossRef]
24. Ayoola, W.A.; Suder, W.J.; Williams, S.W. Parameters controlling weld bead profile in conduction laser welding. *J. Mater. Process. Technol.* **2017**, *249*, 522–530. [CrossRef]
25. Nikhare, N.B.; Arakerimath, R.R. Parametric analysis and heat transfer enhancement of laser welding for different material. *Int. J. Eng. Manag. Res.* **2015**, *ICRAME-2015*, 92–96.
26. Hashemzadeh, M.; Suder, W.; Williams, S.; Powell, J.; Kaplan, A.F.H.; Voisey, K.T. The application of specific point energy analysis to laser cutting with 1 μm laser radiation. *Phys. Proc.* **2014**, *56*, 909–918. [CrossRef]
27. Verhaeghe, G. The effect of spot size and laser quality on welding performance when using high-power continuous wave solid-state lasers. In Proceedings of the ICALEO'2005 Conference, Miami, FL, USA, 31 October–3 November 2005; pp. 264–271.
28. Kawahito, Y.; Mizutani, M.; Katayama, S. Investigation of high-power fiber laser welding phenomena of stainless steel. *Trans. JWRI* **2007**, *36*, 11–15.
29. Bhargava, P.; Paul, C.P.; Mundra, G.; Premsingh, C.H.; Mishra, S.K.; Nagpure, D.; Kumar, A.; Kukreja, L.M. Study on weld bead surface profile and angular distortion in 6 mm thick butt weld joints of SS304 using fiber laser. *Opt. Laser Eng.* **2014**, *53*, 152–157. [CrossRef]
30. Katayama, S.; Kawahito, Y.; Mizutani, M. Elucidation of laser welding phenomena and factors affecting weld penetration and welding defects. *Phys. Proc.* **2010**, *5*, 9–17. [CrossRef]
31. International Organization for Standardization. *EN ISO 13919-1: Welding—Electron and Laser-Beam Welded Joints—Guidance on Quality Levels for Imperfection—Part 1: Steel*; ISO: Geneva, Switzerland, 1996; 9p.
32. International Organization for Standardization. *EN ISO 17639 Destructive Tests on Welds in Metallic Materials—Macroscopic and Microscopic Examination of Welds*; ISO: Geneva, Switzerland, 2003.

Publication V

Grünenwald, S., Unt, A., Salminen, A.
Investigation of the influence of welding parameters on the weld geometry when welding structural steel with oscillated high-power laser beam

Reprinted with permission from
Procedia CIRP
Vol. 74, pp. 461-465, 2018

Available online at www.sciencedirect.com

ScienceDirect

Procedia CIRP 74 (2018) 461–465

www.elsevier.com/locate/procedia

10th CIRP Conference on Photonic Technologies [LANE 2018]

Investigation of the influence of welding parameters on the weld geometry when welding structural steel with oscillated high-power laser beam

Stefan Grünenwald[a],Anna Unt[a], Antti Salminen[a,]*

[a] *Laboratory of Laser Materials Processing, Lappeenranta University of Technology,Tuotantokatu 2, Lappeenranta, 53850 Finland*

* Corresponding author. *E-mail address*: antti.salminen@lut.fi

Abstract

Oscillation of the laser beam has been applied to achieve a positive influence on the efficiency of the welding process and the quality of the weld seam. In this work a 10 kW laser beam from a fiber laser was oscillated with frequencies up to 1000 Hz for bead on plate welds in 15 mm thick structural steel to investigate the influence of beam oscillation on geometrical dimensions of the weld seam. The laser beam was oscillated transversally with a given amplitude for each frequency. The parameter set to be varied was laser power, welding speed and focal point position according to the highest influence on the formation of the weld seam and the welding process. The results obtained show that lower oscillation frequencies in the range of 200 Hz with higher amplitudes in combination with either low welding speeds or higher laser powers up to 10 kW had the greatest influence on the geometry of the weld seam.

Keywords: high power laser; fibre laser; oscillating laser beam; transversal scanning; structural steel.

1. Introduction

Welding with oscillated laser beam is a well-established production process, gaining renewed interest since high power lasers with superior beam quality and virtually unlimited output power became affordable [1]. Laser welding with high frequency beam oscillation is studied as a method to increase the stability of the welding process. Bright beam and process stability at high power levels opens new possibilities for beam manipulation [2]. High-power beams produce deep nail-shaped welds with high depth-to-width ratio, however its applicability is limited because of extreme demands to joint fit-up accuracy [3]. One way to overcome this challenge is wobbling the laser beam over the joint in a predetermined pattern [4]. Research for growing range of applications is motivated also by advances in beam delivery equipment, as smaller dimensions of the processing head improve the joint accessibility and overall flexibility of the welding process [5], [6]. Beam oscillation distributes the beam energy across a wider area and produces fully bridged and defect free joints with excellent geometrical features at the expense of slightly reduced processing speed [7]. In addition, beam oscillation enables control of the cooling rate, which is beneficial for joining dissimilar and difficult to weld materials like aluminum alloys and high strength steels used in automotive and aerospace industries [8]. When oscillating a single mode laser beam to stabilize the melt pool in laser-GMA hybrid welding of 22MnB5 boron alloyed steel, it was found that the beam influence on bead geometry can be neglected [9]. Studies using an oscillated multimode laser beam in welding lap joint in zinc coated steel and ASIS304 presented advantages of welding with small beam diameter at reduced power with oscillation over conventional laser welding, while noting that knowledge of material behavior is crucial for the successful application of this technique [10], [11]. Further parameter studies have shown that beam oscillation in welding butt joint improves the gap bridgeability up to three times [12]. Regardless of joint type, the profile of the weld and surface smoothness have direct influence on the weld quality. Detailed understanding of the formation mechanism of the

10.1016/j.procir.2018.08.150

weld geometry is important for utilization of the whole potential that beam manipulation by oscillation is able to provide.

2. Experimental work

2.1. Material

The material used for the welding experiments were a structural steel of the grade S235J2C with a thickness of 8 mm and for experiments with low welding speeds at a higher laser power the fine-grained structural steel S355MC with thicknesses of 12 mm and 15 mm. The chemical compositions of materials are given in Table 1.

Table 1. Nominal chemical composition of the materials used (wt. %).

Material	C max	Si max	Mn max	P max	S max
S235J2C	0.12	0.03	1.20	0.02	0.02
S355MC	0.09	0.50	1.00	0.02	0.01

2.2. Experimental set-up

An IPG YLR 10000 fiber laser with a 200 µm beam transfer fiber diameter was used for the experiments. For laser beam oscillation the DC-Scanner system from ILV was applied, see Fig. 1. The scanner system was mounted on a 90° Precitec YW 50 welding head, Fig. 2, with a collimation unit of 150 mm and a focusing lens of 300 mm. The scanner is capable of achieving scanning frequencies in the range of 10 - 1000 Hz and producing scan widths from 18 mm to 2 mm depending on the frequency. All of the welding was performed as bead on plate, with the parameter sets given in Table 2. One set of experiments was carried out with a frequency range of 100 - 1000 Hz, all other experiments started with 200 Hz ascending in steps of 200 Hz until 1000 Hz. As a comparison for each parameter set, a reference weld without the beam oscillation was produced.

Table 2. Welding Process Parameters.

Parameter	Unit	Parameter range
Laser Power (P)	kW	5; 6; 8; 10
Welding speed (v_w)	m/min	1; 2; 3
Focal point position (f_{pp})	mm	-10; -5; 0; 5; 10
Scanning frequency (f)	Hz	0; 100; 200; 300; 400; 500; 600; 700; 800; 900; 1000
Scanning amplitude (A)	%	100%
Process gas	-	Argon with 30 l/min

2.3. Evaluation of welded samples

Metallographic preparation of the samples was carried out according to DIN EN ISO 17639. The welds were transversely sectioned at the middle of the weld length, polished and etched using a 2% Nital solution. Macrographs of the cross-sections were inspected for penetration, weld dimensions in five locations of the fusion zone (w1-w5) and HAZ, as shown in Fig. 3. From this data also the angle α of the weld side was calculated.

Fig. 1. DC-Scanner System from ILV used to oscillate the laser beam.

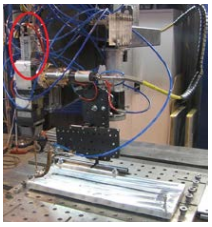

Fig. 2. Experimental set-up, with DC-Scanner marked in red.

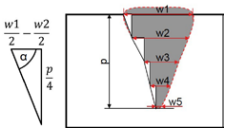

Fig. 3. Weld cross-section measurements: w1 = weld width at top surface (mm), w2 = weld width at 0.25p (mm), w3 = weld width at 0.5p (mm), w4 = weld width at 0.75p (mm), w5 = weld width at 1p (mm), A = area of fusion zone (mm²), α = angle of weld cross-section side

3. Experimental results

The characteristic property of a weld produced with a high-power laser beam is a deep and narrow weld seam with a high depth to width ratio. In order to evaluate the influence of the beam oscillation on the weld seam geometry and to determine the differences between the various frequencies applied, the angle of the weld fusion zone side outline and the width of the fusion zone at different positions was studied. Furthermore, three main process parameters, welding speed, focal point position and laser power were varied in combination with oscillation frequencies in so called parameter sets.

In addition, the penetration depth as well as fusion zone area were considered as well. As a reference for further discussions below, Fig. 4 displays cross-sections from a parameter set where all the welds were made with the full range of frequencies (0 – 1000 Hz), according to Table 2.

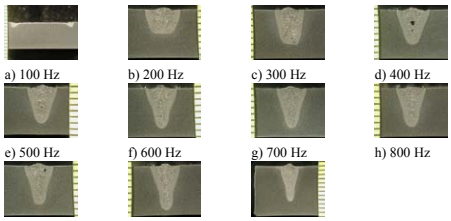

Fig. 4. Cross-sections of welds carried out with frequencies between 100 Hz and 1000 Hz with the parameter set of v_w= 1 m/min, f_{pp}= 0 mm, P = 5 kW.

3.1. Distance from middle of weld cross-section

To compare the weld cross-section geometry resulting from the different scanning frequencies used, regardless of the main parameters, an average value for each of the five measurement locations w1-w5 was calculated and the standard deviation determined by using:

$$s = \sqrt{\frac{\sum_{i=1}^{n}(x-\bar{x})^2}{(n-1)}} \quad (1)$$

where x are the observed values of the sample items, $\overline{x}$ is the mean value of these observations, and n is the number of observations in the sample. To make the measurements comparable and exclude the influence of the different penetration depths, the initial measurement values were standardized by dividing them with the measured penetration depth.

Depicted in Fig. 5 is the average distance from the middle of the weld cross-section at five different positions. The graph is plotted for positive values on the x-axis only, the indicated grey outline of the weld cross-section in the background gives an orientation of the geometrical shape. The graph clearly shows that the welds produced with 200 Hz are the widest – independent from the parameter set applied – and have the highest statistical variance as seen from the upper and lower band of confidence. Welds produced with oscillation frequencies of 400 Hz and higher, including 0 Hz, have a rather narrow band of confidence and are closer together, resembling the geometry of the high-power laser weld the most. These statistically processed results correspond to the cross-sections shown in Fig. 8, where welds with 200 Hz are compared, and cross-sections in Fig. 4, showing the whole set of welds from 0 – 1000 Hz.

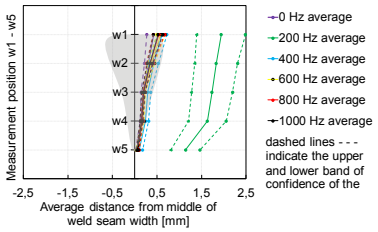

Fig. 5. Evaluation of the standardized average distance from the middle of the weld cross-section at positions w1 – w5.

3.2. Angle of the weld cross-section outline

The angle α of the weld side cross-section outline was calculated by the five widths of the cross-section, w1 – w5. This includes the depth to width ratio by a stepwise consideration of the penetration depth. Fig. 6 shows the average geometric angles of each position w1 – w5, calculated for the individual oscillating frequencies from the respective parameter set variation.

The average angle α for welds produced without oscillation, and an oscillating frequency of 1000 Hz varies in a rather small range, showing that the geometrical outline of the weld cross-section does not differ much, which is shown also in Fig. 7. The samples welded with 1000 Hz at 2 m/min have the same characteristic shape of deep penetration high power laser welds, similar to cross-section k) shown in Fig. 4.

Experiments with a frequency of 200 Hz show a high variance of α in each of the three parameter sets applied. This variance is due to the more or less distinct spike visible on the left and right side of the cross-section, for each parameter set, determining the value measured in position w5 and thus the angle α, compare with Fig. 8, especially cross-sections b), c) and d). Regarding the parameter set for the variation of the focal point position, depicted in the top right graph in Fig. 6, the fluctuation range of α decreases, starting from 400 Hz to a more uniform series of values. This indicates that the influence of the focal point position is less distinct when welding with oscillated high-power laser beams at higher frequencies.

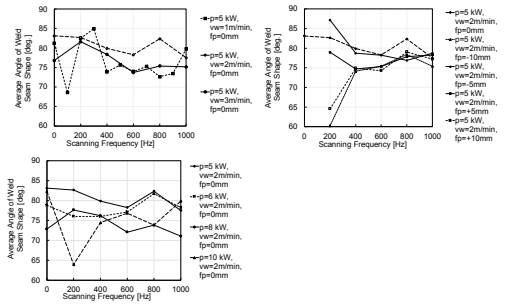

Fig. 6. Evaluation of the average angle α of the weld cross-section shape for parameter set variation of welding speed (top left), focal point position (top right) and laser power (bottom left).

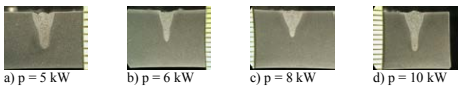

a) p = 5 kW b) p = 6 kW c) p = 8 kW d) p = 10 kW

Fig. 7. Cross-sections of welds carried out with different laser powers with the parameter set of v_w= 2 m/min, f_{pp} = 0 mm, f = 1000 Hz.

3.3. Evaluation of the penetration depth

The graphs on Fig. 9 display the penetration depths of the different experiments according to the three main parameter sets: welding speed, focal point position and laser power.

The variation of the focal point position shows a very uniform behavior, as can also be seen in Fig. 8. Even though the laser beam properties like focal spot size and intensity distribution are affected significantly by changing the focal point position or the inclination angle, as shown for example by [13], influencing also the keyhole behavior, in combination with the oscillating laser beam it does not have a great effect on the penetration depth with the parameters applied in this study.

a) f_{pp}= +10 mm b) f_{pp}= + 5 mm c) f_{pp}= 0 mm d) f_{pp}= - 5 mm e) f_{pp}= - 10 mm

Fig. 8. Cross-sections of welds carried out with different focal positions with the parameter set of vw= 2 m/min, P = 5 kW, f = 200 Hz.

Regarding the variation of the welding speed and laser power, Fig. 9 top left and top right shows that a change of the heat input at a given frequency of the oscillated laser beam will lead to the expected change in penetration depth.

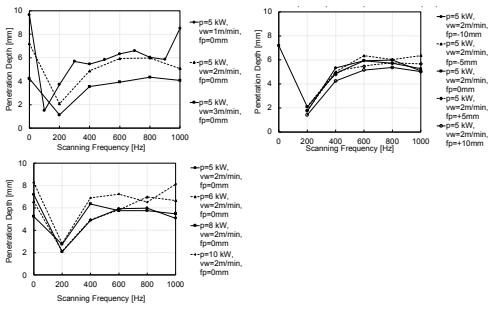

Fig. 9. Evaluation of the penetration depth for parameter set variation of welding speed (top left), focal point position (top right) and laser power (bottom left).

3.4. Evaluation of the weld fusion zone

The area of the fusion zone of the three parameter sets is illustrated in Fig. 10. Variation of the welding speed and laser power are the main factors influencing the dimensions of the measured area. The focal point position does not have a significant effect, keeping welding speed and laser power constant.

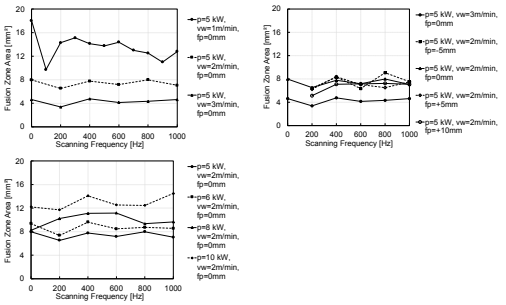

Fig. 10. Evaluation of the fusion zone area for parameter set variation of welding speed (top left), focal point position (top right) and laser power (bottom left).

Regarding the oscillation of the laser beam, it can be seen that at a low frequency of 100 Hz, a downward spike appears. The respective cross-section, Fig. 4 a), shows a low penetration in the middle of the weld cross-section with a more distinct penetration depth on the left and right side. It seems that a keyhole welding process did not take place, but only a partial melting of the surface.

4. Conclusion

A high-power fiber laser with beam oscillation was used to produce bead on plate welds to investigate the influence of the oscillation frequency on the shape of the weld cross-section. In combination with the oscillation frequency varied from 100 Hz to 1000 Hz, the welding speed, laser power and focal point position were varied also. All measures applied to evaluate the weld geometry on a mathematical or statistical basis comply with the original measurements obtained from the cross-sections of each weld. The following findings can be presented:

- Welds with a frequency up to 200 Hz have a high variance regarding the overall weld cross-section width and average angle of the cross-section outline. The penetration depth achieved was the lowest.
- Welds with 400 Hz and more, including welds with 0 Hz are more uniform in shape and variance regarding the obtained results. The highest oscillation frequencies produced similar or same results as were noted with welds without oscillation, i.e. 0 Hz, also concerning penetration depth and fusion zone area.
- Variation of the focal point position in combination with the oscillation frequency has little influence on the weld cross-section geometry at higher frequencies as well as on the penetration depth and fusion zone area.
- The influence of the heat input on the dimensions of the fusion zone area, by varying welding speed and laser power is most distinctive. The influence from oscillation of the laser beam is secondary.

Acknowledgements

This study was funded by Finnish industries and Business Finland in project “DigRob” and Academy of Finland in project “Pamowe”.

References

[1] Zervas, M.N.; Codemard, C.A.: High power fiber lasers: a review IEEE Journal of Selected Topics in Quantum Electronics, 20, 5, (2014) 1- 23
[2] Overton, G. et al.: Laser Marketplace 2014: Lasers Forge 21st Century Innovations, Laser Focus World, 5, (2014)
[3] Bachmann, M.; et al.: Welding with High-power Lasers: Trends and Developments, Physics Procedia, 83 (2016) 15-25
[4] Martukanitz, R.P.; Tressler, J. F.: Mixing it up: Laser stir welding shows promise for the joning of aluminium alloys. Industrial Laser Solutions, 21, 3 (2006) 25-30
[5] Spöttl, M.; Mohrbacher, H.: Laser-based manufacturing concepts for efficient production of tailor welded sheet metals, Adv. Manuf. 2, (2014) 193–202
[6] Schweier, M.; et al.: Spatter formation in laser welding with beam oscillation, Physics Procedia 41, (2013) 20 – 30
[7] Kuryntsev, S.V.; Gilmutdinov, A.K.:The effect of laser beam wobbling mode in welding process for structural steels, Int J Adv Manuf Technol, 81, (2015) 1683–1691
[8] Kraetzsch, M.; et al.: Laser Beam Welding with High-Frequency Beam Oscillation: Welding of Dissimilar Materials with Brilliant Fiber Lasers, Physics Procedia, 12, (2011) 142–149
[9] Gao, X.S.; et al.: Effects of process parameters on weld bead defects in oscillating laser-GMA hybrid welding of lap joints, Int J Adv Manuf Technol, 93, (2017) 1877–1892
[10] Müller, A.; et al.: Laser beam oscillation strategies for fillet welds in lap joints, Physics Procedia, 56, (2014) 458 – 466
[11] Hao, K.; et al.: Weld formation mechanism of fiber laser oscillating welding of austenitic stainless steel, Journal of Materials Processing Technology, 225, (2015) 77–83
[12] Vollertsen, F.; et al.: Developments for laser joining with high-quality seam surfaces, Lightweight Design worldwide 10, 5, (2017) 6-13
[13] Tsoukantas, G.; et al.: On optical design limitations of generalized two-mirror remote beam delivery laser systems: the case of remote welding, Int J Adv Manuf Technol, 32, (2007) 932–941

ACTA UNIVERSITATIS LAPPEENRANTAENSIS

839. GERAMI TEHRANI, MOHAMMAD. Mechanical design guidelines of an electric vehicle powertrain. 2019. Diss.

840. MUSIIENKO, DENYS. Ni-Mn-Ga magnetic shape memory alloy for precise high-speed actuation in micro-magneto-mechanical systems. 2019. Diss.

841. BELIAEVA, TATIANA. Complementarity and contextualization of firm-level strategic orientations. 2019. Diss.

842. EFIMOV-SOINI, NIKOLAI. Ideation stage in computer-aided design. 2019. Diss.

843. BUZUKU, SHQIPE. Enhancement of decision-making in complex organizations: A systems engineering approach. 2019. Diss.

844. SHCHERBACHEVA, ANNA. Agent-based modelling for epidemiological applications. 2019. Diss.

845. YLIJOKI, OSSI. Big data - towards data-driven business. 2019. Diss.

846. KOISTINEN, KATARIINA. Actors in sustainability transitions. 2019. Diss.

847. GRADOV, DMITRY. Experimentally validated numerical modelling of reacting multiphase flows in stirred tank reactors. 2019. Diss.

848. ALMPANOPOULOU, ARGYRO. Knowledge ecosystem formation: an institutional and organisational perspective. 2019. Diss.

849. AMELI, ALIREZA. Supercritical CO2 numerical modelling and turbomachinery design. 2019. Diss.

850. RENEV, IVAN. Automation of the conceptual design process in construction industry using ideas generation techniques. 2019. Diss.

851. AVRAMENKO, ANNA. CFD-based optimization for wind turbine locations in a wind park. 2019. Diss.

852. RISSANEN, TOMMI. Perspectives on business model experimentation in internationalizing high-tech companies. 2019. Diss.

853. HASSANZADEH, AIDIN. Advanced techniques for unsupervised classification of remote sensing hyperspectral images. 2019. Diss.

854. POPOVIC, TAMARA. Quantitative indicators of social sustainability applicable in process systems engineering. 2019. Diss.

855. RAMASAMY, DEEPIKA. Selective recovery of rare earth elements from diluted aqueous streams using N- and O –coordination ligand grafted organic-inorganic hybrid composites. 2019. Diss.

856. IFTEKHAR, SIDRA. Synthesis of hybrid bio-nanocomposites and their application for the removal of rare earth elements from synthetic wastewater. 2019. Diss.

857. HUIKURI, MARKO. Modelling and disturbance compensation of a permanent magnet linear motor with a discontinuous track 2019. Diss.

858. AALTO, MIKA. Agent-based modeling as part of biomass supply system research. 2019. Diss.

859. IVANOVA, TATYANA. Atomic layer deposition of catalytic materials for environmental protection. 2019. Diss.

860. SOKOLOV, ALEXANDER. Pulsed corona discharge for wastewater treatment and modification of organic materials. 2019. Diss.

861. DOSHI, BHAIRAVI. Towards a sustainable valorisation of spilled oil by establishing a green chemistry between a surface active moiety of chitosan and oils. 2019. Diss.

862. KHADIJEH, NEKOUEIAN. Modification of carbon-based electrodes using metal nanostructures: Application to voltammetric determination of some pharmaceutical and biological compounds. 2019. Diss.

863. HANSKI, JYRI. Supporting strategic asset management in complex and uncertain decision contexts. 2019. Diss.

864. OTRA-AHO, VILLE. A project management office as a project organization's strategizing tool. 2019. Diss.

865. HILTUNEN, SALLA. Hydrothermal stability of microfibrillated cellulose. 2019. Diss.

866. GURUNG, KHUM. Membrane bioreactor for the removal of emerging contaminants from municipal wastewater and its viability of integrating advanced oxidation processes. 2019. Diss.

867. AWAN, USAMA. Inter-firm relationship leading towards social sustainability in export manufacturing firms. 2019. Diss.

868. SAVCHENKO, DMITRII. Testing microservice applications. 2019. Diss.

869. KARHU, MIIKKA. On weldability of thick section austenitic stainless steel using laser processes. 2019. Diss.

870. KUPARINEN, KATJA. Transforming the chemical pulp industry – From an emitter to a source of negative CO2 emissions. 2019. Diss.

871. HUJALA, ELINA. Quantification of large steam bubble oscillations and chugging using image analysis. 2019. Diss.

872. ZHIDCHENKO, VICTOR. Methods for lifecycle support of hydraulically actuated mobile working machines using IoT and digital twin concepts. 2019. Diss.

873. EGOROV, DMITRY. Ferrite permanent magnet hysteresis loss in rotating electrical machinery. 2019. Diss.

874. PALMER, CAROLIN. Psychological aspects of entrepreneurship – How personality and cognitive abilities influence leadership. 2019. Diss.

875. TALÁSEK, TOMÁS. The linguistic approximation of fuzzy models outputs. 2019. Diss.

876. LAHDENPERÄ, ESKO. Mass transfer modeling in slow-release dissolution and in reactive extraction using experimental verification. 2019. Diss.

ISBN 978-952-335-438-8
ISBN 978-952-335-439-5 (PDF)
ISSN-L 1456-4491
ISSN 1456-4491
Lappeenranta 2019